Chapter 4

RESULTS AND DISCUSSIONS

4.1 Introduction

The present chapter deals with detailed analyses of heat transfer in square and vertical porous annulus. The various sections and subsections describe the heat transfer analyses in square porous annulus (external and internal heating), conjugate heat transfer in vertical annulus, conjugate double diffusion in vertical porous cylinder, investigation of heat transfer in vertical annulus subjected to discrete heating and finally, the mixed convection analysis in vertical porous cylinder subjected to segmental heating. The thermal equilibrium as well as thermal non-equilibrium approach is adopted for various cases, thus giving the comprehensive details about the effect of geometrical and physical parameters on the heat transfer characteristics and fluid flow in the porous domain. This chapter predominantly explains heat transfer phenomenon which is extended to study the heat and mass transfer as well in one of the cases.

4.2 Investigation of heat transfer in square porous-annulus subjected to outside wall heating

4.2.1 Introduction

This section deals with the heat transfer characteristics in a square porous annulus. Emphasis is given to investigation the effect of width ratio on heat and fluid flow characteristics inside the porous domain. The problem under consideration is represented schematically in Figure 4.2.1 and the related boundary conditions are detailed in chapter 3 section 3.2.3.

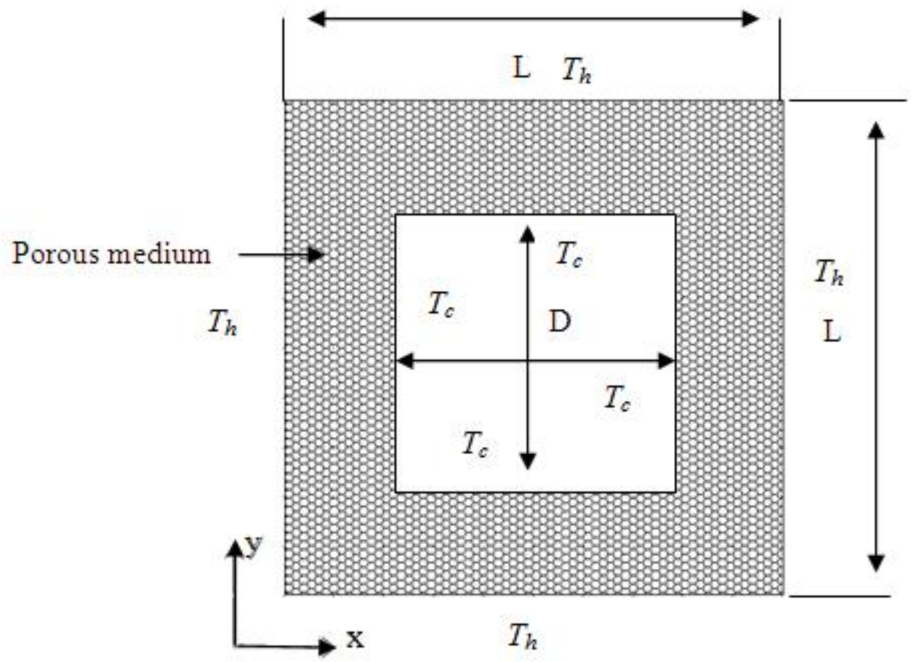

Figure 4.2.1: Schematic of square porous annulus heated at outer walls

4.2.2 Analysis

Figure 4.2.2 shows the streamlines and isothermal lines for width ratio of 0.125, 0.25, 0.375, 0.5, 0.625 and 0.75. This figure is obtained for $Ra = 100, Rd = 0$. It can be seen from Figure 4.2.2 that the fluid circulates in two symmetric sections about the central vertical line along the duct. It is obvious that fluid exhibits negligible movement at the upper portion of duct when $W=0.125$. The isothermal lines at the upper section of the duct are much more straightened as compared to the distorted isotherms at the other section of the cavity which clearly indicates that the conduction is the dominant mode of heat transfer at the upper portion of the cavity. This is further confirmed by the fact that the fluid movement that is the driving force for convection, is minimal at the upper section of cavity for $W=0.125$. The increase in the duct ratio changes the fluid motion from oval to elliptical pattern as shown in Figure 4.2.2. The increase in the width ratio brings in the uniformity in temperature distribution along the porous duct. Figure 4.2.3 shows the effect of an increased Rayleigh number on the fluid and heat transfer of varying duct width ratio. This figure corresponds to $Ra = 200,\ Rd = 0$. The effect of increased Rayleigh number is to increase the streamline magnitude which directly reflects the increase in fluid velocity as expected. It can be seen that the temperature lines at the lower section of the duct are distorted as compared to Figure 4.2.2a, indicating the increased convection current into lower section of the duct which demonstrates enhanced fluid motion. It is observed that a separate fluid circulation cell is formed at the lower section of duct for $0.25<W<0.625$. Figure 4.2.4 shows the streamlines and isotherms for $Ra = 400, Rd = 1$. The increase in the Rayleigh number and radiation parameter leads to considerable increase in the energy content of porous medium at the upper section of the cavity as indicated by isothermal lines in that region. The smaller fluid circulation cell at the bottom section of cavity gains further strength due to the increased Rayleigh number and radiation parameter, thus pushing the main circulation region towards the hot walls. It is obvious from streamlines and isotherms that a considerable variation in fluid velocity and temperature exists at the bottom section of the cavity as compared to the other sections of the cavity. This can be attributed to the fact that fluid has sufficient space to move around at lower region of cavity so that warm fluid can move upwards and cooler fluid can move downwards. However, the fluid is blocked by the wall at upper section of the cavity which acts as a barrier for smooth movement of fluid thus reducing the fluid convection.

a)

b)

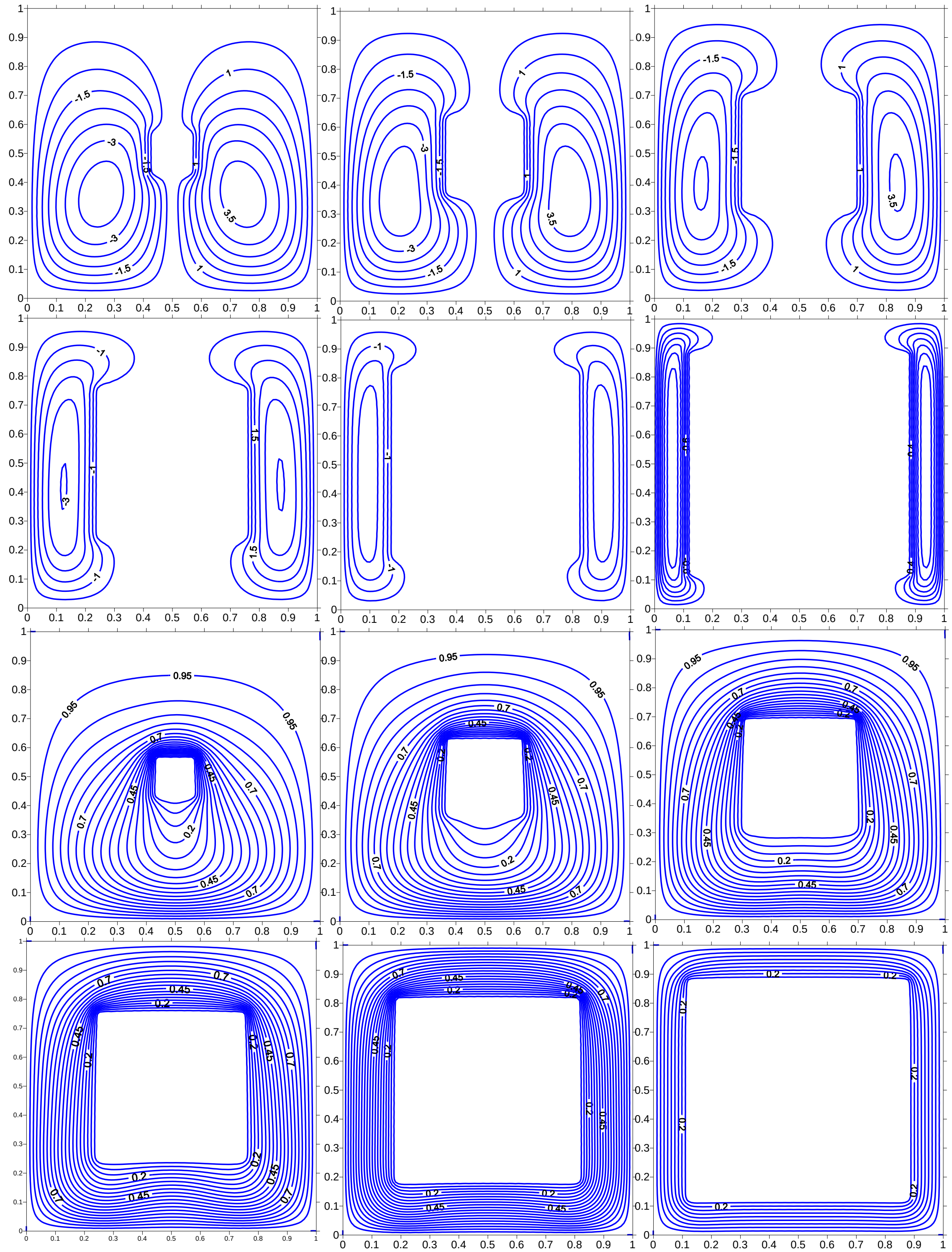

Figure 4.2.2: a) Streamlines b) Isotherms for *Ra=100*, *Rd=0*, W*=0.125*, *0.25*, *0.375* for rows I & III. *W=0. 5*, *0.625*, *0.75* for rows II & IV

a)

b)

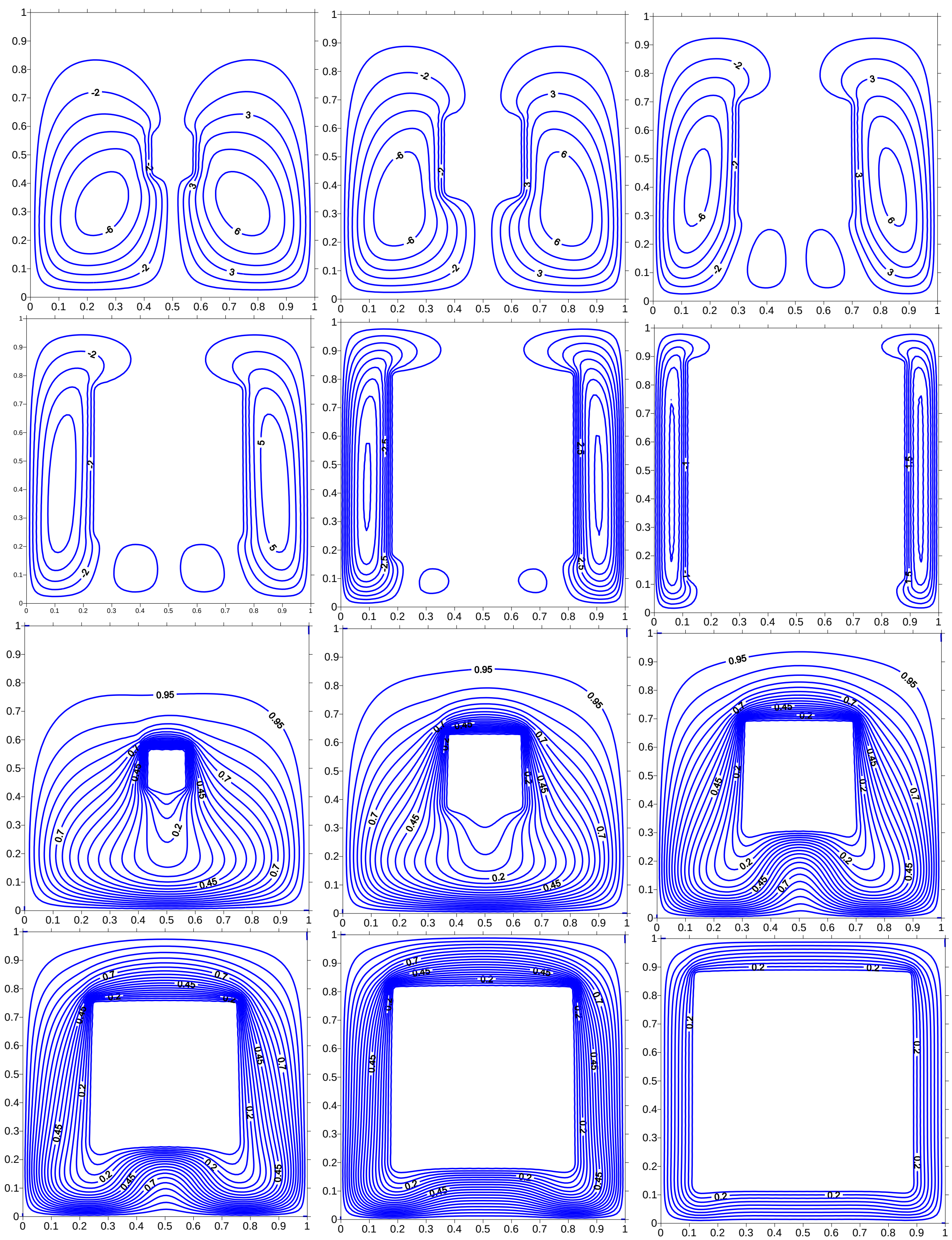

Figure 4.2.3: a) Streamlines b) Isotherms for *Ra=300*, *Rd=0*, W*=0.125, 0.25, 0.375* for rows I & III.   *W=0. 5, 0.625, 0.75* for rows II & IV

a)

b)

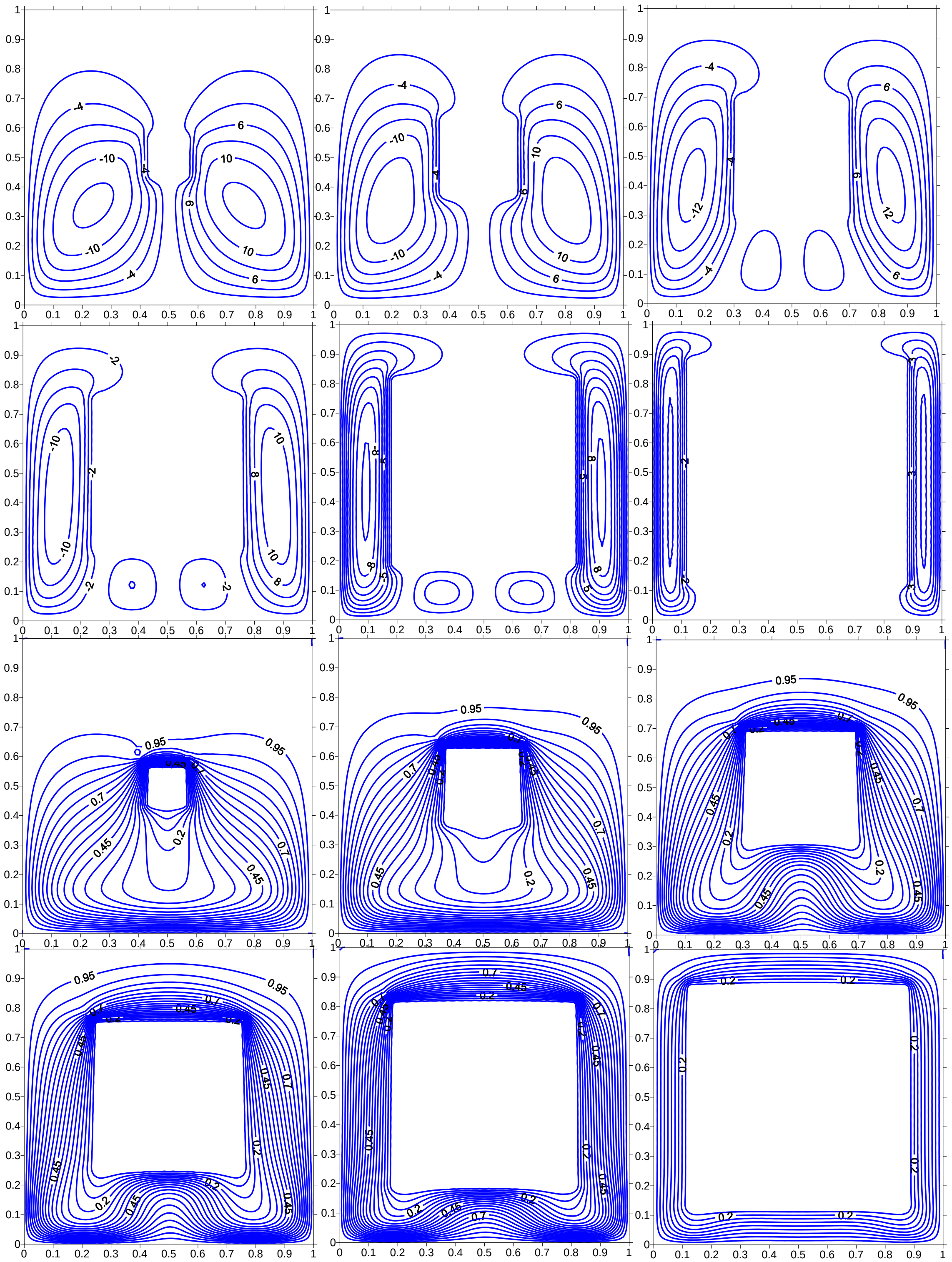

Figure 4.2.4: a) Streamlines b) Isotherms for *Ra=400*, *Rd=1*, W*=0.125*, *0.25*, *0.375* for rows I & III. *W=0. 5*, *0.625*, *0.75* for rows II& IV

Figure 4.2.5 shows the local Nusselt number variation with respect to height and width of the porous duct for $W=0.25$, $Ra=100$ and $Rd=0$. It is to be noted that the letter “L, R, B, T” represents the left, right, bottom and top walls of duct respectively. It is seen that the local Nusselt number at the left and the right walls are equal in magnitude, thus only one line is represented in Figures to represent the Nusselt number at these walls. It is found that the Nusselt number is much higher at the bottom wall compared to other walls. This is due to higher fluid velocity in the lower section of the duct which helps to transfer the high amount of energy from wall to the medium. The local Nusselt number is higher at mid-portion of walls for the top and bottom walls. However, the maxima for the left and right walls occur at the upper section of the walls. The heat transfer rate at the top wall is lower compared to other walls due to very low fluid convection in that region.

Figure 4.2.6 shows the local Nusselt number variation for $W=0.5$, $Ra=100$ and $R_d=0$. It is interesting to note that the Nusselt number oscillates in a wavy form for the bottom wall when $W=0.5$. The amplitude of oscillation increases with increment of the Rayleigh number. The wavy fluctuations of the Nusselt number could be attributed to the formation of a separate flow regime at the bottom portion of the cavity. However, the trend of the local Nusselt number at the left, right and top walls are similar to the case of $W=0.25$. It is interesting to see that the local Nusselt number at the top wall along the width of the porous medium decreases with an increase in the Rayleigh number. This is due to the formation of a separate fluid circulation zone at the bottom wall due to an increase in the Rayleigh number (as obvious from streamline and isotherms), that substantially increases the bottom wall heat transfer thus elevating the temperature of the fluid. The high temperature fluid flows towards the top wall where the heat transfer rate between the top wall and fluid gets retarded due to decreased temperature difference (because of increased fluid temperature). It is observed that the Nusselt number increases with increase in duct ratio.

Figure 4.2.7 illustrates the *Nu* for *W=0.75*, *Ra=100* and *Rd=0*. It is found that the *Nu* for left, right and bottom wall increases for $L \leq 0.3$ remains constant for $L \leq 0.75$ and thereafter decreases. There exist two maxima for the bottom wall *Nu*, near the left and right ends of the inner bottom wall. It is seen that the Nusselt number remains constant for all the walls at *0.3<L<0.75*.

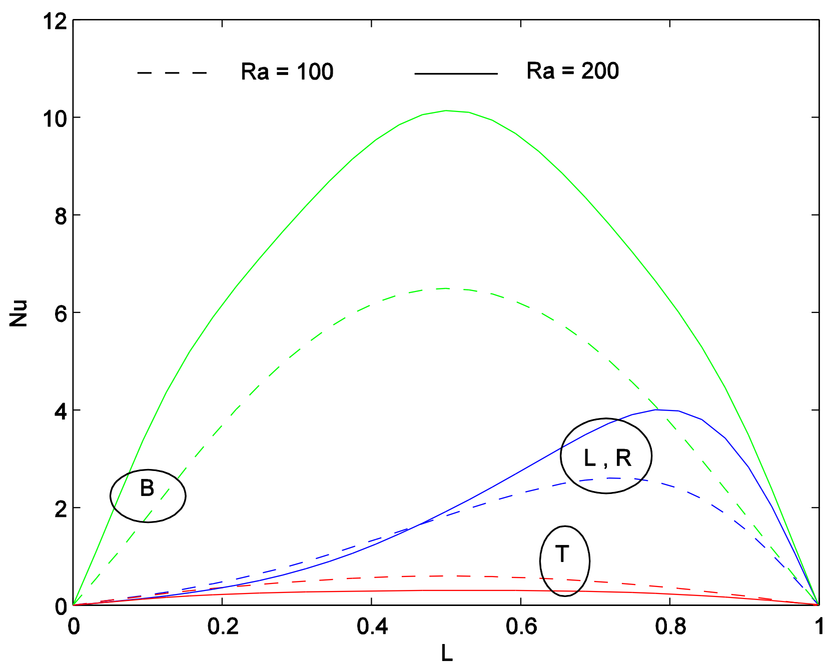

Figure 4.2.5: Local Nusselt number for $W=0.25$, $R_d=0$

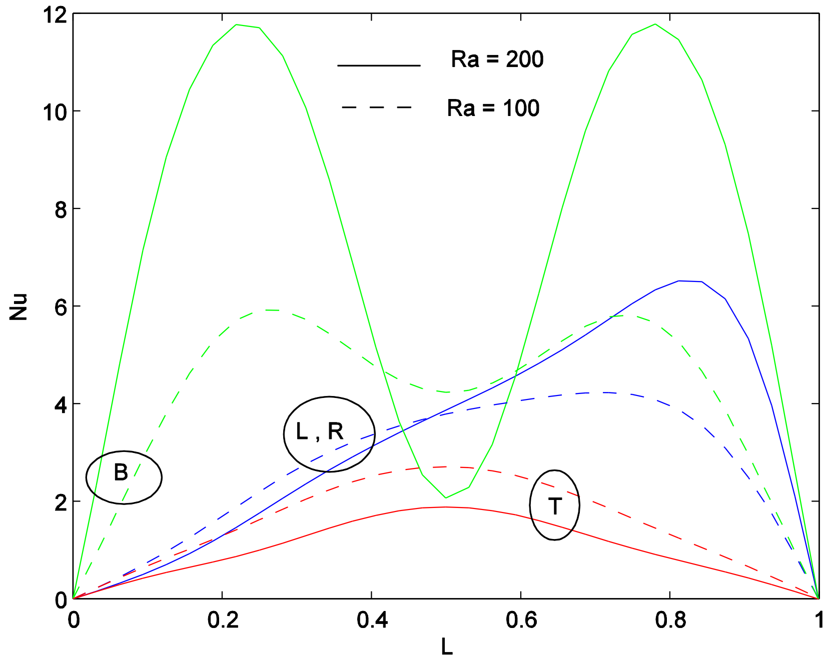

Figure 4.2.6: Local Nusselt number for *W=0.5*, $R_d=0$

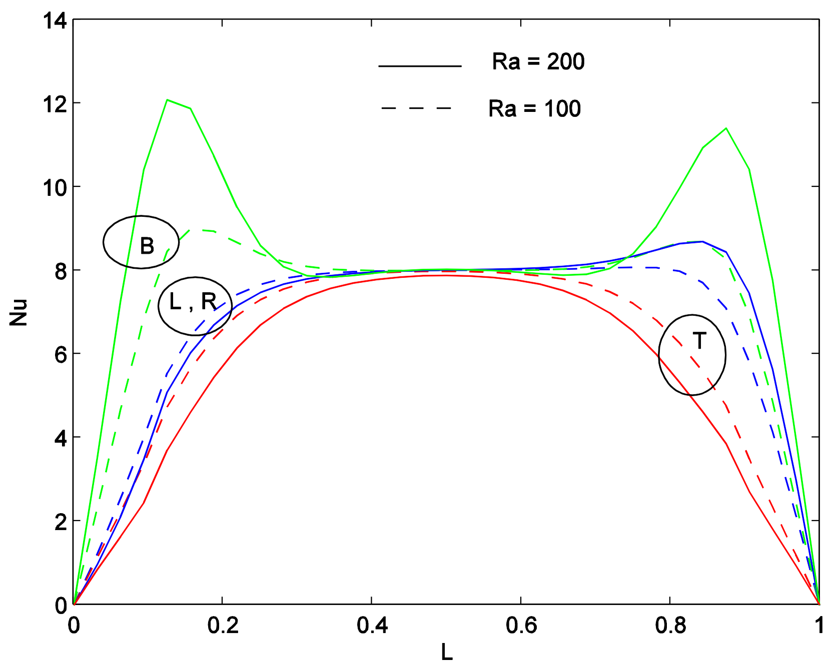

Figure 4.2.7: Local Nusselt number for *W=0.75*, $R_d=0$

Figure 4.2.8 demonstrates the average Nusselt number variation with respect to the width ratio of the duct for$Ra = 100, Rd = 0$. The average Nusselt number increases with increase in the duct width ratio. $\overline{Nu}$ for the bottom wall is higher than the other walls and

$\overline{Nu}$ for the vertical walls is greater than the bottom wall for all values of duct ratio. The total Nusselt number indicated by "Tot" in the Figure is almost equal to the average Nusselt number of vertical walls. It is found that the difference between $\overline{Nu}$ of different walls increases with decrease in duct ratio. Figure 4.2.9 shows the average Nusselt number variation for $Ra = 200, Rd = 0$. It is seen that the trend of average Nusselt number remains the same as that of Figure 4.2.8 but the magnitude of $\overline{Nu}$ increases with increment of Rayleigh number. The similar trend is observed in case of research carried out by (Moya et al., 1987; Baytas and Pop., 1999; Misirlioglu et al., 2005). It is inferred that the increase in Ra has profound effect on $\bar{N}u$. The increase in Rd increases $\overline{Nu}$ as shown in Figure 4.2.10 which belongs to $Ra = 200, Rd = 5$. At the bottom wall, $\overline{Nu}$ is slightly lesser than that of left/right walls at W>0.6. The $\overline{Nu}$ increased by 2.63 times at *W=0.125* when *Rd* is increased from 0 to 5.

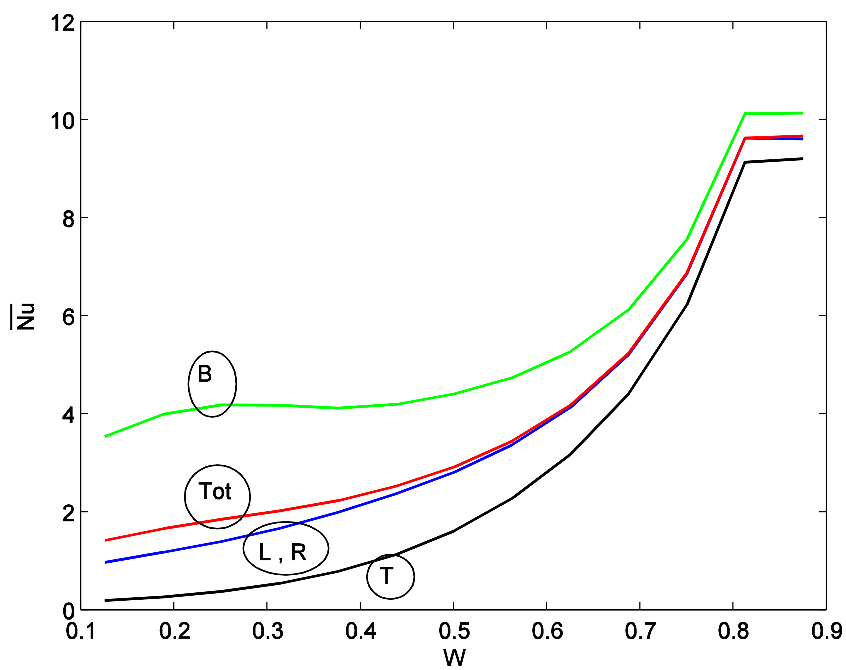

Figure 4.2.8: Average Nusselt number for $Ra=100$, $R_d=0$

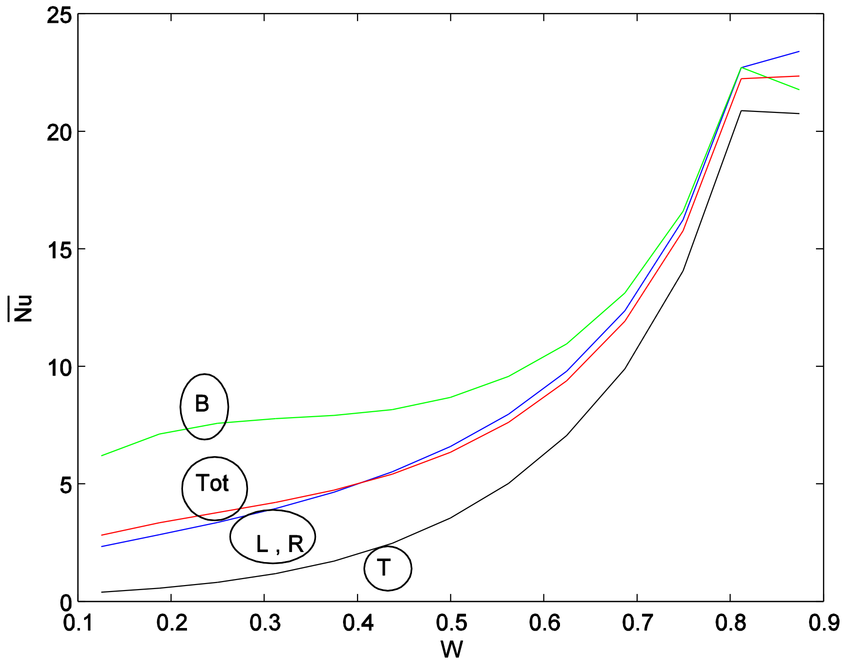

Figure 4.2.9: Average Nusselt number for *Ra=200*, R_d*=0*

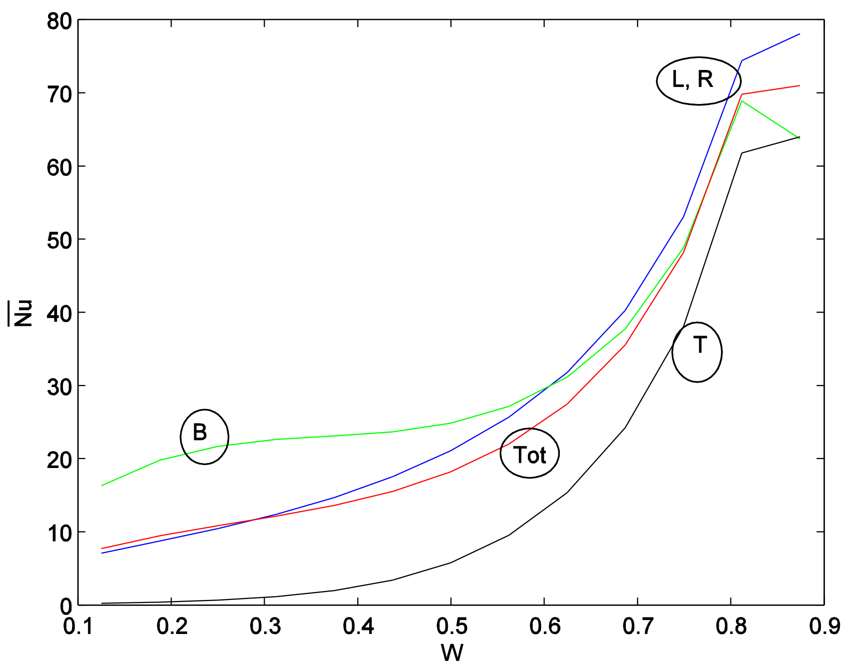

Figure 4.2.10: Average Nusselt number for *Ra=200*, R_d*=1*

4.3 Investigation of heat transfer in square porous-annulus subjected to inside wall heating

4.3.1 Introduction

The current section explains the heat transfer characteristics and fluid flow behaviour in a square porous annulus subjected to the outer boundaries of annulus being exposed to cooler isothermal temperature T_c whereas the inner walls are maintained isothermally at a hot temperature T_h. The thermal equilibrium and thermal non-equilibrium approach was adopted to determine the effects of various parameters on the heat transfer. The schematic representation of the geometry is shown in Figure 4.3.1 and the corresponding boundary conditions are given in Chapter 3 section 3.2.4.

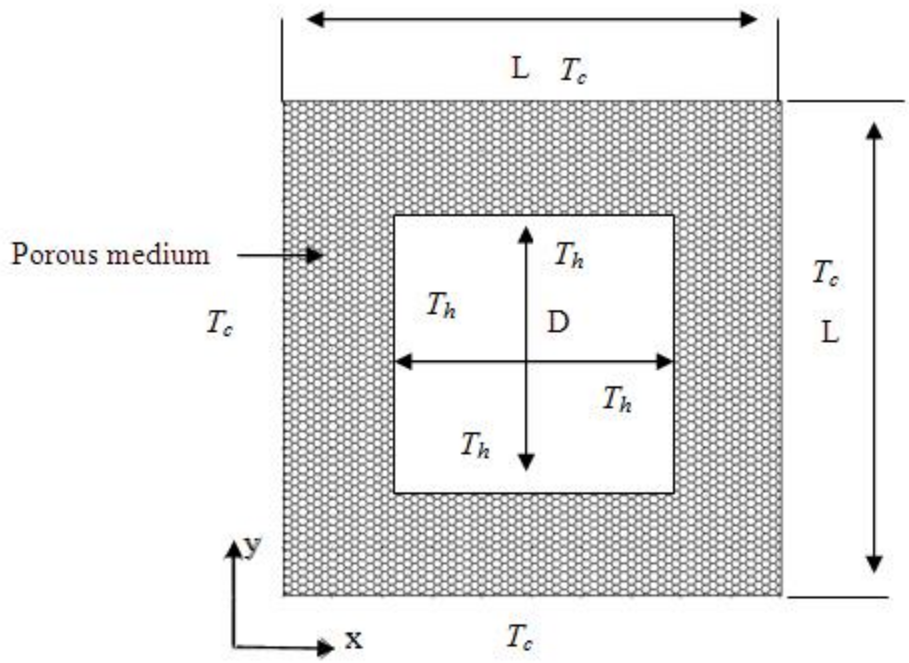

Figure 4.3.1: Schematic of square porous annulus heated at inner walls

4.3.2 Analysis

4.3.2a Thermal Equilibrium

Figure 4.3.2 depicts the streamlines and isothermal lines for width ratio of 0.125, 0.25, 0.375, 0.5 0.625 and 0.75. The width ratio represents the fraction of the hollow portion in the annulus. This figure is obtained for $Ra = 100, Rd = 0,\ \varepsilon = 0$. Since the hollow portion is located centrally, the fluid in the porous region flows in 2 distinct symmetric regimes. The fluid gets heated at the inner walls of the annulus by absorbing thermal energy and moves upwards due to density variation between hot and cold surfaces. The fluid penetrates much deeper into the upper section of porous medium due to a buoyant force created by the inner hot and upper cold walls of the annulus. On the contrary, the fluid does not have space for the vertical movement at the lower section of annulus which inhibits the vertical fluid movement in that section. The influence of the increased Rayleigh number is illustrated in Figure 4.3.3 which is obtained for $Ra = 200, Rd = 0,\ \varepsilon = 0$. The fluid velocity which depends on the stream function increases with increment in the Rayleigh number. The fluid has sufficient energy to sustain the circulation in a separate segment when the width ratio is increased beyond 0.25 until 0.625 which is illustrated by a smaller circulation cell at the upper section of the cavity. A close look at the isotherms of Figure 4.3.3 reveals that the heat transfer rate continuously varies along the top hot wall of the annulus at the lower width ratio, which is evident from the substantial distortion of isotherms. The isotherms are crowded near the bottom hot wall creating a higher thermal gradient. This shows that the convection heat transfer is dominated at the lower section of the annulus and conduction prevails at the top section of the annulus where the isotherms are spread out leading to reduced thermal gradient. Figure 4.3.4 shows the effect of viscous dissipation on the heat transfer rate in the porous region. It be noted that the value $\varepsilon = 0$

represents the case when viscous dissipation is absent. The viscous dissipation is a phenomenon that corresponds to a situation when fluid movement creates friction with solid matrix of the porous medium. This friction is dissipated in the form of heat. Thus it can be viewed as an internal heat generation phenomenon. It is seen that the effect of viscous dissipation does not significantly alter the streamlines and isotherms until $\varepsilon = 0.01$. The increase of ε beyond 0.01 has a distinct effect on the upper section of the annulus which is seen in the form of an additional fluid circulation region. The increased value of a viscous dissipation parameter suppresses the main fluid cell at the upper corner of the annulus, thus creating space for the secondary circulation cell which in turn displaces the isotherms much deeper into the porous medium, indicating increased convective heat transfer. It is seen that a significant portion of porous medium is occupied by isothermal lines having a value of 1 or more than one. This shows that the heat generated due to friction has overpowered the applied heat at the inner walls of the annulus which is an unrealistic situation from practical point of view. Thus it can be said that the limiting value of ε is 0.05, beyond which the situation becomes unrealistic for $Ra = 200$.

a)

b)

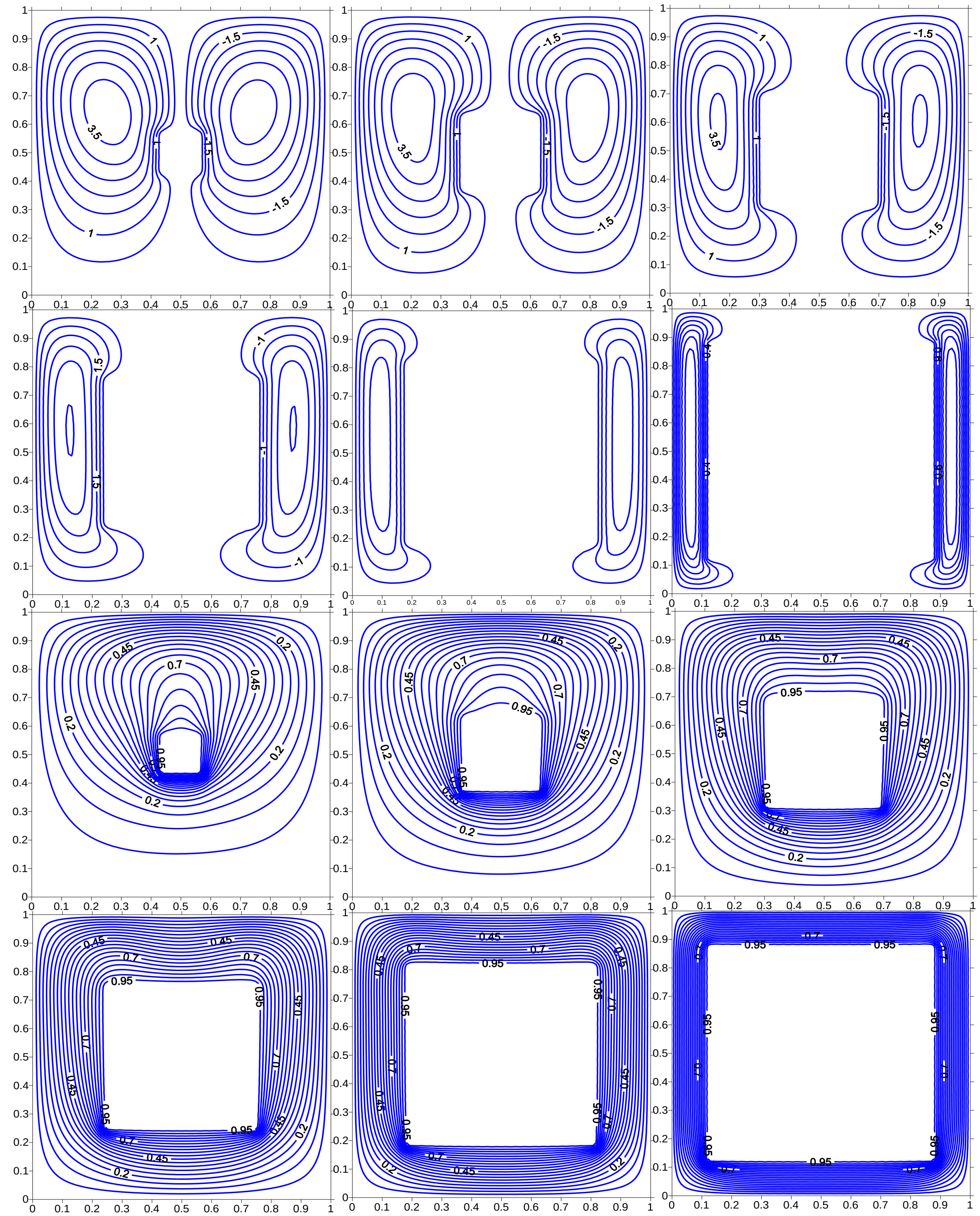

Figure 4.3.2: a) Streamlines b) Isotherms for *Ra=100*, R_d*=0*, $\varepsilon = 0$ *W=0.125, 0.25, 0.375* for rows I & III. *W=0. 5, 0.625, 0.75* for rows II & IV

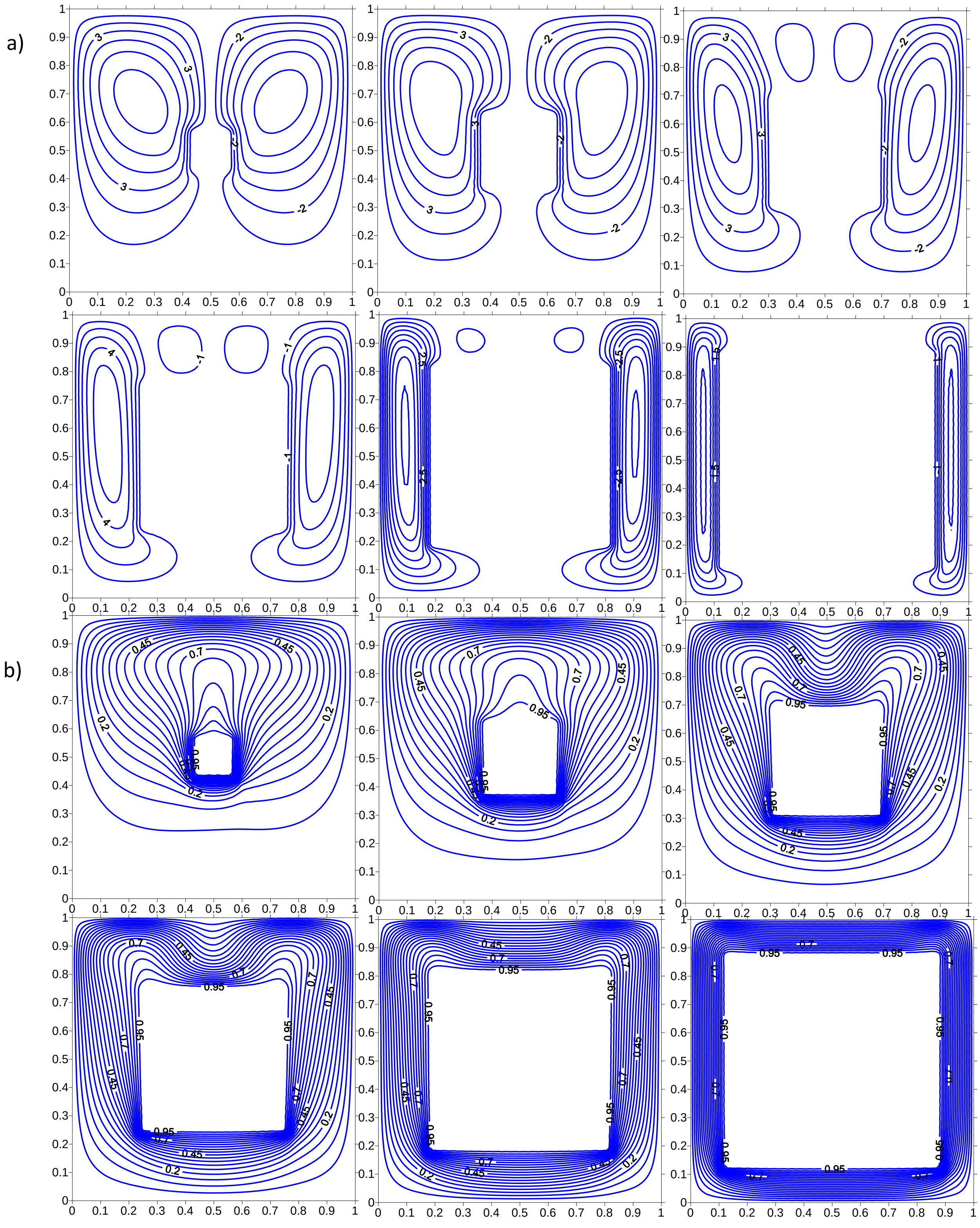

Figure 4.3.3: a) Streamlines b) Isotherms for Ra=200, R_d=0,$\varepsilon = 0$ W=0.125, 0.25, 0.375 for rows I & III. W=0. 5, 0.625, 0.75 for rows II & IV

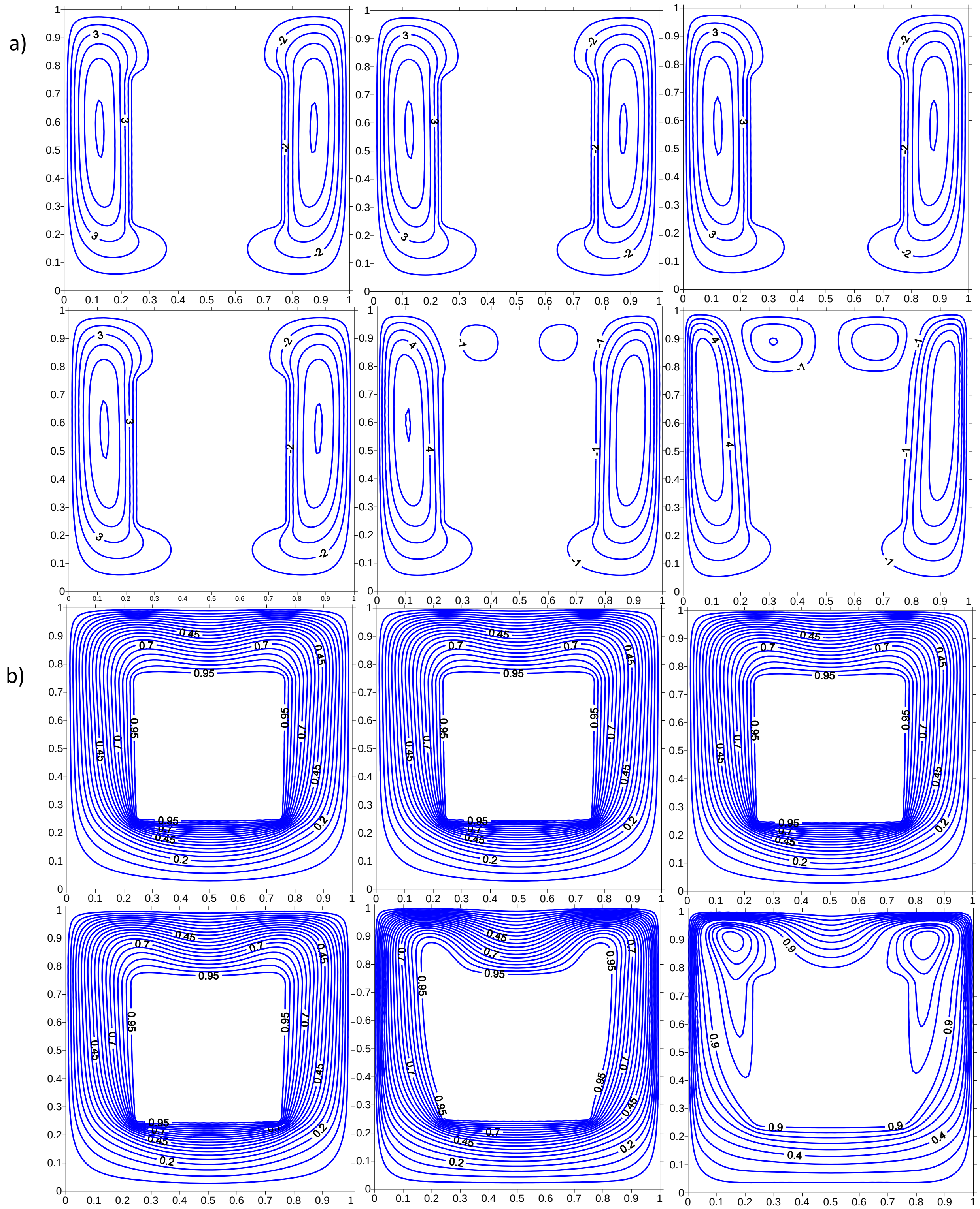

Figure 4.3.4: a) Streamlines b) Isotherms for $Ra=100$, $R_d=0$, $W = 0.5$

$\varepsilon = 0,\ 0.0001\ , 0.001\ , 0.01\ , 0.05\ , 0.1$ for rows I & III.

The local Nusselt number at left/right, bottom and top walls of annuls having applied boundary temperature of T_h varies differently as shown in figure 4.3.5. The letters L,R B & T represent the left, right, bottom and top walls of the annulus where T=T_h. This figure corresponds to $Ra = 100$, $Rd = 0, \varepsilon = 0$, It be noted that the local Nusselt number for the left and right hot walls is equal in magnitude, thus only one line is shown in the figure to represent the Nusselt number for both the vertical walls. The Nusselt number of the left/right walls decreases continuously with increase in the height of the wall. It is interesting to see that the Nusselt number for the left/right and bottom walls is equal for certain length and width of hot walls. However, the Nusselt numbers for left/right walls keep decreasing while that of bottom wall increases after certain width of the wall to form a symmetric pattern of variation. The Nusselt number at the top hot wall varies in different patterns according to the width ratio of the annulus. At *W=0.25*, the Nusselt number decreases with increment in the width and then starts increasing from the mid portion until end of the annulus-width. It varies in a parabolic shape along the width of the annulus. The increase in the width ratio changes the pattern of *Nu* variation along the width of the annulus. At W=0.375, *Nu* decreases and then remains almost constant for major portion of the width before increasing at the other end of the wall. For *W=0.5* and *0.625,* the *Nu* varies in a wave of small amplitude. It is interesting to note that the Nusselt number for all the four hot walls is equal for the major part of the wall height/width when *W=0.75*. Figure 4.3.6 shows the Nu variation due to increased Rayleigh number (*Ra=200*) keeping all other parameters the same as that of Figure 4.3.5. The heat transfer rate increases with respect to increased Rayleigh number as expected. The variation at the bottom and top hot walls are higher when the Rayleigh number is increased in comparison to that of Figure 4.3.5. The amplitude of *Nu* at the top wall increased due to increased fluid velocity. As seen in figure 4.3.5, the *Nu* of all the walls for the major part of hot surface is equal at *W=0.75,* even for the higher Rayleigh number. The effect of viscous dissipation is reflected in figure 4.3.7 which shows the variation of Nusselt number at $Ra = 200$, $Rd = 0, \varepsilon = 0.01$. It is seen that the heat transfer rate at the bottom hot wall for *W=0.25* is almost zero when viscous dissipation parameter is increased to 0.01. This indicates that the temperature close to the bottom wall is very much similar to that of bottom wall temperature. The combined effect of radiation parameter and viscous dissipation is illustrated in fig 4.3.8- 4.3.10. The figures are plotted for width ratio of 0.25 and 0.5. It is seen that the Nusselt number increases substantially with increase in radiation parameter. The Nusselt number at the left/right wall shows the increment by almost 64% when R_d is varied from 0.1 to 1.

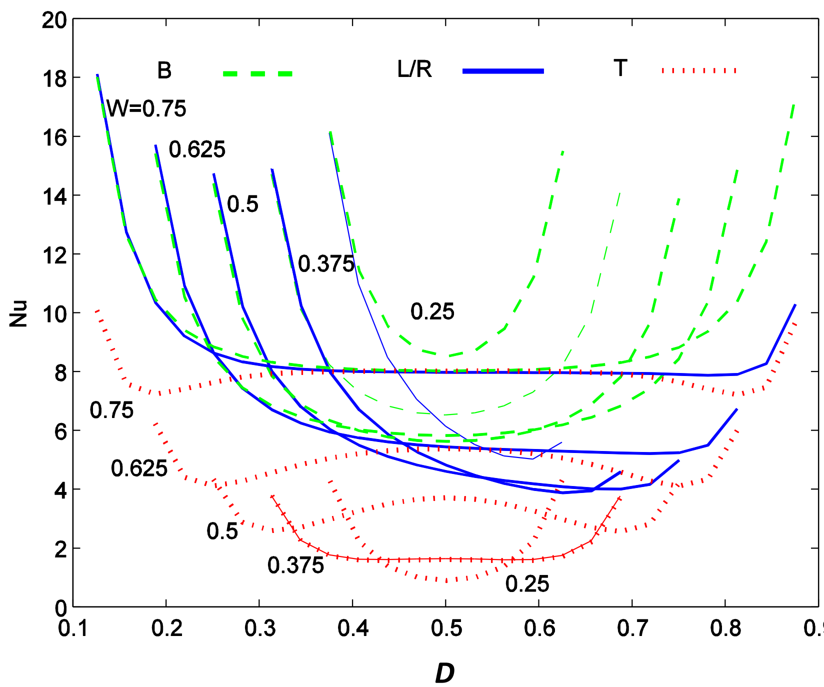

Figure 4.3.5: Local Nusselt number for $Ra=100$, $R_d=0$, $\varepsilon = 0$

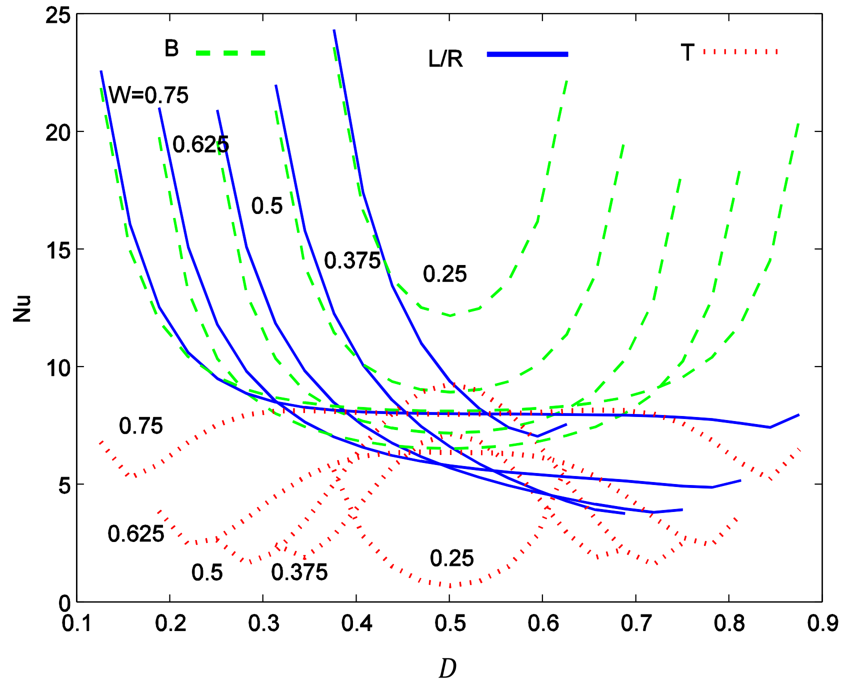

Figure 4.3.6: Local Nusselt number for *Ra*=200, R_d=0, ε=0

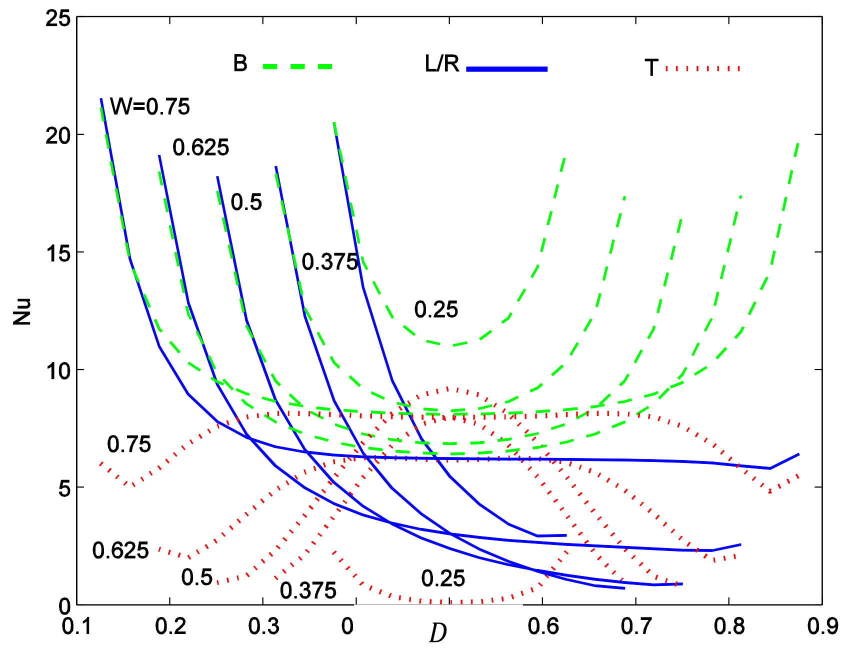

Figure 4.3.7: Local Nusselt number for *Ra=200*, R_d*=0*, $\varepsilon = 0.001$

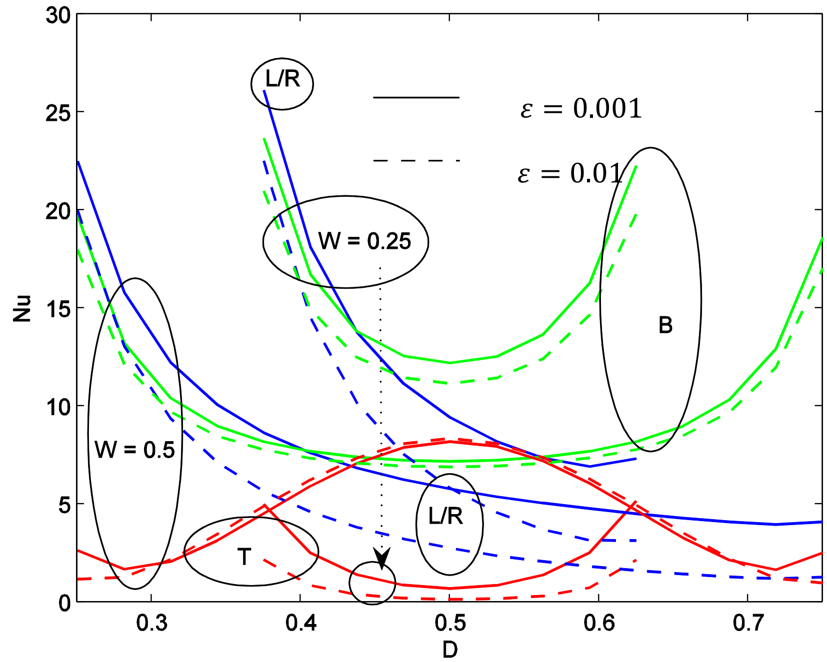

Figure 4.3.8: Local Nusselt number for *Ra=200*, R_d*=0.1*

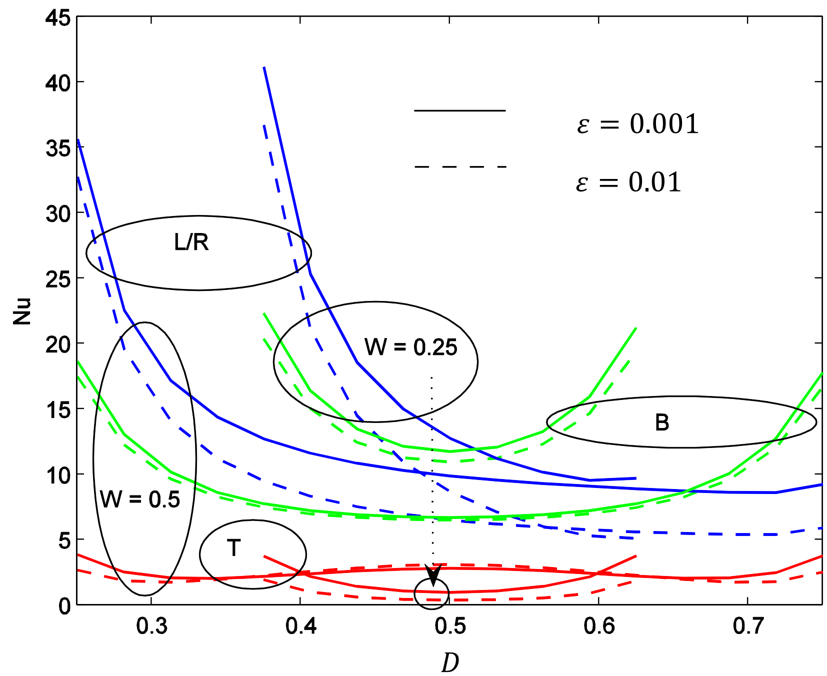

Figure 4.3.9: Local Nusselt number for *Ra=200*, R_d*=1*

The average Nusselt number at all the walls and total average Nusselt number is shown in Figure 4.3.11 for *Ra=100*, $R_d = 0$. The average Nusselt number decreases initially with increase in the width ratio and then increases due to further increase in the width ratio. It is noticed that $\overline{Nu}$ at vertical walls is almost equal to that of total average Nusselt number of the annulus. Thus it can be said that $\overline{Nu}$ at any point on vertical wall is the value of overall Nusselt number of the annulus. Nusselt number $\overline{Nu}$ at top wall is the least and that of bottom wall is highest among all the 4 walls of annulus. The effect of increased viscous dissipation is to reduce the Nusselt number at hot surface. This can be explained in way that the viscous dissipation leads to fluid friction which generates heat in the porous medium thus reducing the temperature gradient near the walls, which in turn reduces the Nusselt number. Figure 4.3.12 shows the variation of average Nusselt number along the width ratio for two values of the radiation parameter at Ra=100,$\varepsilon = 0$. As expected the Nusselt number increases with increase in radiation parameter. The difference between the Nusselt number of various walls is highest at $W=0.125$ for $R_d=0$, and this difference goes on decreasing with increase in the width ratio of the annulus. This is because of the reason that the increased width ratio brings in uniformity of temperature distribution in the porous medium as seen from isothermal lines of Figure 4.3.2. However, the difference of average Nusselt number is found to be highest at $W=0.825$ when $R_d=1$. It is found that the average Nusselt number remains constant for $W>0.825$.

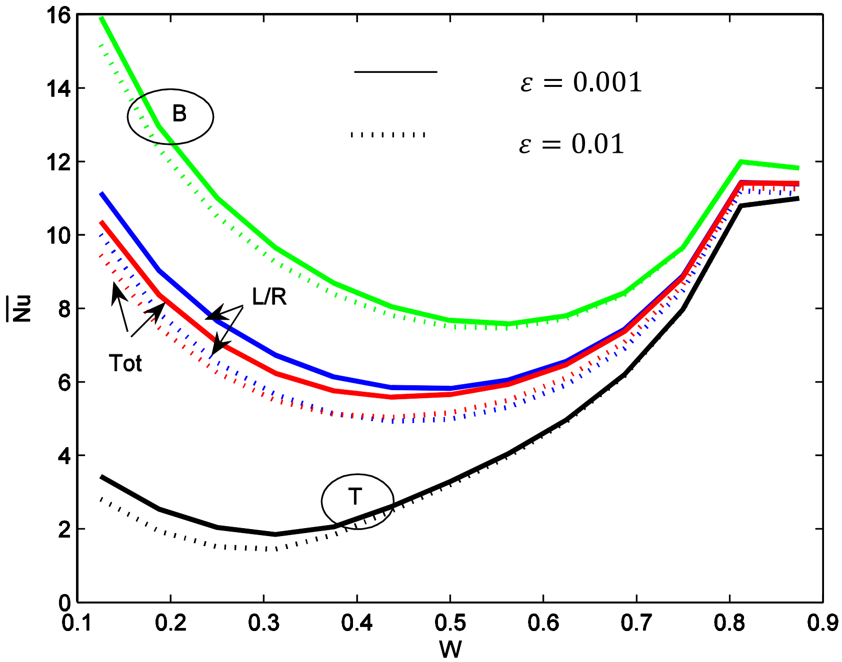

Figure 4.3.10: Average Nusselt number Vs. W for $Ra=100, R_d=0$

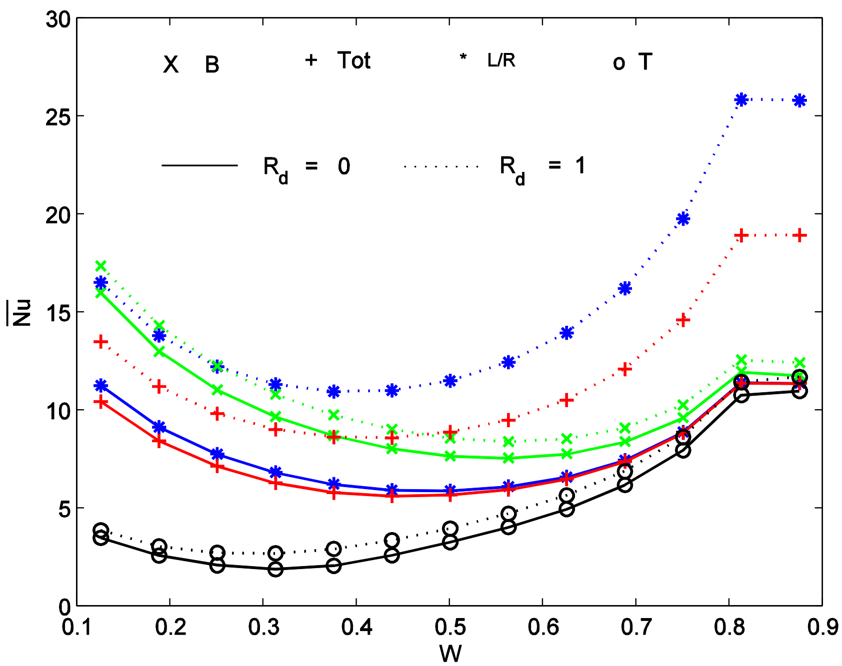

Figure 4.3.11: Average Nusselt number Vs. W for $Ra=100$, $\varepsilon = 0$

4.3.2b Thermal Non-equilibrium

The following section describes the heat transfer characteristics when two equation energy model is utilized. Figure 4.3.12 shows the streamlines and isotherms for fluid and solid phase of porous medium for $Ra = 100$, R_d= $0, \varepsilon = 0, H = 5$ & $Kr = 2$. The first, second and third column of Figures 4.3.13 & 4.3.14 represent the streamlines, fluid isotherms and solid isotherms respectively. It is obvious from Figure 4.3.13 that the thermal non equilibrium effects are much stronger for the case when width ratio is smaller as compared to that of higher width ratio. The fluid isotherms are distorted at upper section of the domain which indicates that the convection current is higher in that region. It is seen that the isotherms of fluid and solid are similar to each other for W>0.5, indicating that thermal equilibrium approaches when width ratio is increased. The increase in width ratio decreases the porous medium thickness which in turn reduces the thermal resistance allowing the fluid and solid to attain similar temperature. Figure 4.3.14 shows the effect of radiation and viscous dissipation on streamline and isotherms. This figure corresponds to $Ra = 100$, R_d= $1, \varepsilon = 0.005, H = 5$ & $Kr = 2$. The maximum value of stream function has increased due to combined effect of increase in viscous dissipation and radiation parameter. It is also observed that the temperature level in the porous domain increased due to increased viscous dissipation and radiation. This can be attributed to the fact that the increase in viscous dissipation acts as heat generation agent which increases the temperature of porous domain.

Figures 4.3.14- 4.3.16 show the local Nusselt number variation along the hot surface for *W=0.25, 0.5 and 0.75* respectively at $Ra = 200$, R_d= $1, \varepsilon = 0.001, H = 5$ & $Kr = 2$. It is seen from Figure 4.3.14 that the Nusselt number for solid phase is higher than that of fluid phase at top surface. This indicates that there is discrepancy in the temperature of solid and fluid near top surface. It also shows that the temperature gradient of solid phase is higher than that of fluid phase. It may be noted that the higher value of Nusselt number represents lower temperature in the vicinity of hot surface. This reflects that in case of lower fluid Nusselt number the heat is being transferred from fluid to solid in the vicinity of hot surface. However the Nusselt number for fluid phase is higher than solid Nusselt number at left/right and bottom surface. It is noted that the difference between fluid and solid Nusselt number decreases continuously along the height of hot surface. This may be attributed to fact that the fluid temperature increases as it moves upward by absorbing more thermal energy from the hot surface which in turn reduces the temperature difference between hot surface and fluid. This decreased temperature difference reduces the fluid Nusselt number. It is further observed that the solid Nusselt number at bottom surface is slightly higher than that of left/right and bottom surface. The increase in width ratio from 0.25 to 0.50 leads fluid Nusselt number to vary in a small wavy form at top surface as shown in figure 4.3.15. It is also observed that the solid number is equal at all hot surfaces when width ratio is increased, as indicated by single dotted line in Figure 4.3.16.

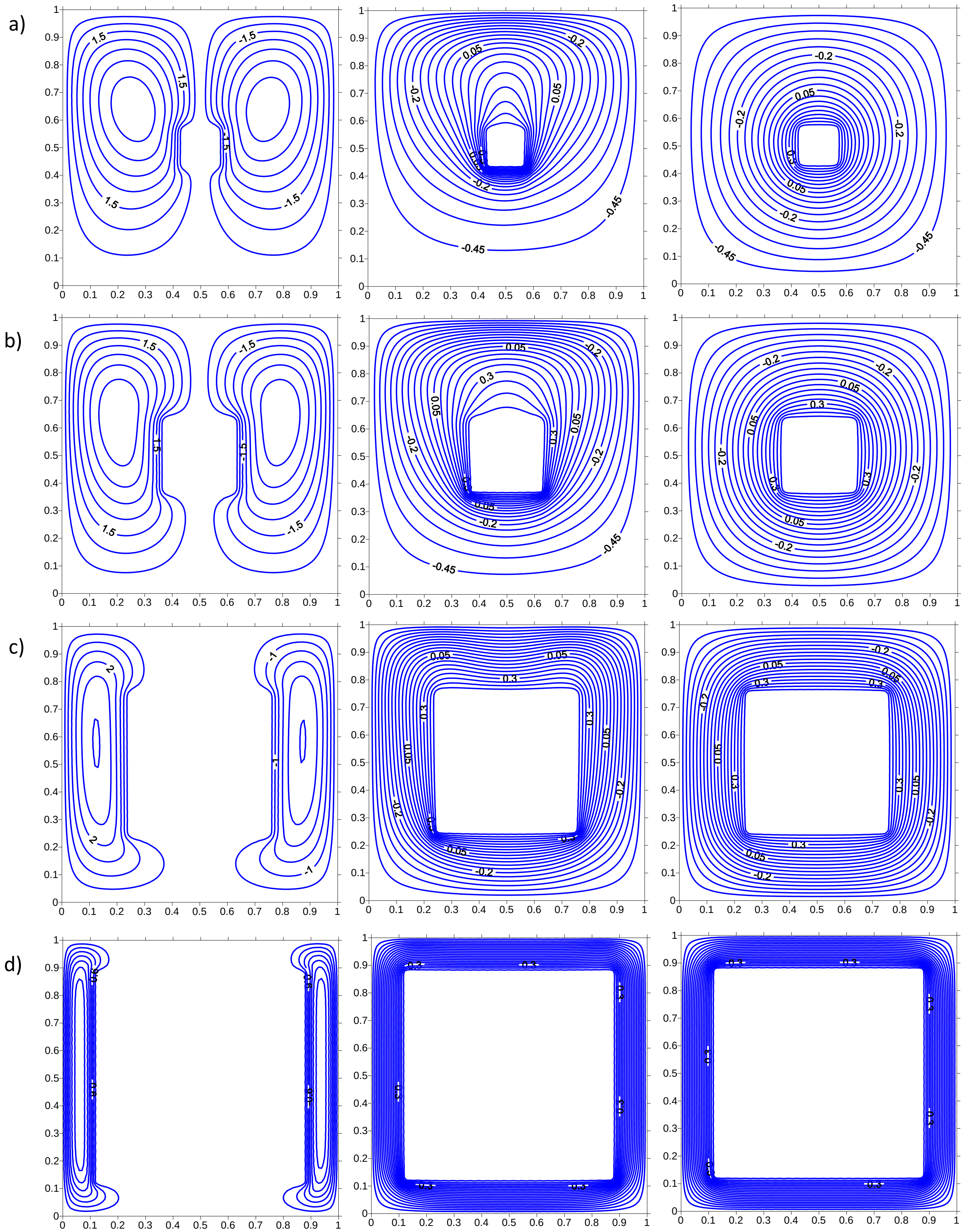

Figure 4.3.12: Streamlines (left) Fluid Isotherms (center) Solid Isotherms (right) for $Ra=100$, $R_d=0$, $H=5$, $Kr=2$, $\varepsilon = 0$, $W = 0.125, 25, 50$ & 75

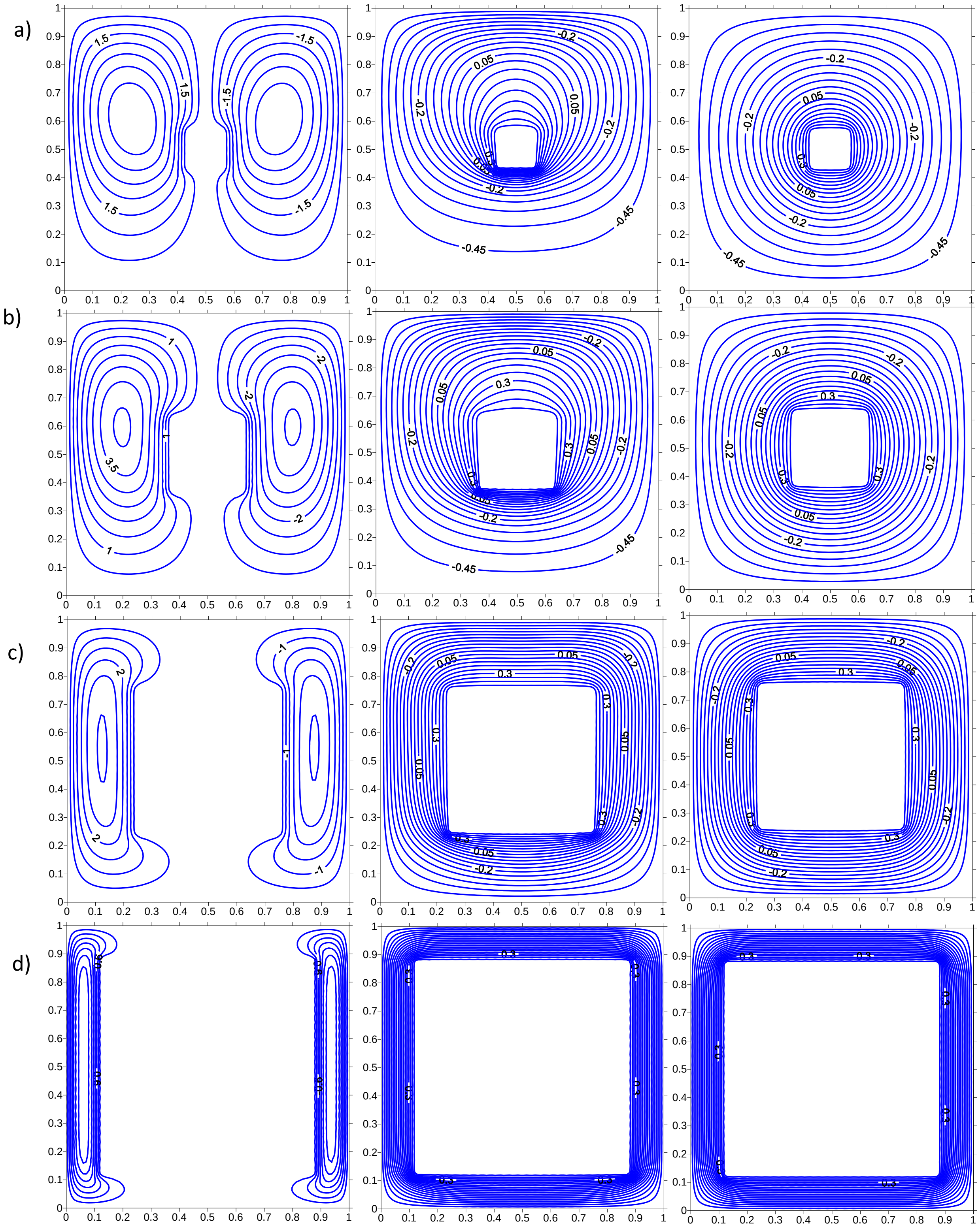

Figure 4.3.13: Streamlines (left) Fluid Isotherms (center) Solid Isotherms (right) for Ra=100, R_d=1,H=5,Kr=2, $\varepsilon = 0.005$, $W = 0.125, 25, 50$ & 75 .

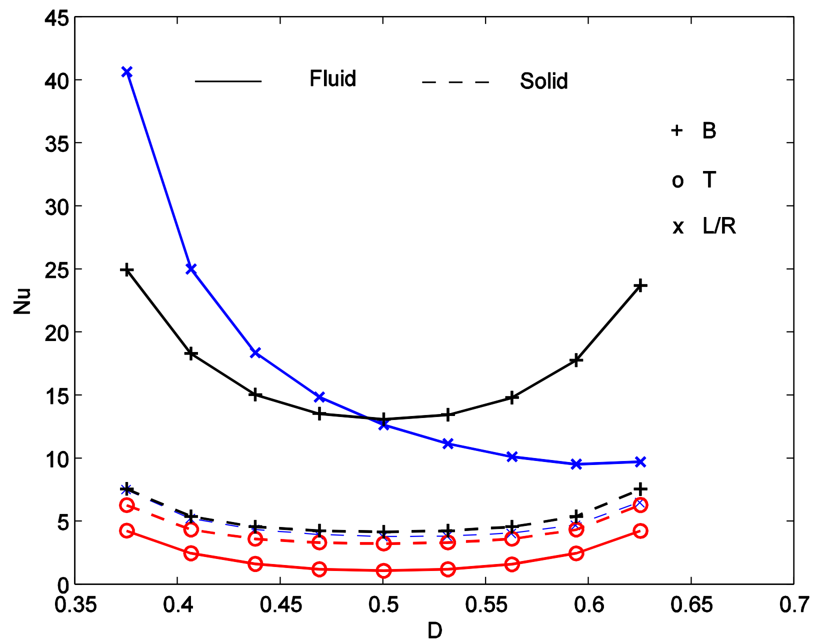

Figure 4.3.14: *Nu* for fluid and solid at *W=0.25*, $Ra = 200$, $Rd = 0, \varepsilon = 0, H = 5$ & $Kr = 2$

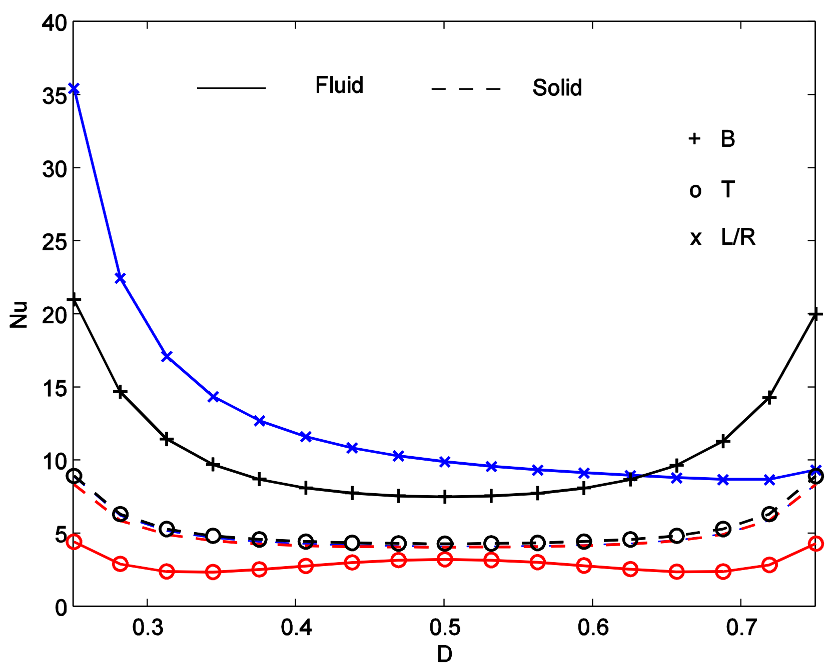

Figure 4.3.15: *Nu* for fluid and solid at *W=0.50*, $Ra = 200$, $Rd = 0, \varepsilon = 0, H = 5$ & $Kr = 2$

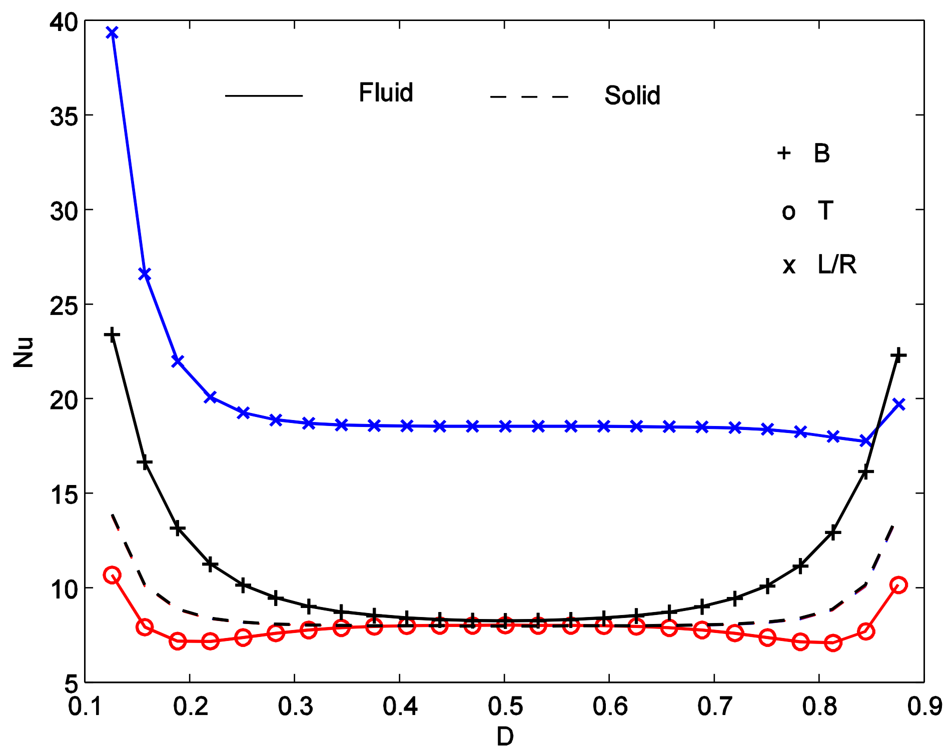

Figure 4.3.16: *Nu* for fluid and solid at *W=0.75*, $Ra = 200$, $Rd = 0, \varepsilon = 0,$

$H = 5$ & $Kr = 2$

4.3.2c Comparison of the results

Table 4.3.2c: Comparison the of outside and inside wall heating

Parameters	Outside heating	Inside heating
Nusselt number	There is substantial difference in *Nu* of bottom wall and left/right wall	*Nu* is almost equal for half of width for bottom wall and left/right wall
Width ratio W, Rayleigh Number Ra,	Nusselt number oscillates for bottom wall when W= 0.5 &oscillation increases with increase in the Rayleigh number.	*Nu* for major part of the hot wall is same at W=0.75. Fluid velocity increased with increase in Rayleigh number Ra.
streamlines	Increased fluid movement at bottom surface of annulus	Increased fluid movement at upper section
Isotherms	More distorted at top surface of annulus	More distorted at bottom section

4.3.2d Validation of the Results

The present research work has been validated to the previously published research work by eminent researchers and it is found to be in good agreement with those results. Table 4.3.2 shows the comparison and validation of the present result with the open literature.

Table 4.3.2d: Validation of results with the open literature

Author	$Ra = 10$	$Ra = 100$
(Walker and Homsy.,1978)		3.097
(Bejan., 1979)		4.2
(Beckermann et al., 1986)		3.113
(Moya et al., 1987)	1.065	2.801
(Baytas and Pop., 1999)	1.079	3.16
(Misirlioglu et al., 2005)	1.119	3.05
(Gross et al.,1986)		3.141
(Manole and Lage., 1992)		3.118
Present	1.0798	3.2005

4.4 Investigation of conjugate heat transfer in porous annular cylinder

4.4.1 Introduction

The conjugate heat transfer applications are chiefly found in the electronic cooling, where it is employed to regulate the undesired higher temperature to increase the efficiency of the electronic devices. Thus the present section deals with the detailed study pertaining to the heat transfer and fluid flow analysis in vertical annulus. The physical model of conjugate heat transfer in an annular porous cylinder along with the boundary conditions is shown in Figure 4.4.1 as discussed in chapter 3 section 3.3

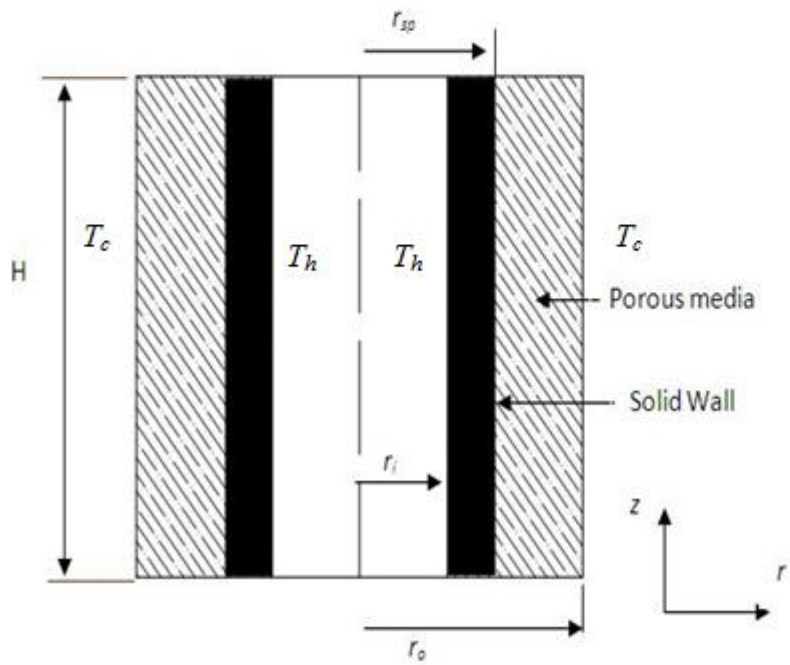

Figure 4.4.1: Schematic of porous annulus with solid wall

4.4.2 Analysis

The results are presented in terms of Nusselt number at the solid-porous interface which is a measure of heat transfer from the solid wall to porous medium. Apart from Nusselt number, the temperature distribution at the solid-porous interface and the streamlines along with isothermal lines are presented for various physical and geometric parameters with emphases on solid wall thickness and the conductivity ratio. Figure 4.4.2 illustrates the effect of the solid wall thickness on the temperature distribution at the solid porous interface for $Ra = 200, Rr = 1, Ar = 5$. At low value of Kr, the temperature along the interface is almost constant when the wall thickness is higher in comparison to the porous thickness. The temperature along the interface layer increases with decrease in the solid wall thickness. This happens because of decease in the thermal resistance in the wall with decease in the wall thickness. It is also observed that the temperature variation from bottom to top of the porous solid interface increases with increase in the wall thickness when *Kr=0.1*. However the temperature along the interface layer is almost constant for higher wall thickness when conductivity ratio is increased from 0.1 to 10.

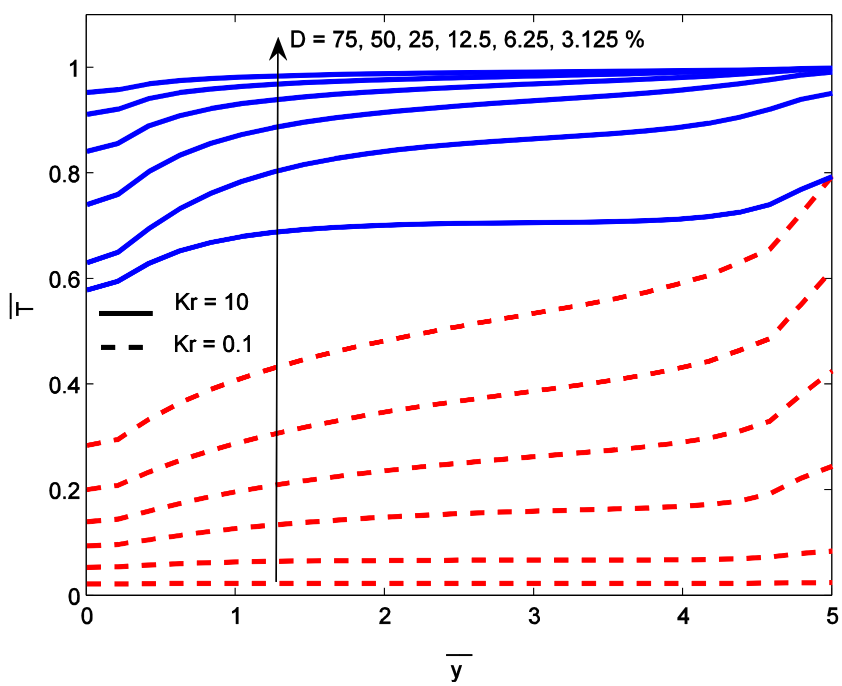

Figure 4.4.2: Effect of wall thickness on interface temperature

Figure 4.4.3 illustrates the temperature along the solid-porous interface for different values of conductivity ratio at $Ra = 200, Rr = 1, Ar = 10$. The temperature along the solid porous interface is relatively constant for very low and high values of conductivity ratio. The increase in the conductivity ratio leads to increase in the temperature in the solid-porous interface. It may be noted that the higher values of *Kr* indicates better thermal conductivity in the solid wall as compared to that of porous region. The increased conductivity ratio is associated with increase in the thermal conductivity of solid wall which in turn reduces the thermal resistance in the wall, leading to decrease in the temperature difference between the hot wall and solid-porous interface. Since temperature of hot wall is maintained constant, the increase in Kr leads to increase in the interface temperature.

Figure 4.4.4 illustrates the temperature variation at just beneath the top wall of cylinder along radial direction. This figure corresponds to $Ra = 200, Rr = 1, Ar = 5$. As expected the temperature along the solid wall decreases linearly and then temperature profiles become non-linear as it enters into porous region of the cylinder. The temperature gradient at hot surface i.e. $\bar{r} = r_i$ decreases with increase in the solid wall thickness as well as increase in conductivity ratio.

Figure 4.4.5 shows the temperature variation along the radial direction at center of the cylinder for $Ra = 200, Rr = 1, Ar = 5$. It is seen that the temperature gradient is lesser at the mid of the cylinder as compared to that of the top portion of the cylinder. This indicates that the heat transfer rate increases along the height of the cylinder from bottom until top. It is interesting to note that the temperature variation along the porous region is almost linear for *Kr =10 and D=0.75,* suggesting that the conduction mode of heat transfer is dominant at these values of conductivity ratio and the thickness ratio. Figure 4.4.6 depicts the temperature along the radial direction for various values of conductivity ratio at $Ra = 200, Rr = 1, Ar = 10$. It is obvious from Figure 4.4.6 that the temperature gradient increases with the increase in the conductivity ratio and the height of the cylinder as explained previously.

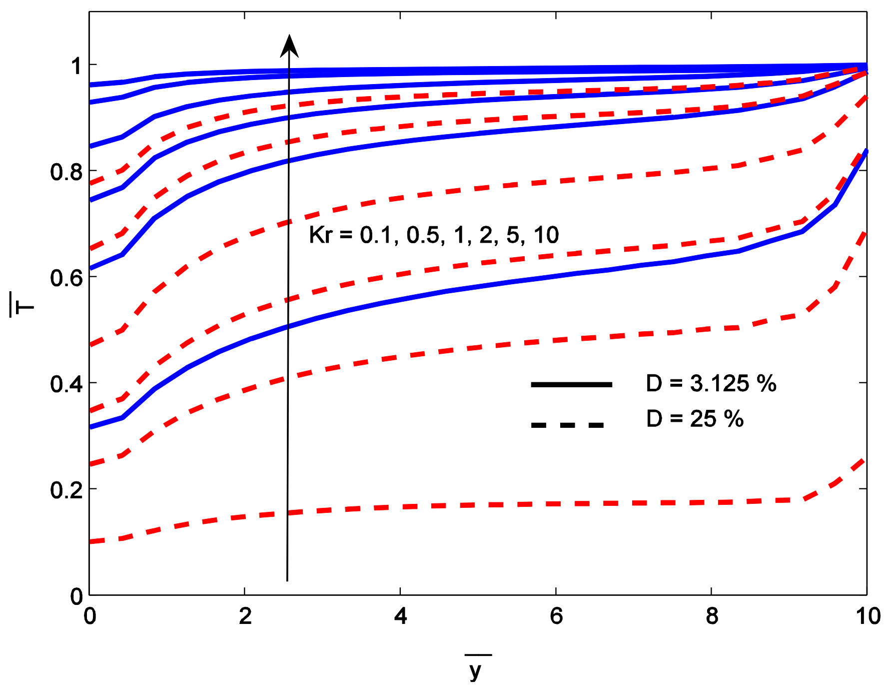

Figure 4.4.3: Temperature variation along the solid-porous interface when conductivity ratio

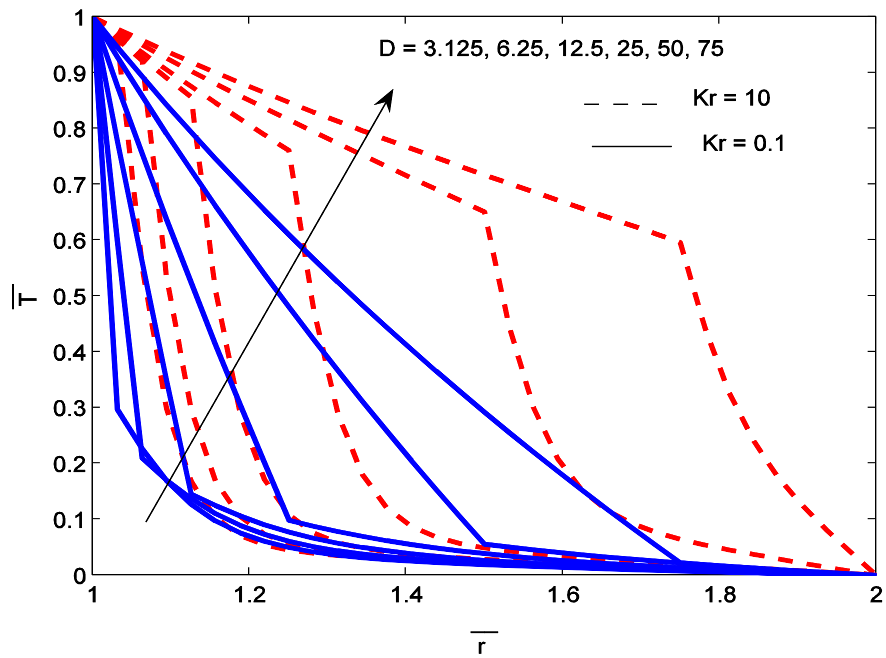

Figure 4.4.4: Temperature along the radial direction beneath the top surface of the cylinder

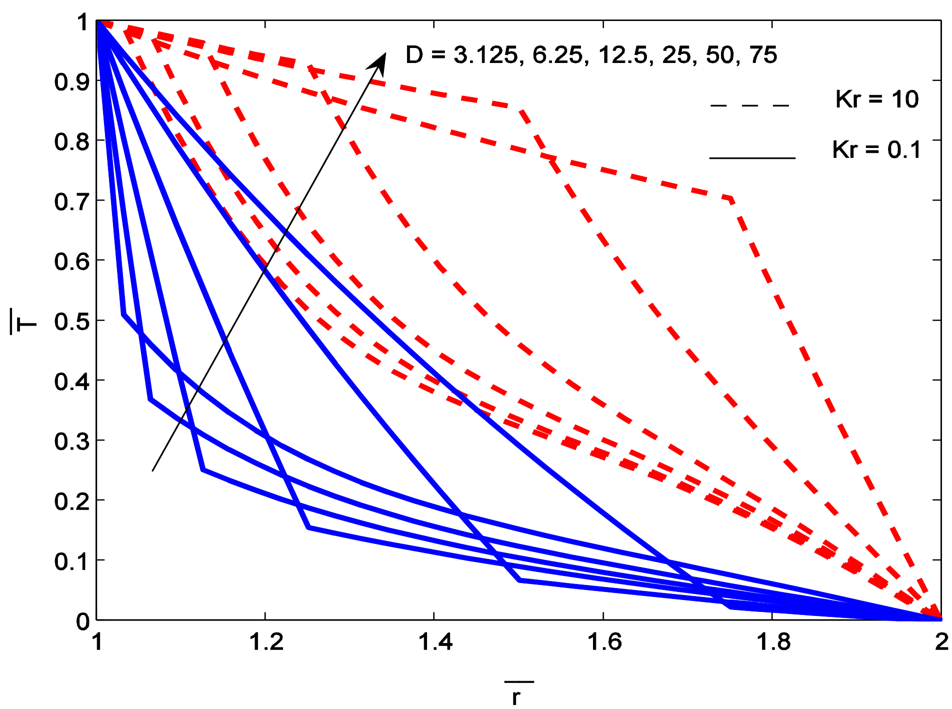

Figure 4.4.5: Temperature along the radial direction at mid of the cylinder

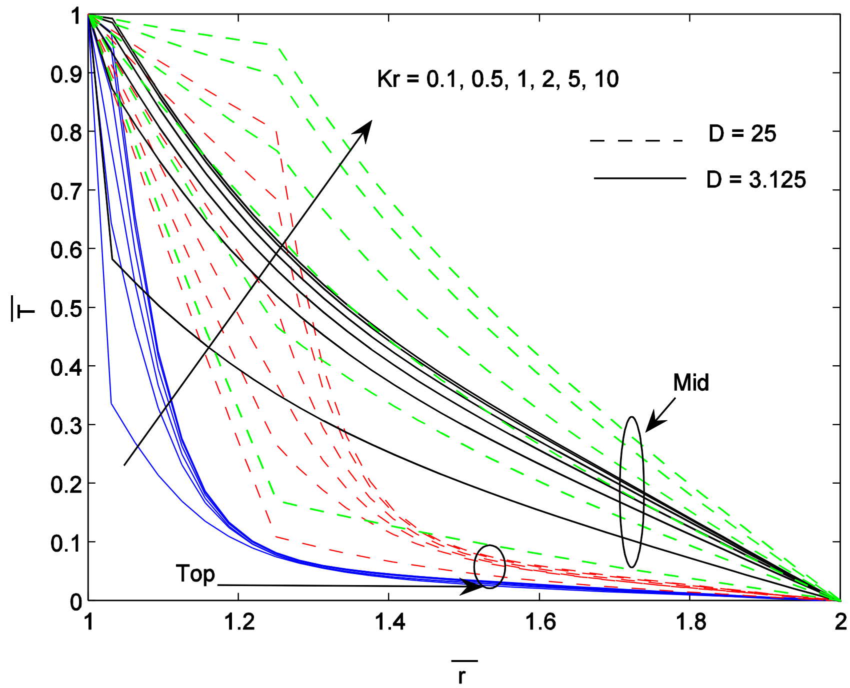

Figure 4.4.6: Temperature along the radial direction at top and mid of the cylinder

Figure 4.4.7 shows the isothermal and streamlines for D = 3,125, 12.5 and 50% which indicates that the wall thickness is 1/32, 1/8 and ½ times the total thickness of the annulus. The figure is obtained at $Ra = 100, Rr = 1, Ar = 1, Kr = 0.5$. It is clear from streamlines that the maximum value of the stream function reduces with increase in the wall thickness and the fluid flow becomes weaker; the flow cell changes the shape from being near circular to oval shape when solid wall thickness is increased. The isothermal lines straighten with increase in the wall thickness which indicates that there is increase in the conduction mode of heat transfer due to increase in the solid wall thickness. This can be related to the fact that the fluid velocity decreases with increase in the wall thickness as highlighted by streamlines thus reducing the energy transportation by fluid convection which makes the conduction to dominate. Figure 4.4.8 illustrates the streamlines and isothermal lines for $Ra = 100, Rr = 1, Ar = 1, Kr = 5$. The increase in the conductivity ratio leads to increase in the value of maximum stream function which increases the fluid velocity thus the convective heat transfer in the porous region of the cylinder.

Figure 4.4.9 demonstrates the heat and fluid flow behaviour in terms of isotherms and streamlines for *Kr=0.1,1 and 10.* The figure is obtained for $Ra = 100, Rr = 1, Ar = 1, D = 25\%$. It be noted that the value *Kr = 1* indicates that the thermal conductivity of solid and the porous region are equal. As shown in figure, the increase in conductivity ratio increases the magnitude of stream function. At *Kr = 0.1,* the fluid flows in a smooth pattern from left to right surface in a near circular shape cell. However the increase in conductivity ratio makes the fluid to move from lower left region to upper right surface of the cylinder in an oval shaped cell. The isotherms indicate that the thermal gradient varies along the height of the cylinder thus varying the local heat transfer rate.

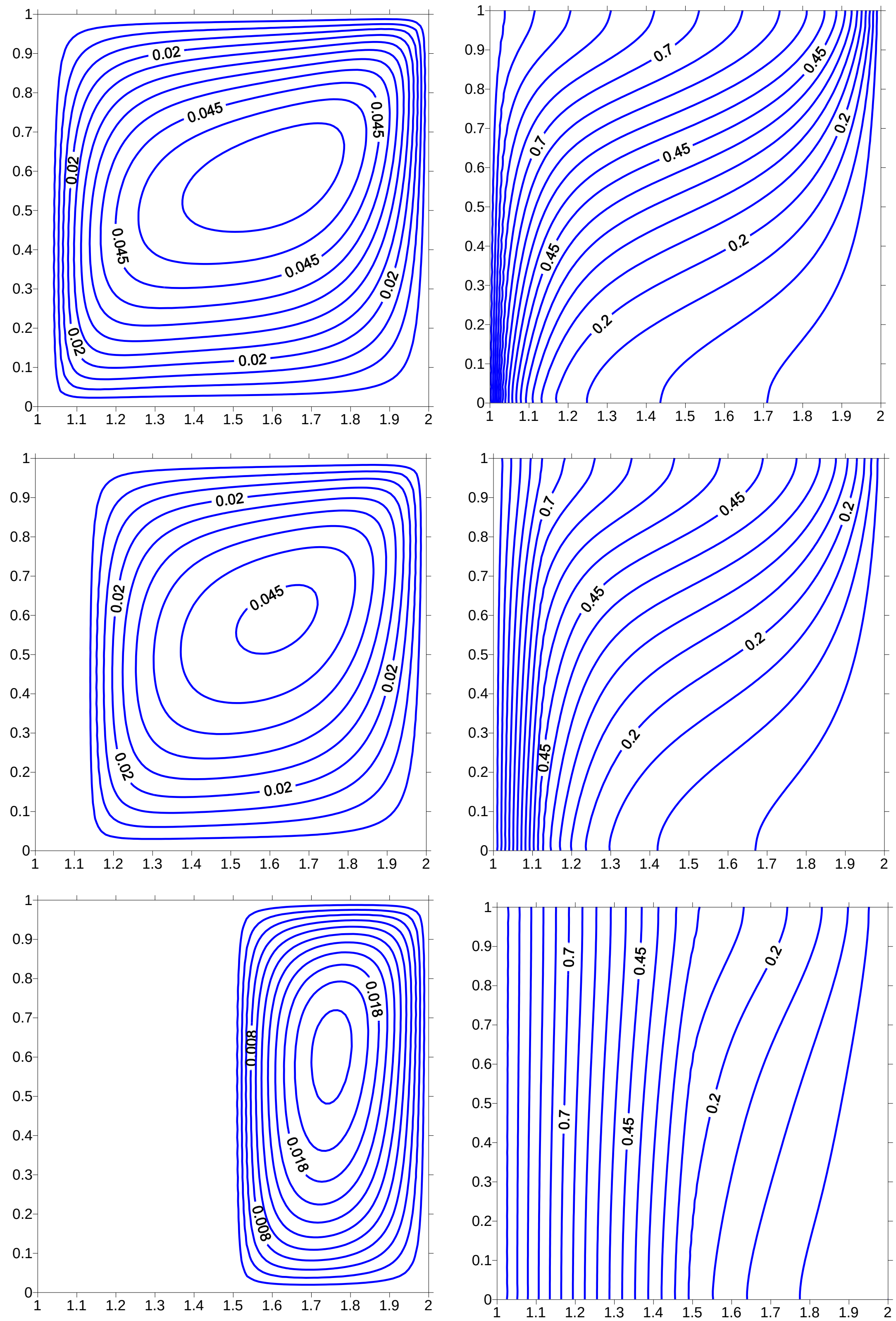

Figure 4.4.7: Stream lines (left) and isotherms (right) for *D* = 3.125, 12.5 50% , *Kr* =0.5

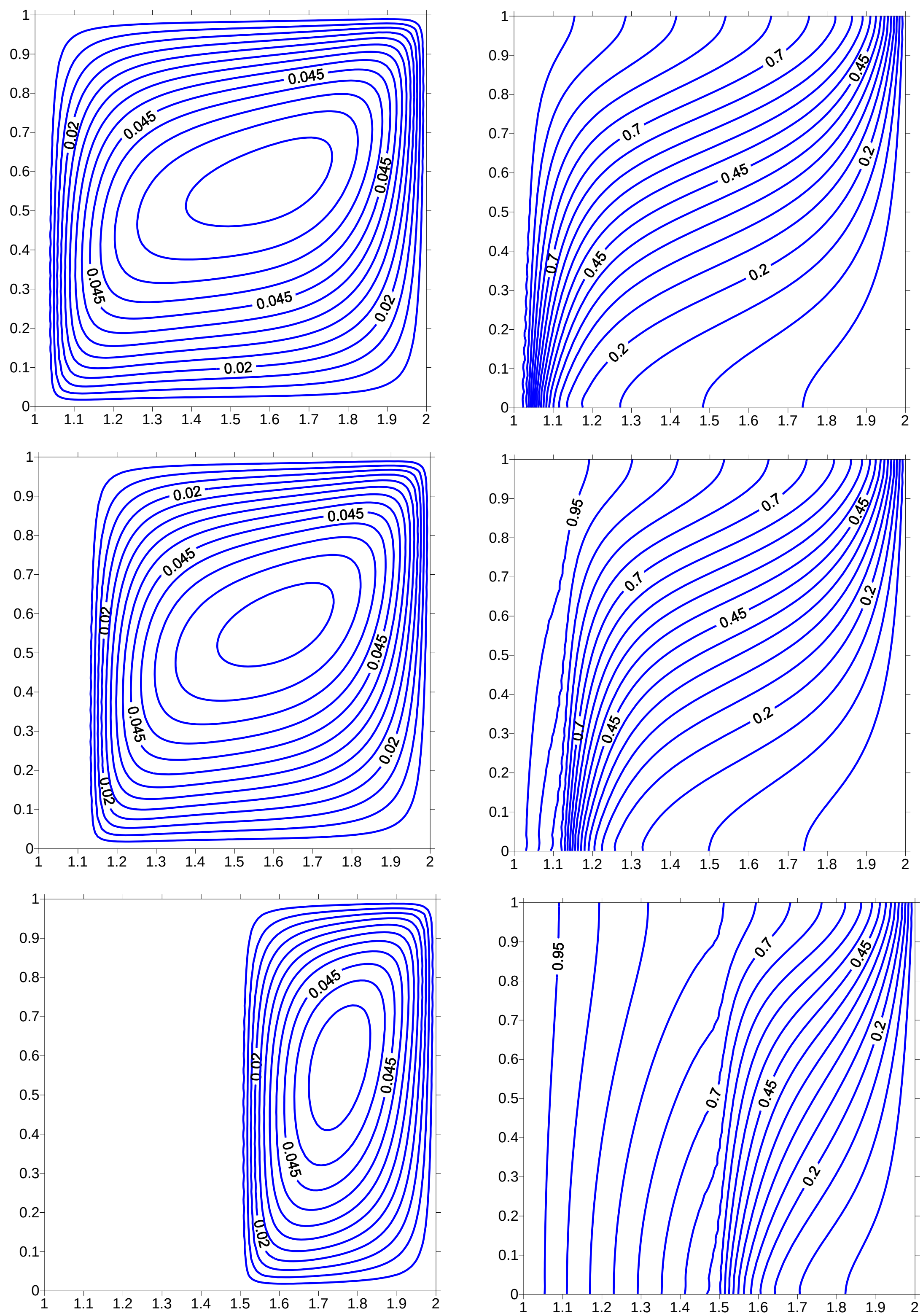

Figure 4.4.8: Stream lines (left) and isotherms (right) for D = 3.125, 12.5 50% , Kr =5

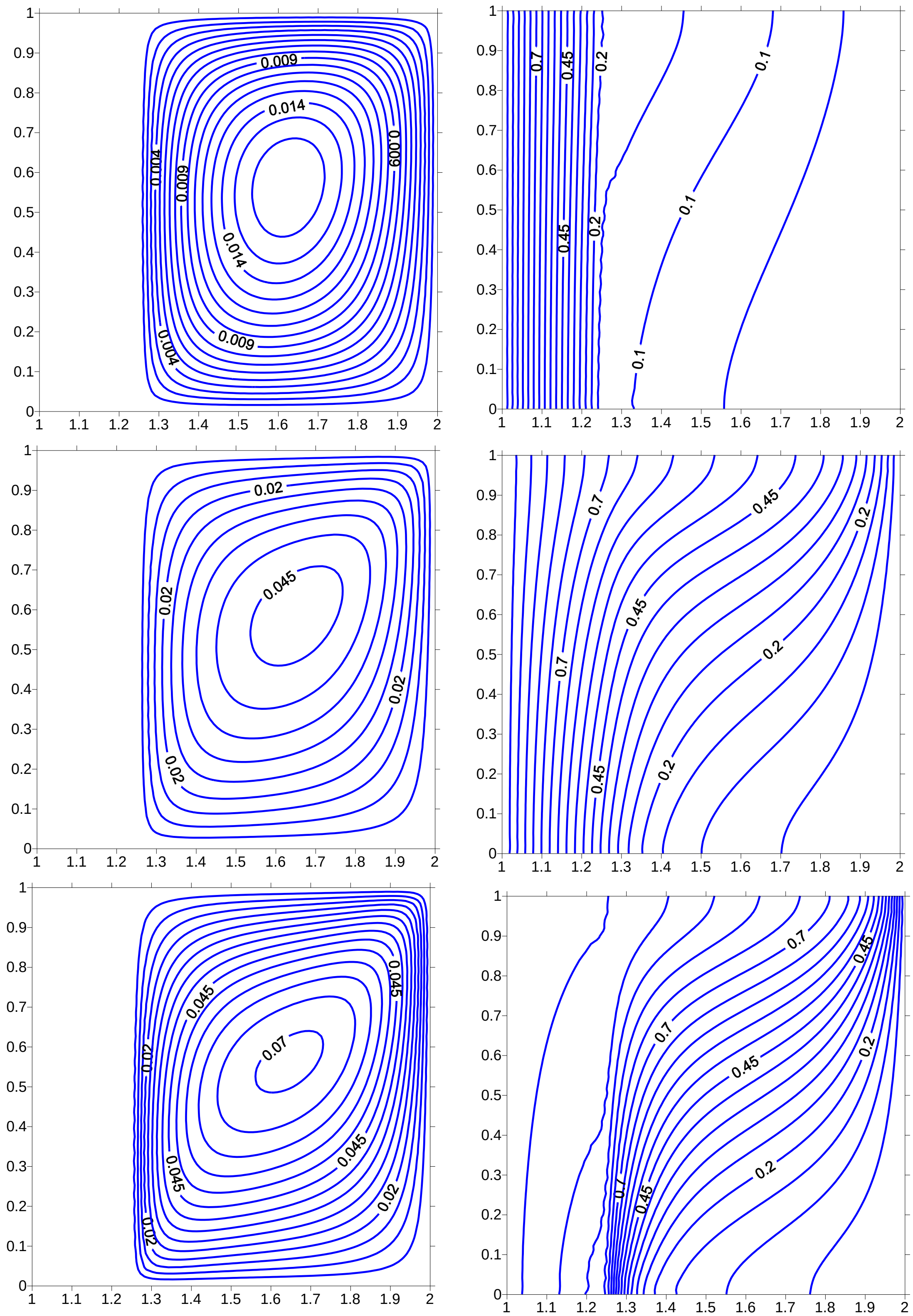

Figure 4.4.9: Stream lines (left) and isotherms (right)for *Kr* = 0.1, 1, 10, *D* = 25%

Figure 4.4.10 depicts the heat transfer behaviour in terms of average Nusselt number when the solid wall thickness is varied from 3.125 to 75 % at three values of aspect ratio. It be noted that the Nusselt number indicates the heat transfer rate from the solid porous interface to the porous medium. The figure is obtained by setting the parameters $Ra = 100, Rr = 1$. It is observed that the Nusselt number decreases with the increase in the solid wall thickness. This is a result of the decreased thermal gradient due to increase in the thickness of the wall. It is observed that the effect of aspect ratio is negligible when porous conductivity is much higher than that of the solid wall conductivity. As the value of Kr increases the effect of aspect ratio also increases. At Kr = 10 and Ar =0.5, the Nusselt number variation is almost linear with respect to the increase in wall thickness. This could be a result of decrease in the convective heat transfer because of reduced fluid velocity. At Kr =10 and Ar = 1,3 , the Nusselt number decreases with increase in *D* until a point and then starts increasing which is not the case for lower values of *Kr*.

Figure 4.4.11 demonstrates the effect of wall thickness and the conductivity ratio on Nusselt number at $Ra = 100, Rr = 1, \ Ar = 2$. The increase in the thermal conductivity ratio increases the Nusselt number thus increasing the heat transfer rate. It is observed that the higher value of *Kr* leads to increase in $\overline{Nu}$ with increase in D whereas the lower values of *Kr* leads to decrease in $\overline{Nu}$ with respect to increase in D.

Figure 4.4.12 shows the average Nusselt number variation with respect to the conductivity ratio. The figure is obtained at $Ra = 100, Rr = 1, \ Ar = 2$. The variation in Nusselt number is sensitive with change in *Kr* for higher wall thickness ratio and lower conductivity ratio. It is intersting to note that the heat transfer rate is not much affected due to change in wall thickness at $Kr \approx 8$ and $D \geq 6.25$.

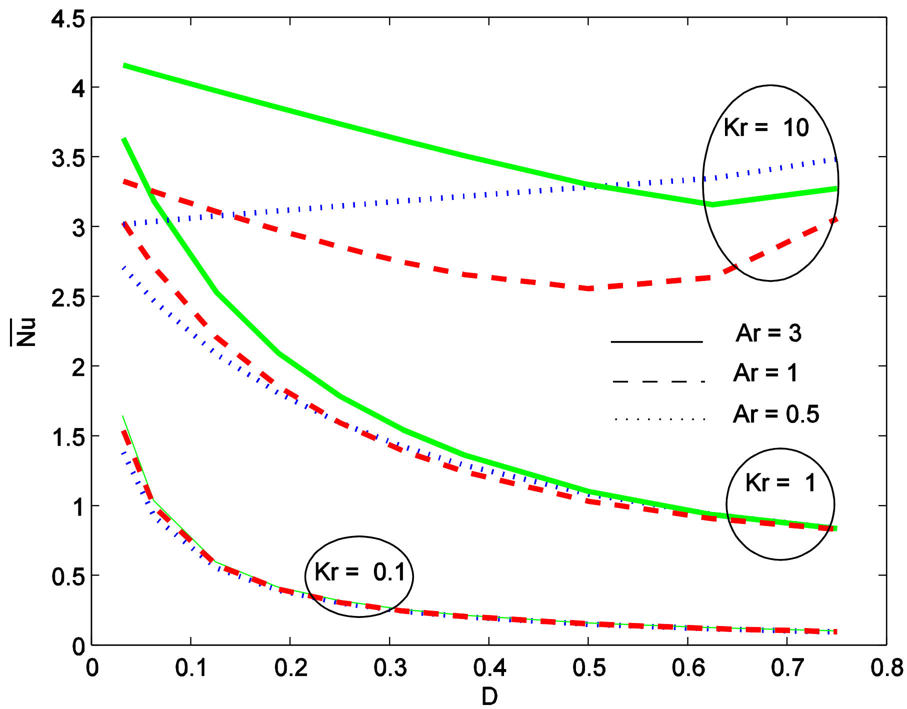

Figure 4.4.10: $\overline{Nu}$ Vs D for various aspect ratio

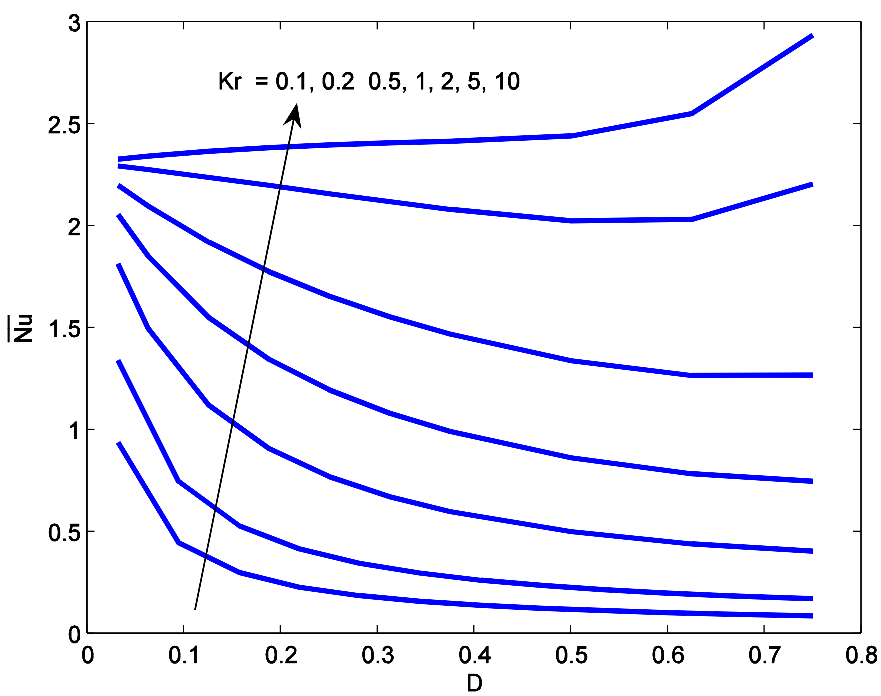

Figure 4.4.11: $\overline{Nu}$ Vs D for various conductivity ratio

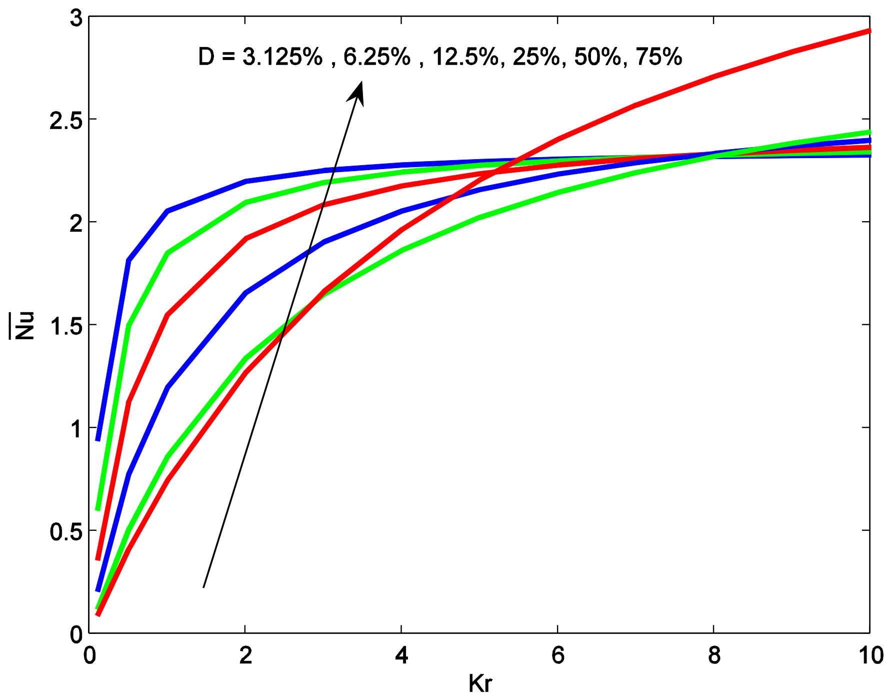

Figure 4.4.12 : $\overline{Nu}$ Vs Kr for various wall thickness

Figure 4.4.13 shows the effect of radius ratio for various values of conductivity ratio at $Ra = 100,\ Ar = 2$. As in case of aspect ratio, the effect of radius ratio is negligible when thermal conductivity of porous region is much higher than that of the solid region. The effect of radius ratio increases with increase in the conductivity ratio. At low thickness ratio, the nusselt number is higher when radius ratio is high. Howvere this trend reverses for larger thickness of the solid wall. Figure 4.4.14 illustrates the effect of radius ratio and conductivity ratio at $Ra = 100,\ Ar = 2$. For smaller conductivity ratio, the Nusselt number increases rapidly with increase in Kr and thereafter the variation in $\overline{Nu}$ smaller.

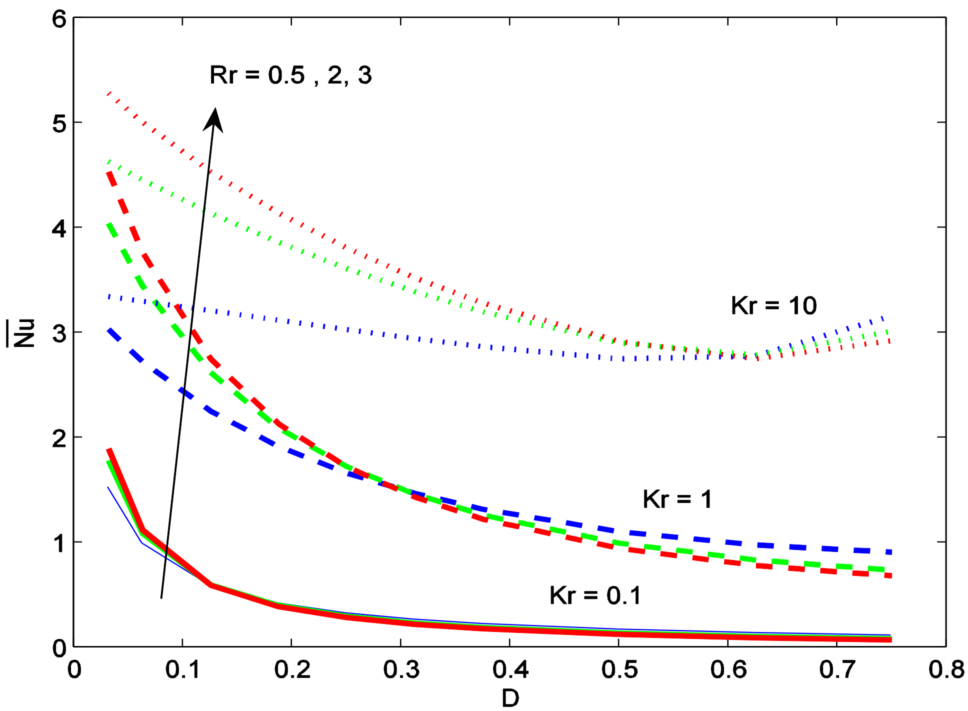

Figure 4.4.13: $\overline{N}u$ Vs D at different radius ratio

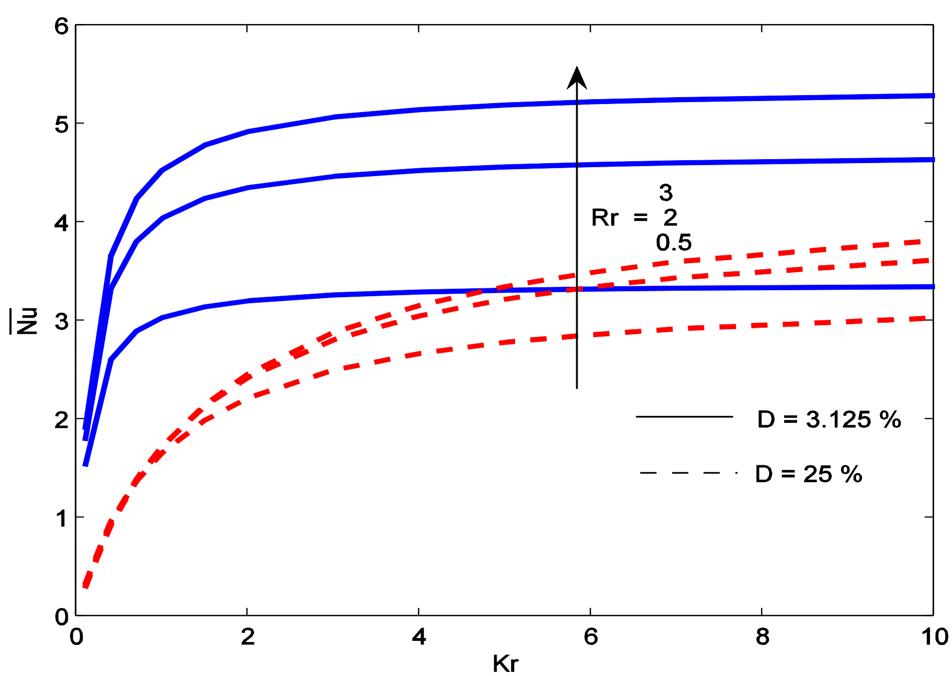

Figure 4.4.14: $\overline{N}u$ Vs. Kr at different radius ratio

Figure 4.4.15 and 16 reflects the effect of Rayleigh number for various values of solid wall thickness and the conductivity ratio. The figures are obtained by setting the variables $Rr = 1, \ Ar = 5$. As expected, the Nusselt number is higher for the case of higher Rayleigh number due to increased fluid velocity which in turn helps to carry more amount of heat from the solid-porous interface to the porous medium. For a given wall thickness, the effect of Rayleigh number is substantial when solid conductivity is much higher than the porous conductivity. For instance, the Nusselt number at *D=3.125%* increased by 86% at *Kr = 1* when Rayleigh number in changed from 50 to 200. However, the corresponding increase in $\overline{Nu}$ is found to be 97% for Kr *=10.*

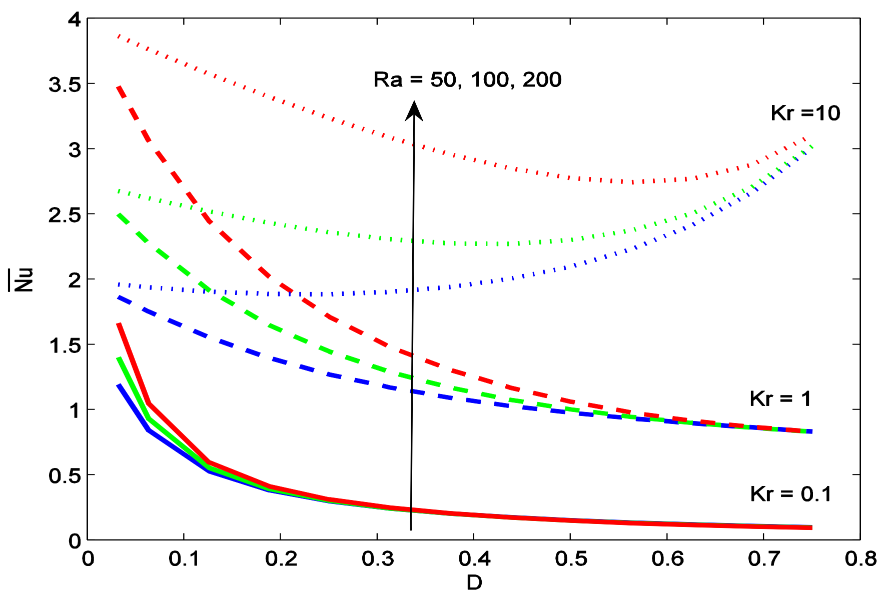

Figure 4.4.15: $\overline{Nu}$ Vs D at different Rayleigh number

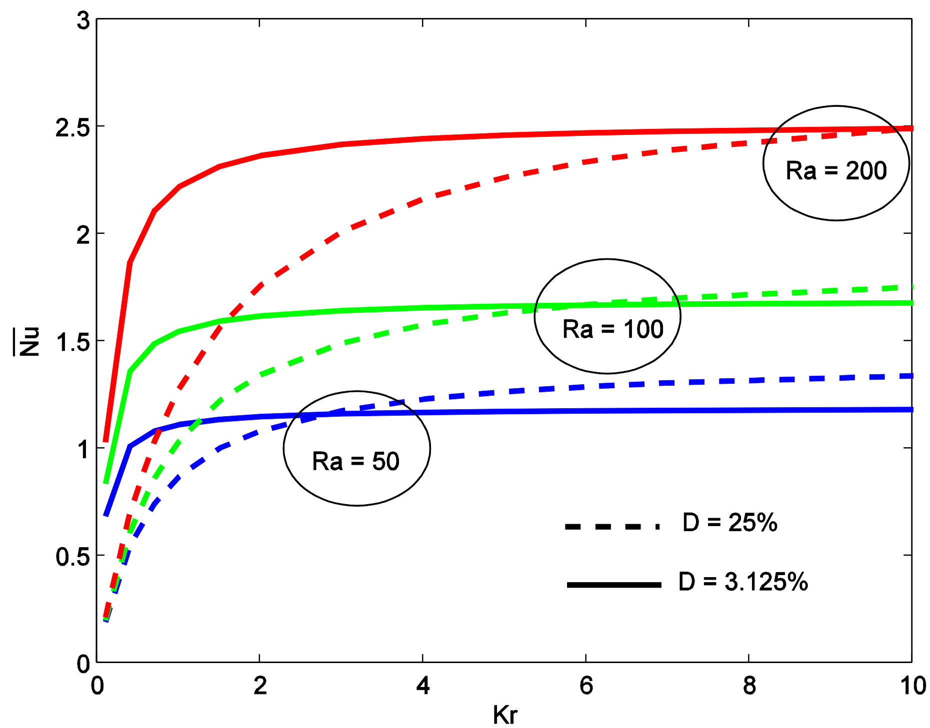

Figure 4.4.16: $\overline{Nu}$ Vs. Kr at different Rayleigh number

4.4.3 Validation of the Results

The present research work has been validated to the previously published research work by eminent researchers and it is found to be in good agreement with those results. The table 4.4.3 validates the present results with the published data by eminent researchers.

Table 4.4.3: Comparison of results for different aspect ratio at $Ra = 100,\ Rr = 1, D = 0$

Aspect ratio	$\overline{Nu}$			
	Prasad and Kulacki, 1984)	(Rajamani et.al, 1995)	(Nath and Satyamurthy,1985)	Present
3	3.70	3.868	3.81	3.8838
5	3.00	3.025	3.03	3.0638
8	2.35	2.403	2.45	2.4249

4.5 Conjugate heat transfer in an annulus with porous medium fixed between solids

4.5.1 Introduction

The current research is focused to study the heat transfer in a porous medium sandwiched between two solid walls of an annular vertical cylinder. The prime focus of current study is to evaluate the effect of solid wall thickness, the influence of variable wall thickness at inner and the outer radius, the conductivity ratio and the solid wall conductivity ratio on the heat transfer characteristics of the porous medium. The application such as increased insulation of the space is achieved by inserting the porous material between the two conducting layers. Also the enhancement or retardation of the heat transfer rate is achieved by means of porous material insertion in many applications.

The schematic representation of the physical model is shown in Figure 4.5.1 along with boundary conditions as explained in chapter 3 section 3.4.

The problem under investigation is discussed for different physical and geometric parameters involved. Emphasis is given to the thickness of the solid walls at the inner and outer surfaces along with the conductivity ratio and solid conductivity ratio. Results are discussed in terms of Nusselt number at the solid-porous interface which is a measure of heat transfer from the solid wall to porous medium. Apart from Nusselt number, the temperature distribution at the solid-porous interface and the streamlines along with isothermal lines are presented for various physical and geometric parameters.

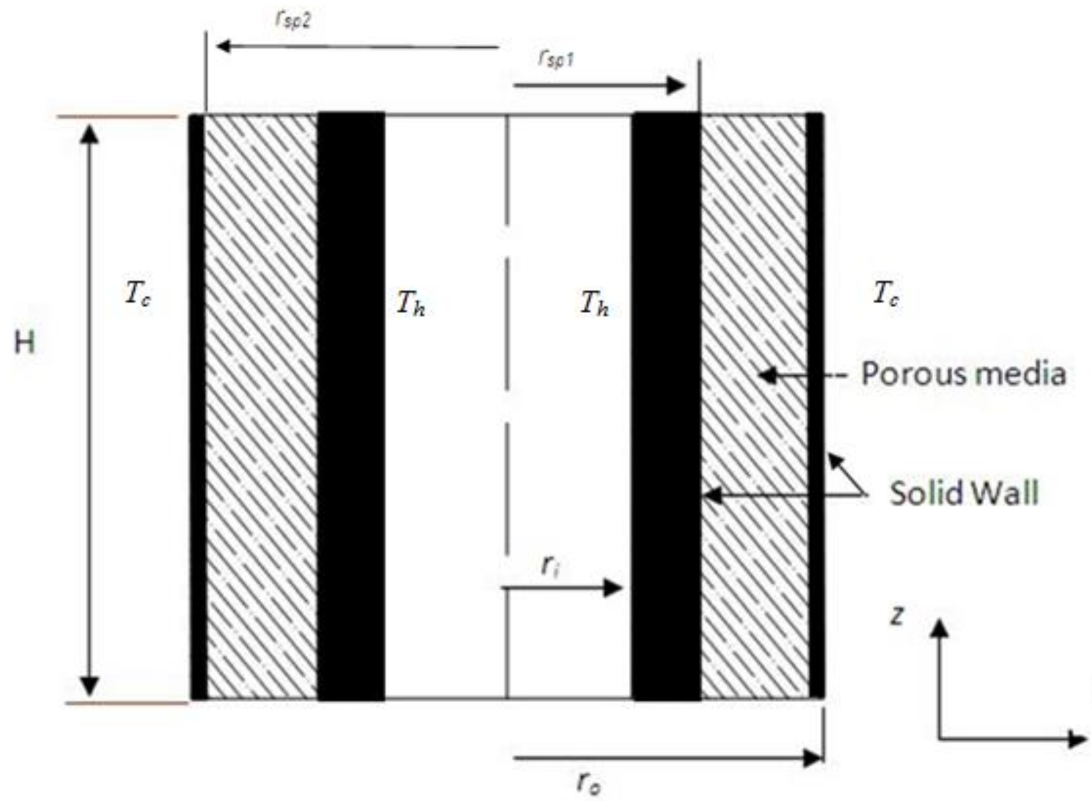

Figure 4.5.1: Schematic of conjugate heat transfer in annular porous cylinder with two solid walls

4.5.2 Temperature profile

The boundary conditions of current problem are such that the inner and outer surfaces are maintained at T_h and T_∞ respectively which means that the heat has to travel from inner radius towards outer radius because of temperature difference in radial direction. The applied temperature exists on the left and right surfaces of the inner and outer solid walls. The heat transfer from solid wall to the porous medium and then from porous medium to outer solid depends on the temperature profile at the solid-porous interfaces. These profiles are in turn dependent on the solid wall thickness and the physical properties of walls. Since the domain includes two solid walls at inner and outer surfaces, it is important to know the temperature variations along the interfaces and the medium to judge the heat transfer characteristics of the whole domain.

Figures 4.5.2- 4.5.3 illustrate the effect of solid wall thickness on the temperature distribution at the inner and outer surface solid porous interface for *DL = 3.125, 6.25, 12.5, 25, 37.5 & 50 %* at *DR* = 6.25 and 25 %. Figures 4.5.2-4.5.5 corresponds to $Ra = 200, Rr = 1, Ar = 5, Kr = 10, Krs = 2$. It is observed that the temperature of solid-porous interface at r_{sp1} is very close to that of the applied temperature T_h when the wall thickness *DL* is small but the temperature of interface at higher values of *DL* is substantially different from that of T_h. This is because the heat travels quickly in thinner wall as compared to that of thick wall thus the temperature variation along the thickness is small. The temperature increases along the height of the cylinder. The variation of temperature at lower section of the cylinder is sharp as compared to other sections. The fluid moment near the interface creates sharp variation in temperature at the lower part of cylinder by absorbing heat near that region and then moving upwards where the already elevated fluid temperature does not allow further absorption of heat due to reduced temperature difference between fluid and the interface region at upper section of cylinder. The increase in the wall thickness at outer surface, *DR* does not affect the interface temperature T_{sp1} for lower values of *DL*. However, the increase in *DR* reduces the interface temperature at upper section of cylinder for higher value of *DL*. The trend of temperature variation T_{sp2} for the porous-solid interface at outer surface as shown in figure 4.5.3 is completely different from that of inner surface temperature T_{sp1}. At r_{sp2}, the temperature increases gradually for most of the cylinder height until almost *Ar*=75 % and then the increase is rapid for upper section. The fluid which has brought energy from rsp1 losses its most of the heat to the upper part of r_{sp2} thus temperature in that region is higher as compared to the other sections of the interface r_{sp2}. At lower part of cylinder and given value of $\bar{z}$, the temperature is higher for higher inner wall thickness. It is also observed that the temperature along r_{sp2} is higher for higher wall thickness at outer surface. The increased wall thickness *DR* is achieved at the cost of reduced porous thickness which in turn decreases thermal resistance along the depth of porous medium thus increasing the temperature along rsp2 as depicted in figures 4.5.4 and 4.5.5. It be noted that figure 4.5.5 shows the temperature variation for two values of *Krs* which indicates the relative thermal conductivity of two solid walls. In Figure 4.5.5, the height of the cylinder varies from left to right for $Krs = 2$ and right to left for $Krs=0.5$. Figures 4.5.6 and 4.5.7 illustrate the effect of solid conductivity ratio *Krs* on interface temperature r_{sp1} and r_{sp2} respectively. These figures correspond to the values $Ra = 300, Rr = 1, Ar = 5,$ when both the solid wall has equal thickness of 6.25% and 25 %. The temperature along r_{sp1} does not vary much for higher wall thickness. It is seen that the T_{sp1} is higher when the conductivity of left solid wall is higher than the solid wall at outer surface of cylinder leading to higher value of *Krs*, for a given value of porous medium thermal conductivity. *Krs* is high. The effect of *Krs* reduces considerably when the porous conductivity is much lesser than the inner surface solid wall conductivity (higher *Kr*).

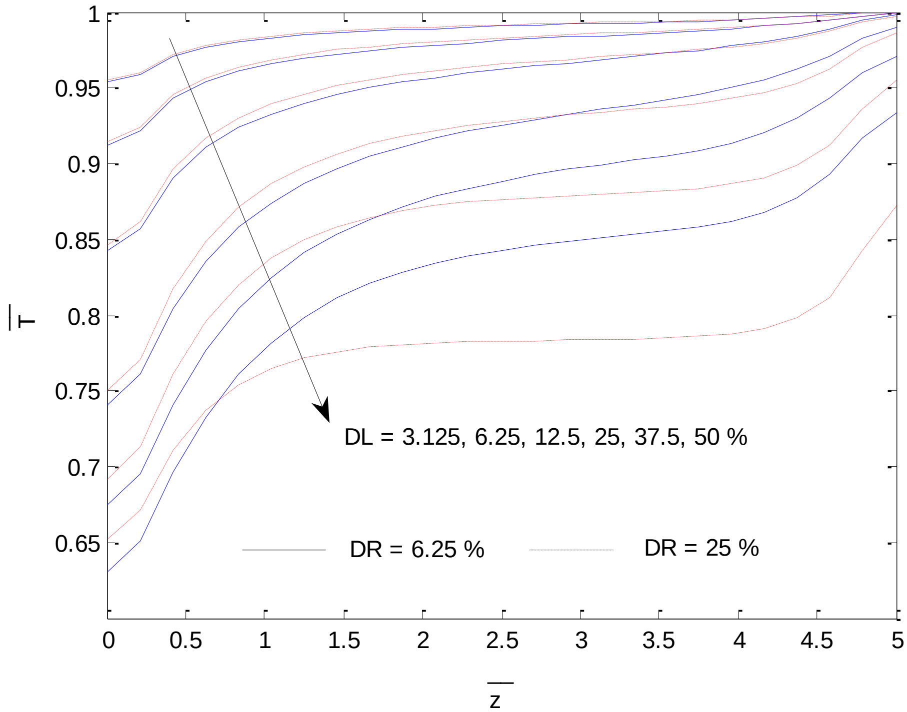

Figure 4.5.2: Temperature along r_{sp1} when *DL* varies

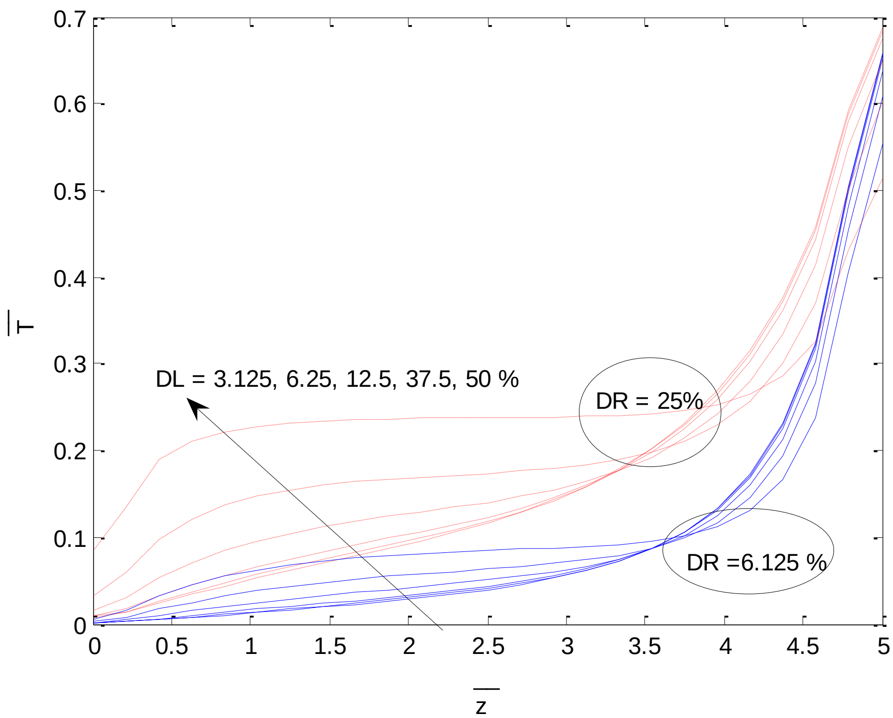

Figure 4.5.3: Temperature along r_{sp2} when *DL* varies

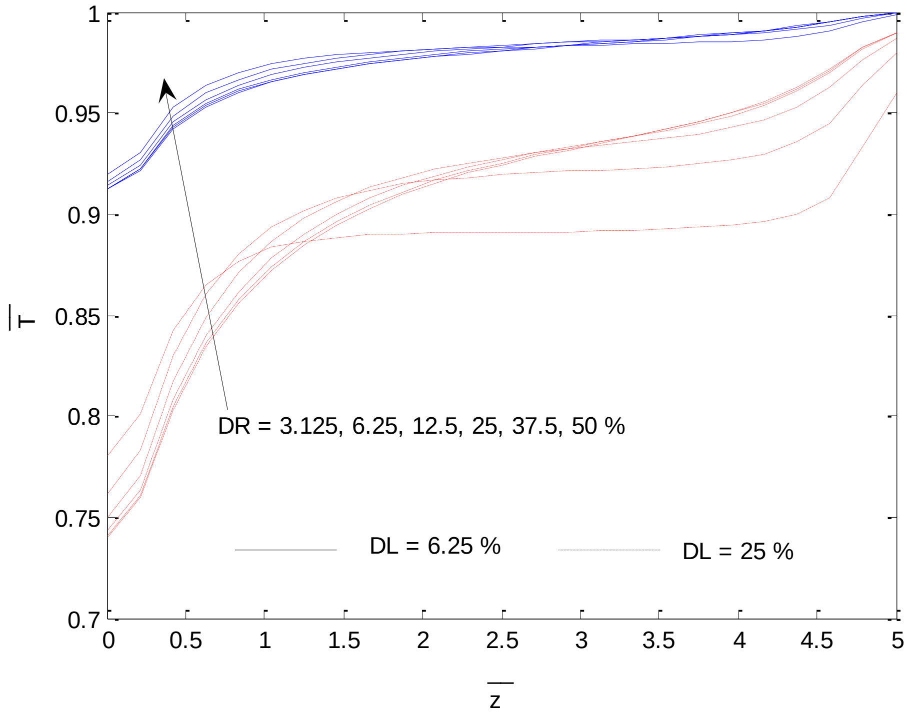

Figure 4.5.4: Temperature along r_{sp2} when DR varies

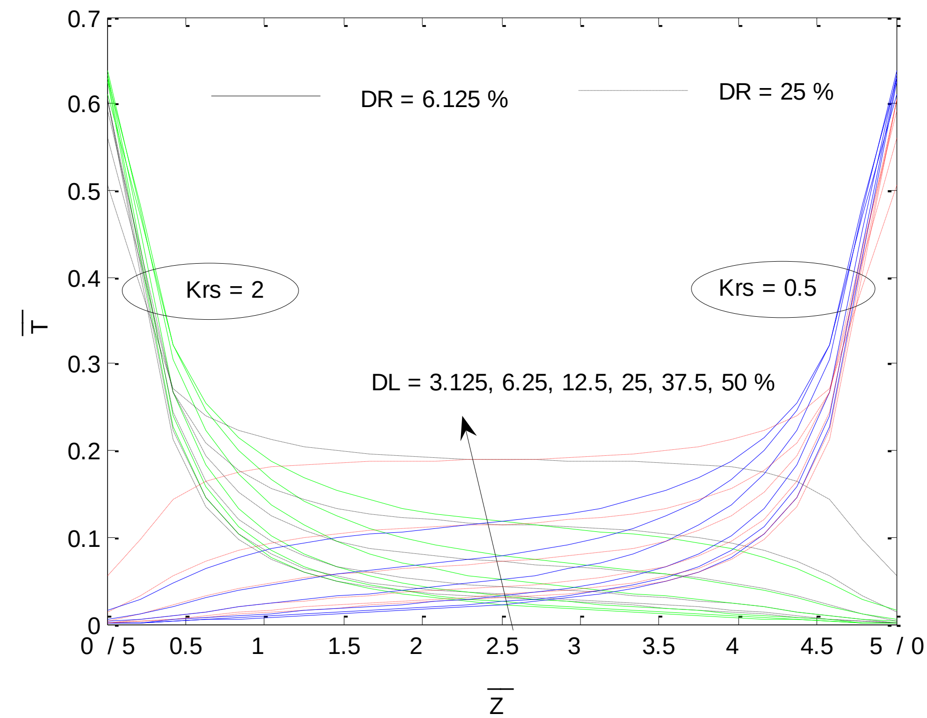

Figure 4.5.5: Temperature along r_{sp2} when DR varies

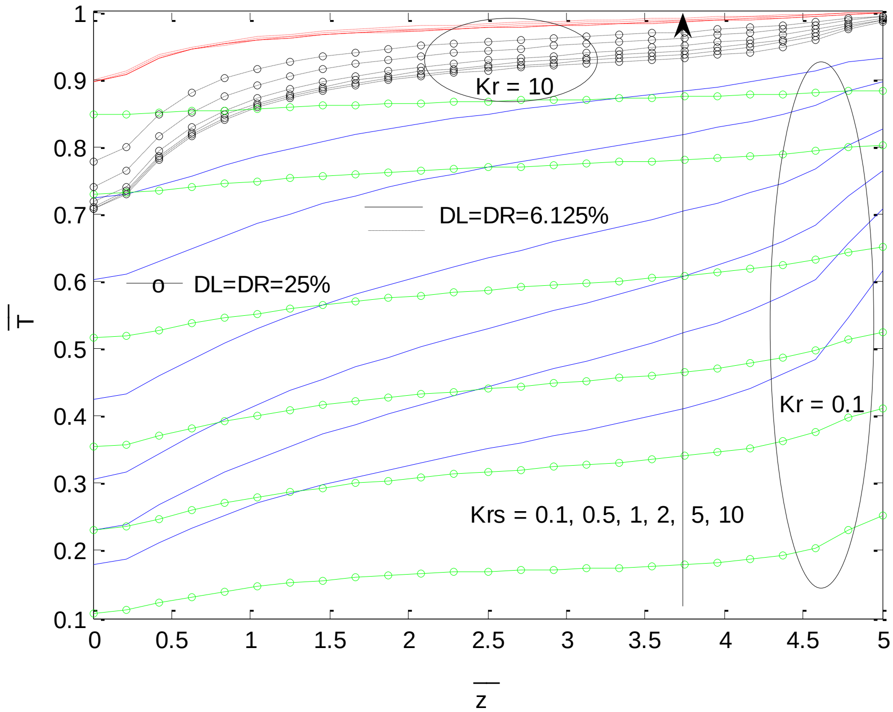

Figure 4.5.6: Temperature along r_{sp1} when *Krs* varies

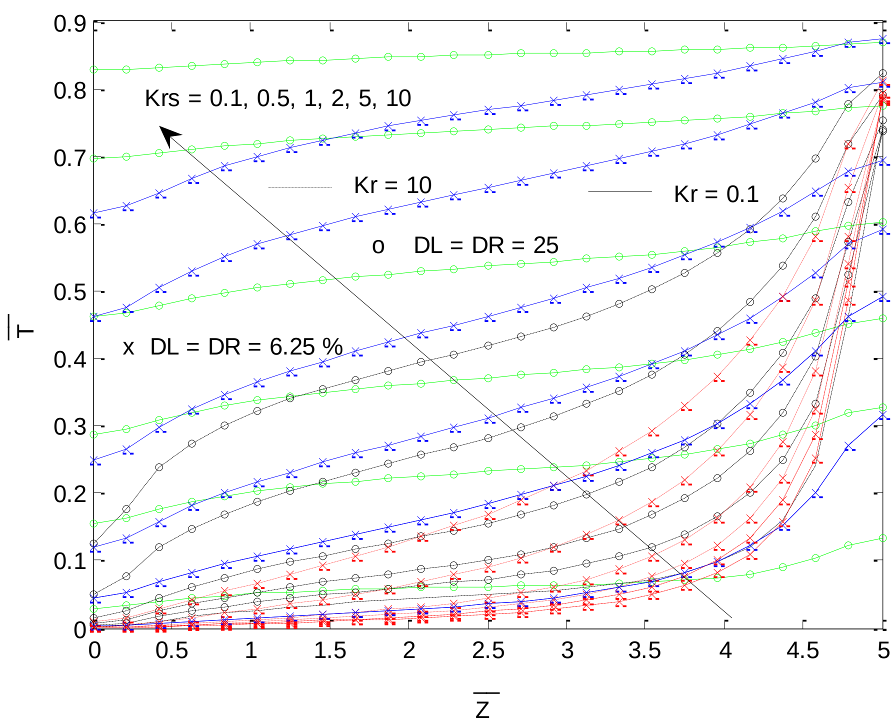

Figure 4.5.7: Temperature along r_{sp2} when *Krs* varies

4.5.3 Streamlines and Isotherms

The fluid flow pattern and the temperature variation in the domain can be well described with the help of streamlines and the isothermal lines which basically represents the areas of constant values of stream function and the temperature. The effect of solid wall thickness variation when *DL=DR* is shown in Figure 4.5.8. This figure is obtained by setting $Ra = 200, Rr = 1, Ar = 5, Kr = 10, Krs = 5$ isotherms are placed left and streamlines on right side of the figure for three values of inner and outer wall thickness. It is seen that the left solid wall is occupied by high temperature lines indicating that the energy is transferred quickly from inner radius to r_{sp1} because of high conductivity of the inner solid (*Kr=10*). The outer solid is occupied by low temperature isotherms because of low conductivity of outer solid. At low values of DL/DR, the fluid gains thermal energy at the lower left segment of cylinder and then moves towards the right upper segment losing its energy to outer surface before flowing back towards the left segment of cylinder thus completing the cycle. The flow pattern is oval shaped from lower left to upper right segment of annulus. The increased wall thickness shifts the flow direction from being oval to near elliptical from bottom to top of annulus.

Figure 4.5.9 indicates the effect of varying inner solid wall thickness by keeping the constant values $Ra = 200, Rr = 1, Ar = 5, Kr = 10, Krs = 5, DR = 6.25\%$. There is slight straightening of isotherms with increase in the wall thickness which indicates that the convection has reduced. This is further vindicated by reduction in the value of stream with increase in *DL*. The reduced stream function leads to reduction the fluid velocity which in turn retards the heat transfer rate at the solid porous interface. The effect of varying the outer wall thickness is shown in Figure 4.5.10 which is obtained at $Ra = 200, Rr = 1, Ar = 5, Kr = 10, Krs = 5, DL = 3.125\%$. It is obvious from figure 4.5.10

that the isotherms have considerably straightened when *DR* is varied from 6.25 to 50 %. This reflects that the heat transfer due to convection reduces when *DR* is increased. The value of stream function reduces with increase in DR. thus it can be said that the increase in the either wall thickness reduces the fluid velocity inside the porous medium.

The effect of solid conductivity ratio on the streamline and isotherms is shown in Figure 4.5.11. $Ra = 200, Rr = 1, Ar = 5, Kr = 10, DL = 25\%, DR = 25\%$ are the various parameters in the Figure correspond to. An increase in solid conductivity ratio reduces the thermal gradient as indicated by spread out isotherms due to increase in *Krs*. The fluid velocity is reduced due to increase in *Krs* as indicated by streamlines.

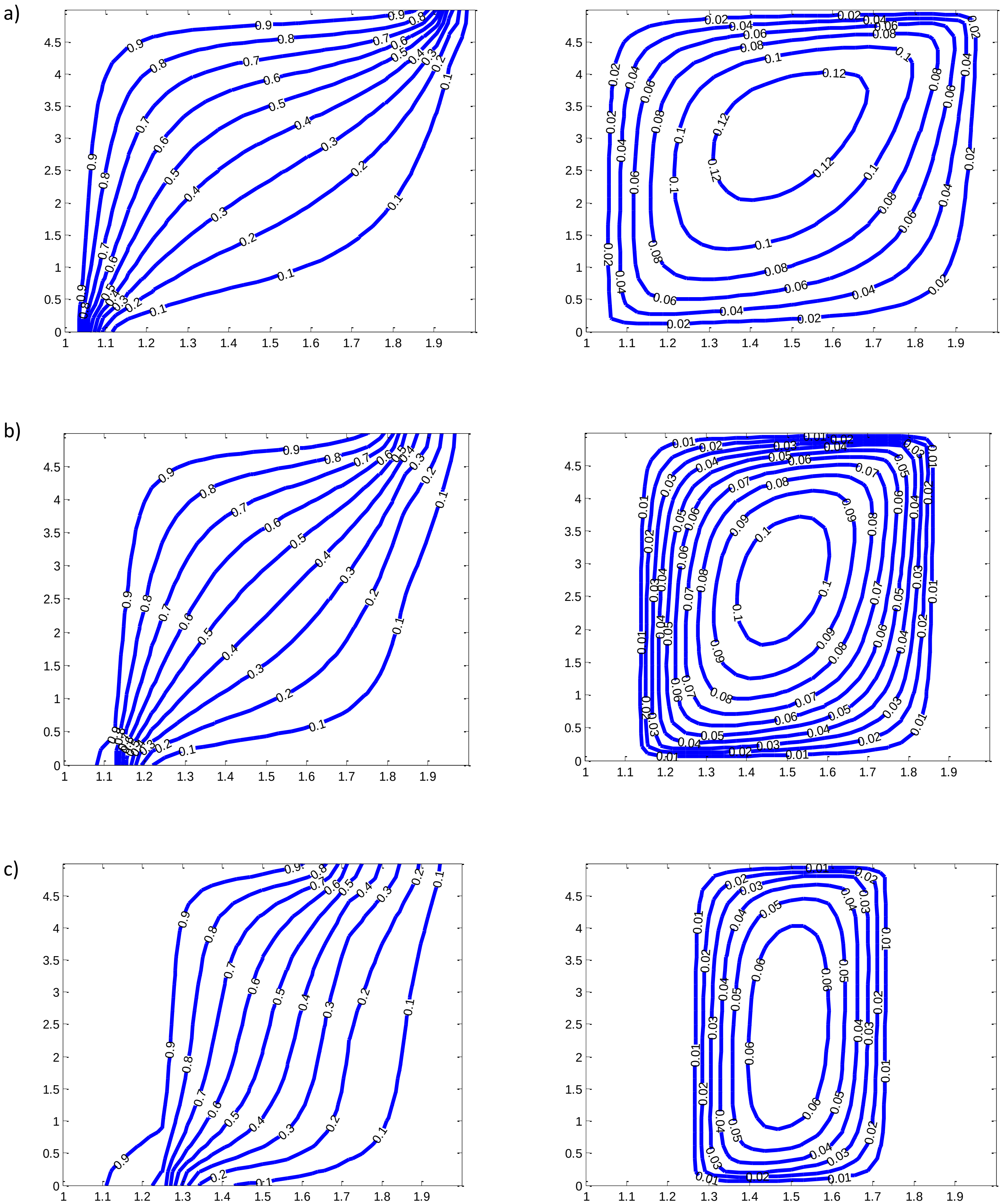

Figure 4.5.8: Isotherms (Left), Streamlines (Right) for a) *DL=DR=6.25 % b) DL=DR=12.5 % c) DL=DR=50%* *at* $Ra = 200, Rr = 1, Ar = 5, Kr = 10, Krs = 5$

a)

b)

c)

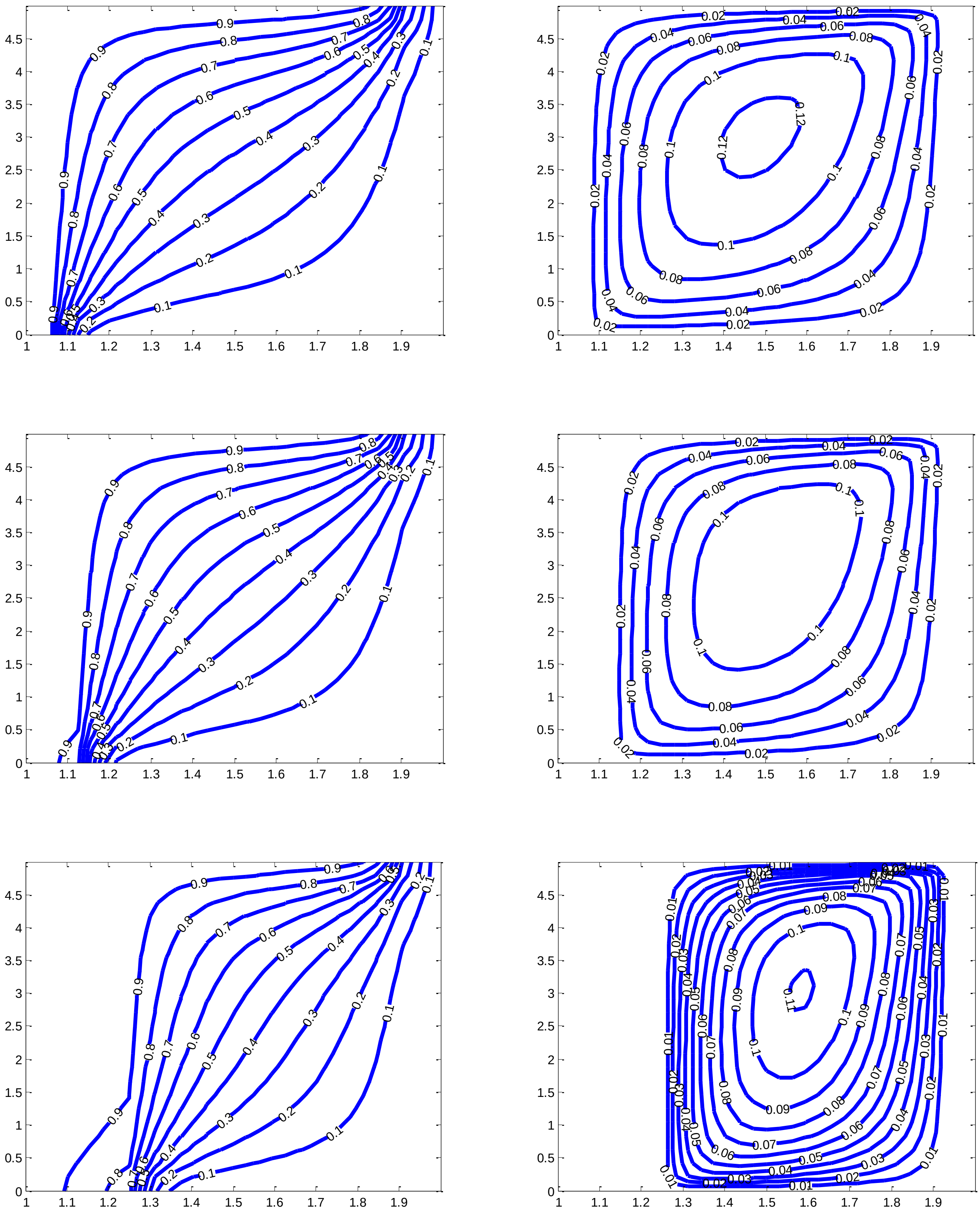

Figure 4.5.9: Isotherms (Left), Streamlines (Right) for a) *DL*=6.25 % b) *DL*=12.5 % c) *DL*=50% at

$$Ra = 200, Rr = 1,\ Ar = 5,\ Kr = 10, Krs = 5,\ DR = 6.25\%$$

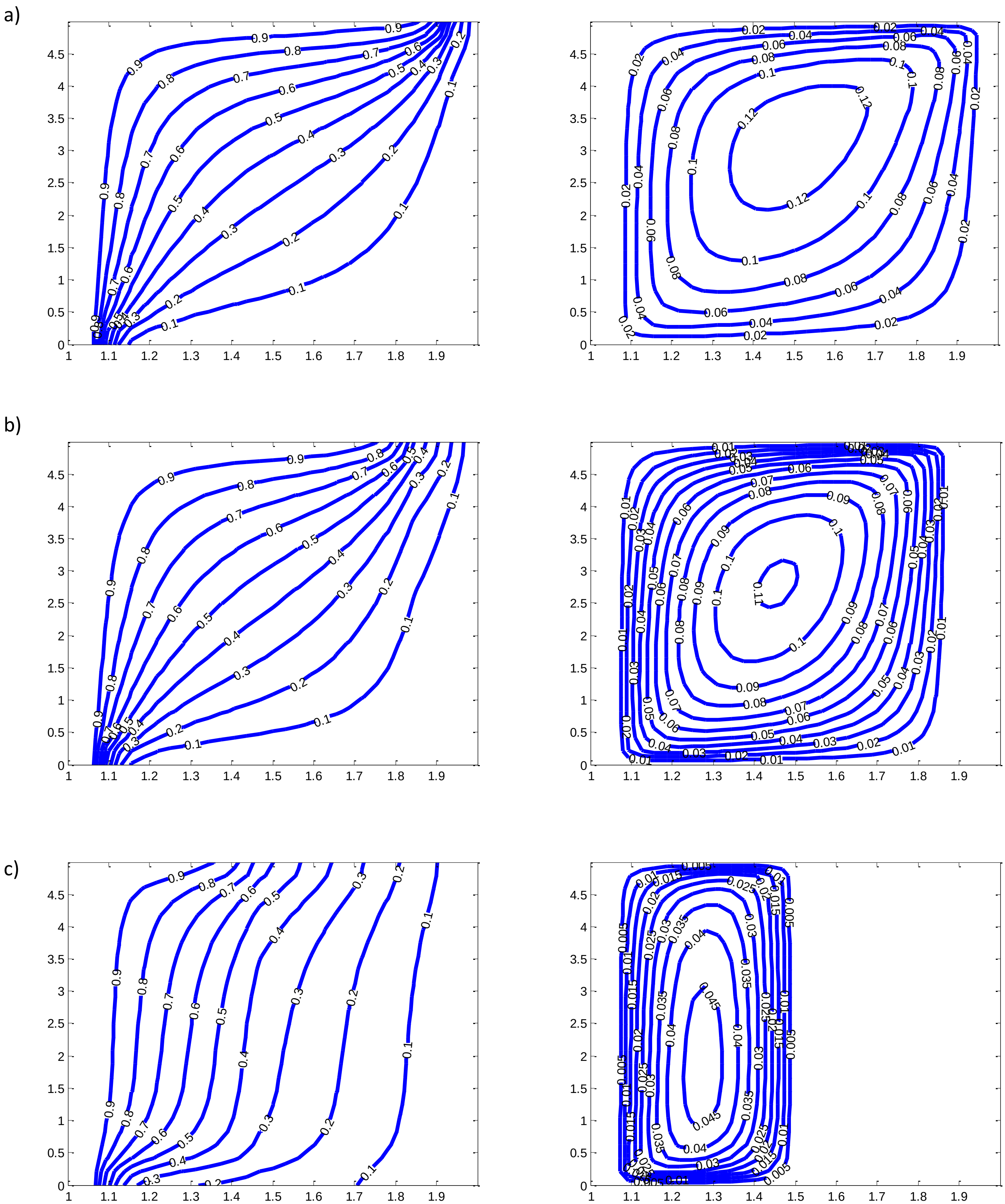

Figure 4.5.10: Isotherms (Left), Streamlines (Right) for a) *DR*=6.25 % b) *DR*=12.5 % c) *DR*=50% at

$$Ra = 200, Rr = 1, \ Ar = 5, \ Kr = 10, Krs = 5, \ DL = 3.125\%$$

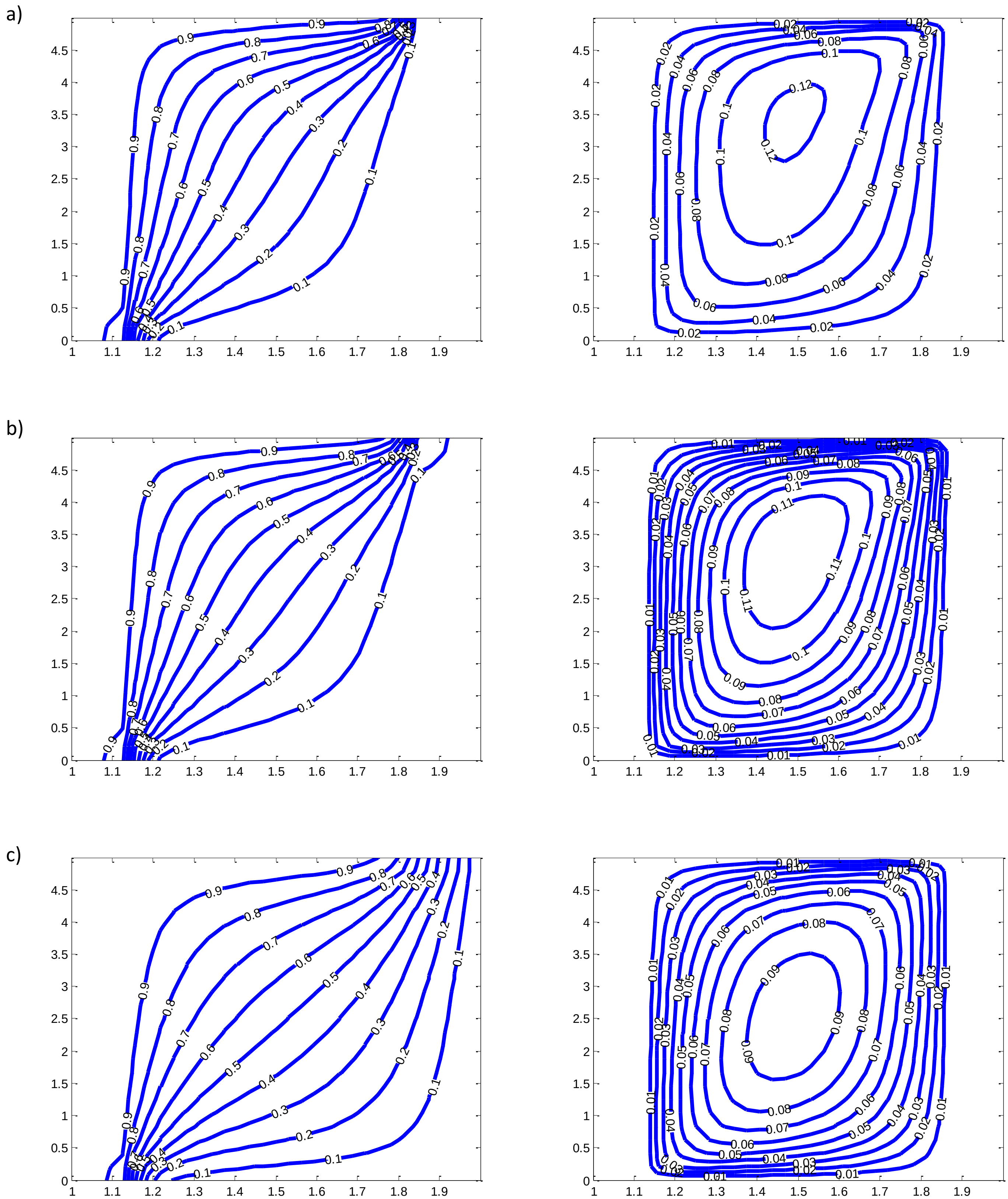

Figure 4.5.11: Isotherms (Left), Streamlines (Right) for a) Krs = 0.1 b) Krs = 1 c) Krs = 10 at $Ra = 200, Rr = 1, Ar = 5, Kr = 10, DL = 25\%, DR = 25\%$

4.5.4 Heat transfer behaviour in terms of Nusselt number

The heat transfer from inner radius towards outer radius of the annular solid-porous-solid domain can be described with the help of Nusselt number. Nusselt number basically highlights the convective heat transfer relative to conduction. The following section discusses the variation of Nusselt number due to changes in various physical and geometric parameters. Figure 4.5.12 shows the average Nusselt number at rsp1 due to change in *DL*. This figure is obtained by setting $Ra = 200, Rr = 1, Ar = 5, Kr = 10$. It is observed that the average Nusselt number $\overline{Nu}$ decreases with increase in the wall thickness *DL* for thin outer wall thickness. However for thicker outer wall thickness, the $\overline{Nu}$ initially decreases with respect to *DL* and then increases with further increase in *DL*. The decrease of $\overline{Nu}$ with respect to increase in *DL* is a result of reduction in the T_{sp1} due to increased thermal resistance created by thickening solid wall at inner surface. However the increase in $\overline{Nu}$ at higher outer wall thickness is associated with increased thermal gradient across r_{sp1} which offsets the effect of decreased interface temperature T_{sp1}. The increase in conductivity ratio *Kr* reduces the heat transfer rate as indicated by Figure 4.5.13 that belongs to $Ra = 100, Rr = 1, Ar = 1, DR = 6.25$. The effect of *Kr* diminishes as the solid wall thickness *DL* increases. The $\overline{Nu}$ variation is almost linear when the relative conductivity of inner solid is small compared to that of porous conductivity.

The effect of outer wall thickness DR on heat transfer rate is depicted in Figure 4.5.14 which is obtained by setting $Ra = 100, Rr = 1, Ar = 1, DR = 6.25$. The Nusselt number decreases with increase in the *DR*. The variation of heat transfer with respect to change in DR is almost linear as shown in Figure 4.5.14. The thermal conductivity ratio of inner and outer solid which is denoted by *Krs*, plays an important role in determining the heat transfer characteristics inside the solid-porous-solid domain. The value *Krs>1* indicates that the conductivity of inner solid is higher than that of outer solid and vise-versa for *Krs<1*. It is seen that the heat transfer rate decreases with increase in the *Krs* as illustrated by Figure 4.5.15. However, this decrease is negligible when the porous conductivity is much higher than that of inner solid conductivity. The decrease of heat transfer with increase in *Krs* can be explained in a way that the increased solid conductivity ratio is associated with decrease in the thermal conductivity of outer solid. The decrease in the outer solid conductivity contributes to increase in the overall thermal resistance of porous-solid combination which in turn reduces the Nusselt number at r_{sp1}. The increase in *Krs* is also associated with increase in the inner wall conductivity k_{s1} by keeping outer solid conductivity at constant value. In such condition, the overall thermal resistance of the whole domain decreases due to increase in k_{s1} leading to increase in heat transfer rate as shown in Figure 4.5.15 ($Ra = 100, Rr = 1, Ar = 1$) where the Nusselt number increased due to increase in *Kr*. The effect of Rayleigh number on Nusselt number is shown in Figure 4.5.16 is obtained at $DL = 12.5, DR = 12.5, Rr = 1, Ar = 10$ .As expected, the heat transfer rate increases with Rayleigh number. For a given value of *Krs*, the effect of Rayleigh number is higher when *Kr* is high. The high Rayleigh number and *Kr* lead to increased fluid energy and velocity, which reflects in increased Nusselt number.

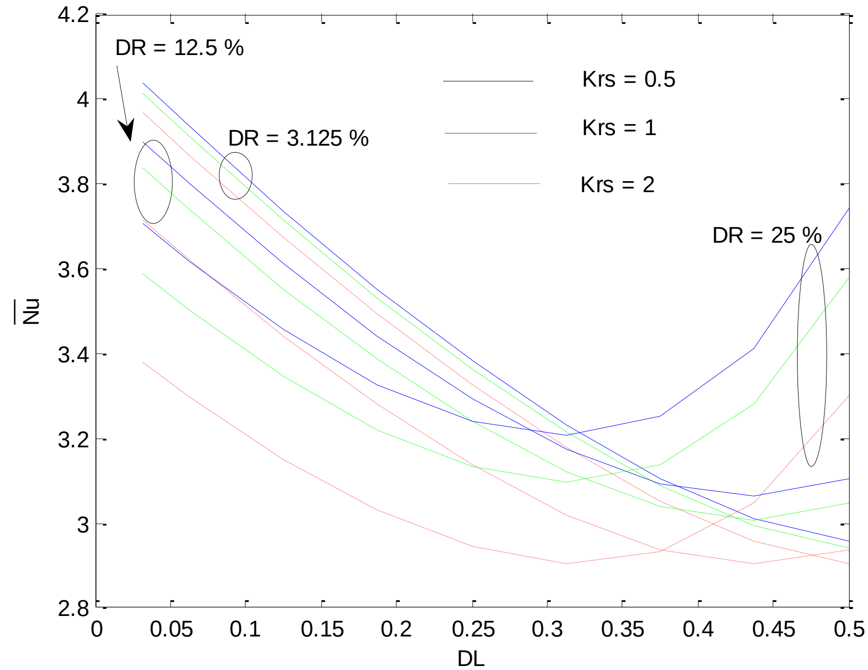

Figure 4.5.12: $\overline{Nu}$ variation with respect to D_L

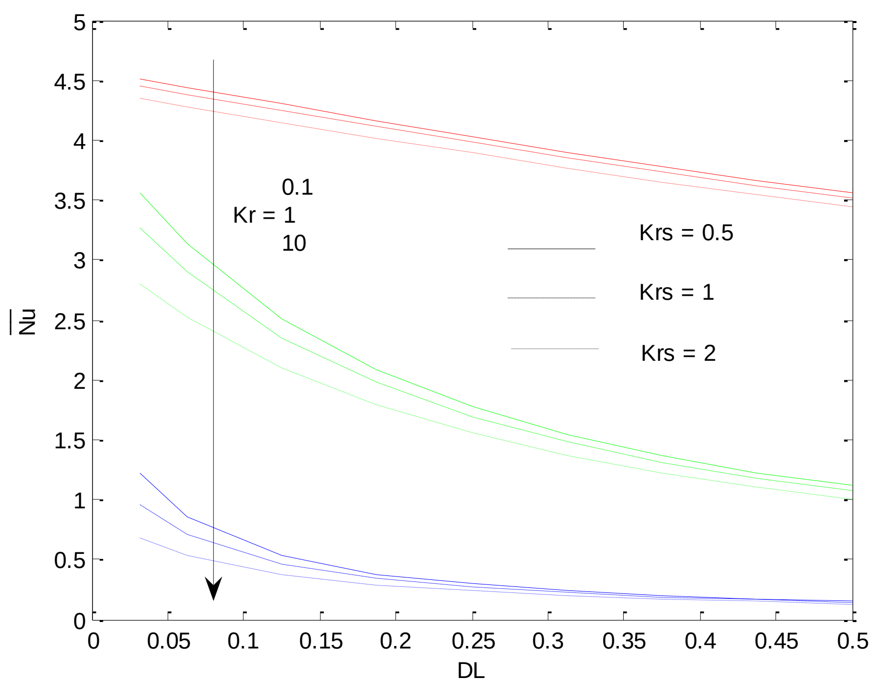

Figure 4.5.13: $\overline{Nu}$ variation with respect to D_L for various thermal conductivity ratios

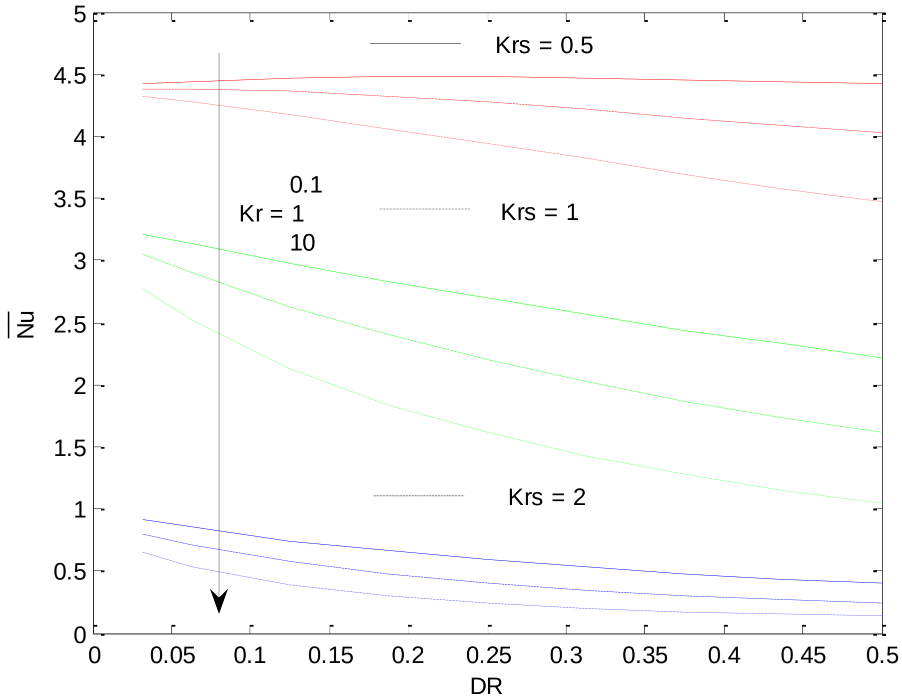

Figure 4.5.14: $\overline{Nu}$ variation with respect to D_L

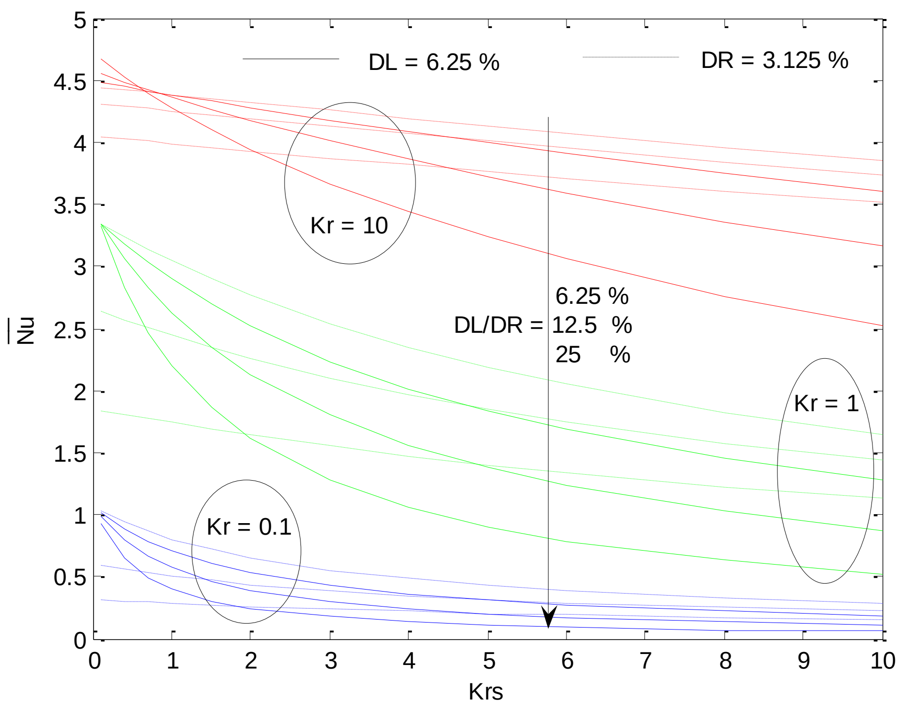

Figure 4.5.15: $\overline{Nu}$ variation with respect to Krs

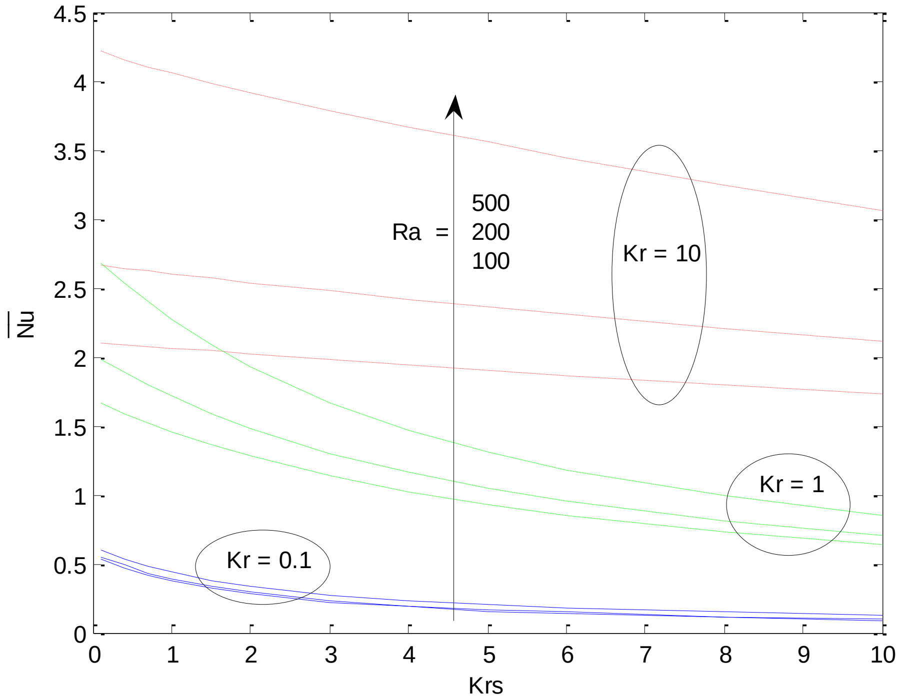

Figure 4.5.16: Effect of Rayleigh number on $\overline{N}u$

4.6 Study of conjugate double diffusion in a vertical porous cylinder

4.6.1 Introduction

The present section deals with the investigation of conjugate heat and mass transfer in an annular vertical cylinder having a solid wall at the inner surface. Emphasis is given on investigation of the effect of variation of the solid wall thickness and the thermal conductivity ratio between solid and porous medium. The applications involving heat and mass transfer in nature such as drying of vegetables, percolation of pollutants through soil and transpiration in plants are examples of heat and mass transfer phenomena. The schematic of the geometry is shown in Figure 4.6.1 and the corresponding boundary conditions are given in chapter 3 section 3.5.

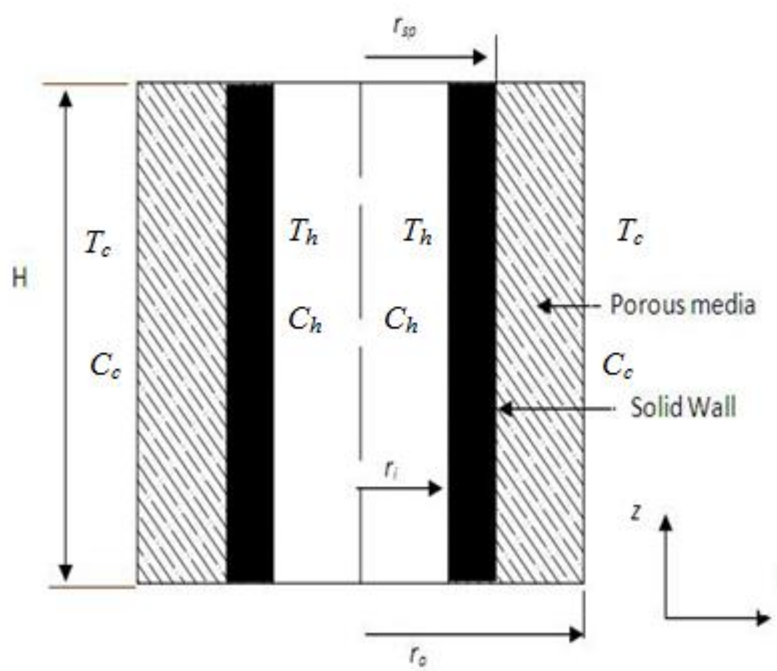

Figure 4.6.1: Conjugate heat and mass transfer in an annular porous cylinder

4.6.2 Analysis

The following section predicts the temperature profile, concentration profile, Nusselt number and Sherwood number for conjugate heat and mass transfer in porous annulus. Emphasis is given to the thickness of solid wall along with the conductivity ratio between solid and porous medium.

4.6.2a Temperature and concentration profile

The thermal boundary conditions of current problem are such that the inner and outer surfaces are maintained at T_h and T_c respectively. This will force the heat to be transferred from inner surface through the solid section and then towards the outer radius across the porous medium due to temperature difference in radial direction. Similarly the mass has to travel from solid porous interface towards the outer radius due to concentration difference in the radial direction. The heat transfer from solid wall to the porous medium depends on the temperature profile at the solid-porous interfaces. These profiles are in turn dependent on the solid wall thickness and the physical properties of walls. It is worth to know the temperature variations along the interface and the medium to judge the heat transfer characteristics of the whole domain.

Figure 4.6.2 illustrates the effect of the solid wall thickness on the temperature distribution at the solid porous interface for $Kr = 0.1, Le = 1, Ra = 100, Rr = 1, Ar = 2$. D indicates the fraction of solid thickness compared to the total thickness of domain between inner and outer radii. The figure is plotted for two values of buoyancy ratio $N=-0.5, 0.5$. The parameter N indicates the relative importance of concentration and thermal buoyancy force. It may be noted that N is positive for thermally assisting flow and negative for thermally opposing flow. $N = 0$, indicates the absence of concentration buoyant force and flow is driven by thermal buoyancy only. The temperature along the interface increases with increase in cylinder height for assisting flow. It is seen that the temperature difference at top and bottom of the cylinder along the interface decreases with increase in the solid thickness. At high value of wall thickness, the temperature along the height is almost constant. For opposing flow at *N*=-0.5, temperature increases along the cylinder height for *D*=3.125%. However the increase in the solid wall thickness leads to decrease in the temperature along the cylinder height. Figure 4.6.3 shows the effect of increasing the thermal conductivity ratio between the solid and the porous medium which belongs for $Kr = 1$ keeping all other parameter same as that of Figure 4.6.2. It can be seen that the temperature at the interface wall has increased compared to that of Figure 4.6.2. This is because of increase in thermal conductivity ratio leads to better heat transfer in solid wall thus increasing the temperature of solid wall. As in previous case, the increase in solid wall thickness decreases the temperature of solid porous interface due to increase in the thermal resistance for heat transfer in the domain. It is found that the temperature of interface is almost equal for assisting and opposing flow for *D*=75%. Figure 4.4.4 shows the temperature along the radial direction at just beneath the top of the cylinder. The figure belongs to $Le = 1, Ra = 100, Rr = 1, Ar = 2$. The figure shows the temperature for two values of thermal conductivity ratio *Kr =0.1 & 1* and buoyancy ratio *N=0.5 &-0.5*. It be noted that the figure is plotted with $\bar{r} = 1\, to\, 2$ from left to right for *Kr = 0.1* and right to left for *Kr = 1*. It is obvious from Figure 4.6.4 that the temperature variation inside the solid wall is linear. Temperature along the domain in radial direction increases with increase in the solid wall thickness. Temperature gradient at the inner surface decreases with increase in the solid wall thickness which indicates that the heat transfer decreases with increases in the solid wall thickness. This happens because of increase in thermal resistance due to increase in thickness. The temperature in the domain for opposing flow is higher as compared to the assisting flow.

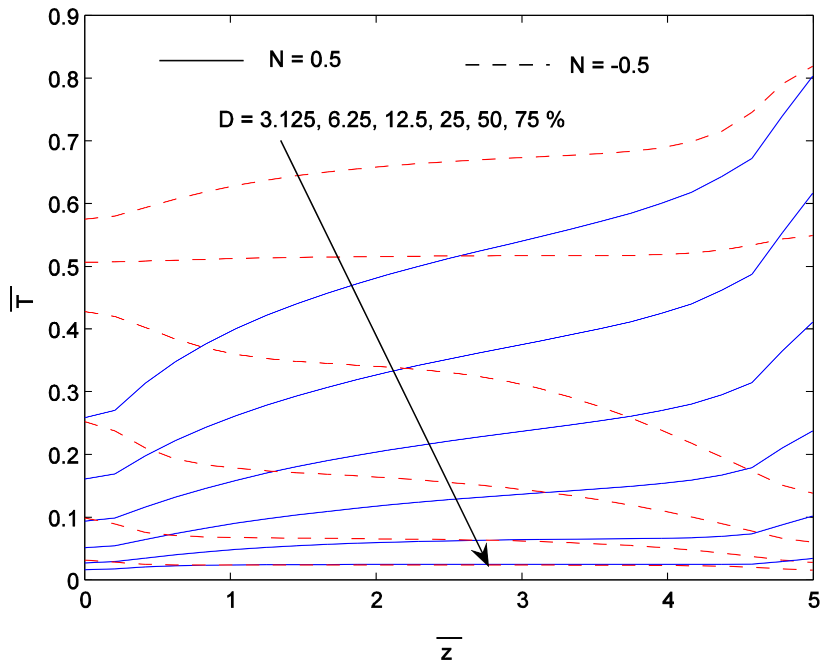

Figure 4.6.2: Temperature at interface for $Kr = 0.1$,

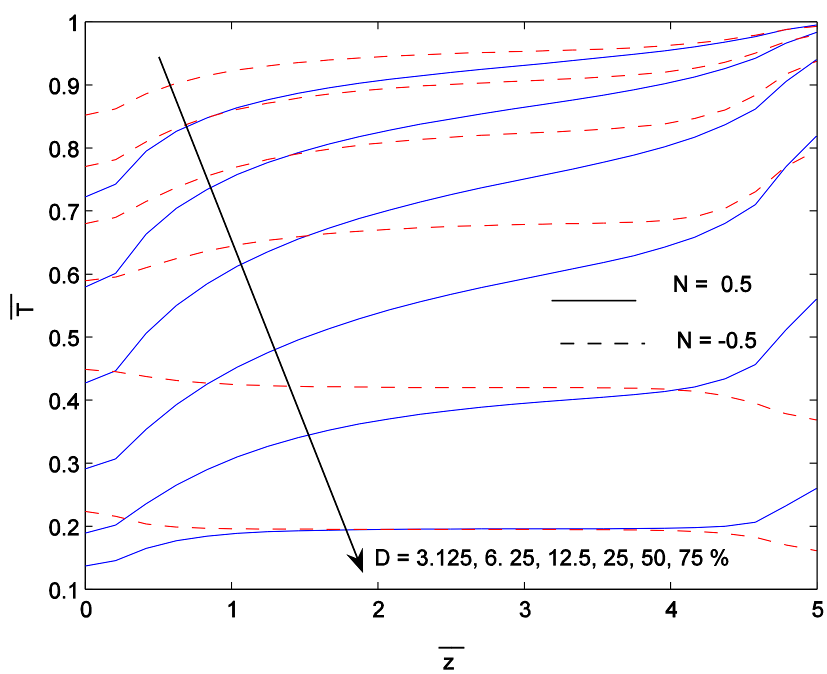

Figure 4.6.3: Temperature at interface for $Kr = 1$,

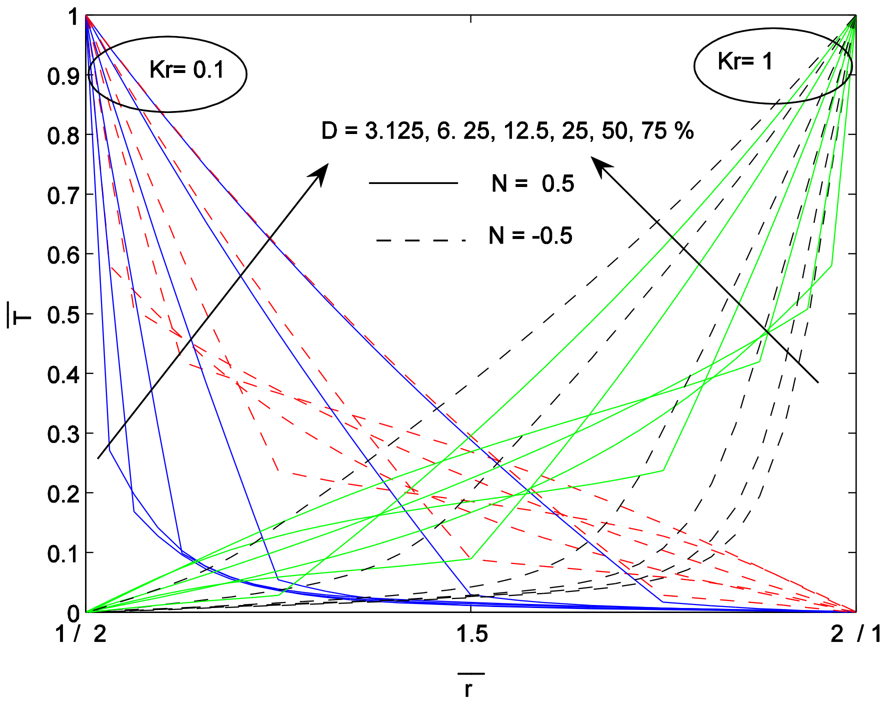

Figure 4.6.4: Temperature along radial direction

Figure 4.6.5 illustrates the effect of solid wall thickness on concentration profile along the cylinder height at just beside the solid porous interface in porous medium. This figure is obtained by setting the variables as $Le = 1, Ra = 100, Rr = 1, Ar = 2, Kr = 0.1$. It is seen that the concentration increases along the height of cylinder for assisting flow and decreases for opposing flow. This in turn leads to decrease in concentration gradient for assisting flow and increases for opposing flow along the height. The increase in concentration for assisting flow is substantial until 20% of the cylinder height which is followed by gradual increase. It is observed that the concentration is almost equal for assisting and opposing flow for D=75%. It is further seen that concentration increases with increase in solid wall thickness for assisting flow and decreases for opposing flow. Figure 4.6.6 shows the concentration variation along the radial direction at just beneath the top surface of the cylinder. This figure corresponds to $Le = 1, Ra = 100, Rr = 1, Ar = 5, Kr = 0.1$.

It is seen that the concentration profile is affected due to change in the thermal conductivity ratio of solid and porous region. The concentration gradient is higher at top of the cylinder for higher thermal conductivity ratio. The increase in solid wall thickness reduces the concentration gradient.

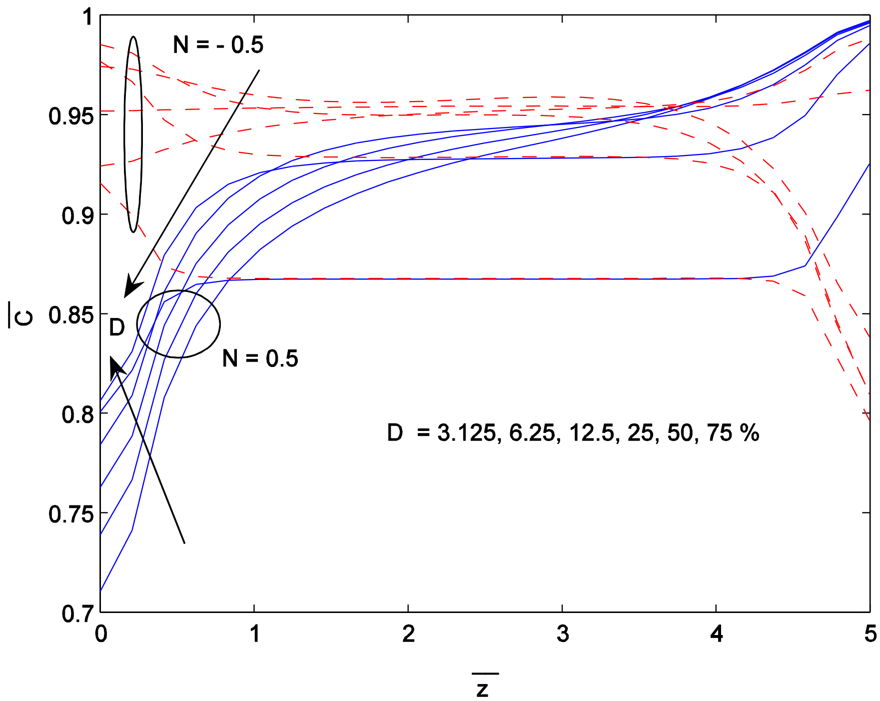

Figure 4.6.5: Concentration profile adjacent to solid porous interface

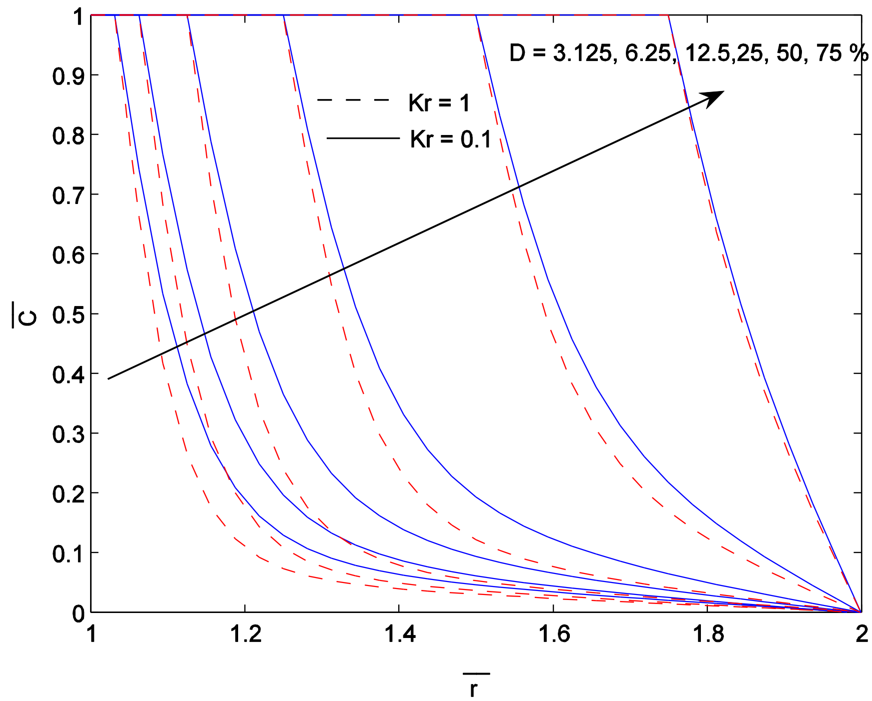

Figure 4.6.6: Concentration profile along the radial direction

The Figure 4.6.7 shows the orientation of the isotherms, iso-concentration and streamlines for *N=2 and -2*. The other constant parameters are set as $Le = 1, Ra = 100, Rr = 1, Ar = 5, Kr = 0.5$. When the buoyancy ratio changes from +2 to -2 the orientation of isotherms, iso-concentration lines and the streamlines changes completely, demonstrating the effect of assisting and opposing nature of buoyancy forces. The isotherms indicate that the heat transfer is higher at upper and lower section of cylinder for assisting and opposing flow respectively. Similar behaviour is observed for iso-concentration lines creating the higher concentration gradient in upper and lower region of cylinder which in turn leads to greater mass transfer at those sections of cylinder. The fluid flows from lower right to upper left corner and vice versa for assisting and opposing flows respectively.

Figure 4.6.8 demonstrates the effect of Lewis number on isotherms, iso-concentration and streamlines with the rest of the constant parameters set as *Ar=10 Rr=1 D=25, Kr=0.5 Ra=100, N=0.5*. The isotherms and iso-concentration lines move towards the hot surface with increase in the Lewis number. The effect of changing the solid wall thickness is depicted in figure 4.6.9 which is obtained for *Ar=5, Rr=1, Le=1, Kr=0.5 Ra=100*. The solid wall thickness is increased from 6.25% to 50 %. The isotherms are distorted at low wall thickness as compared that of high wall thickness which indicates that the convection is higher at low wall thickness. The heat transfer in upper part of cylinder is high for smaller wall thickness. This is because of the fact the fluid circulates more vigorously at upper section of cylinder as shown by the streamlines. The increase in wall thickness brings in the smoothness of fluid flow. The mass transfer is higher at upper part of cylinder for small wall thickness and the increase in the wall thickness leads to straighten the iso-concentration lines.

Figure 4.6.10 indicates the influence of thermal conductivity ratio between the solid wall and porous medium for the parameters *Ar=5, Rr=1, Le=1, Kr=0.5, Ra=100*. It is seen that the isotherms and iso-concentration lines move towards the hot surface due to increase in the thermal conductivity ratio. This means that the heat and mass transfer increases with increase in the thermal conductivity ratio between solid and porous medium. This could be attributed to the reason that the increase in *Kr* leads to reduction of thermal resistance in the medium which in turn enhances the heat transfer.

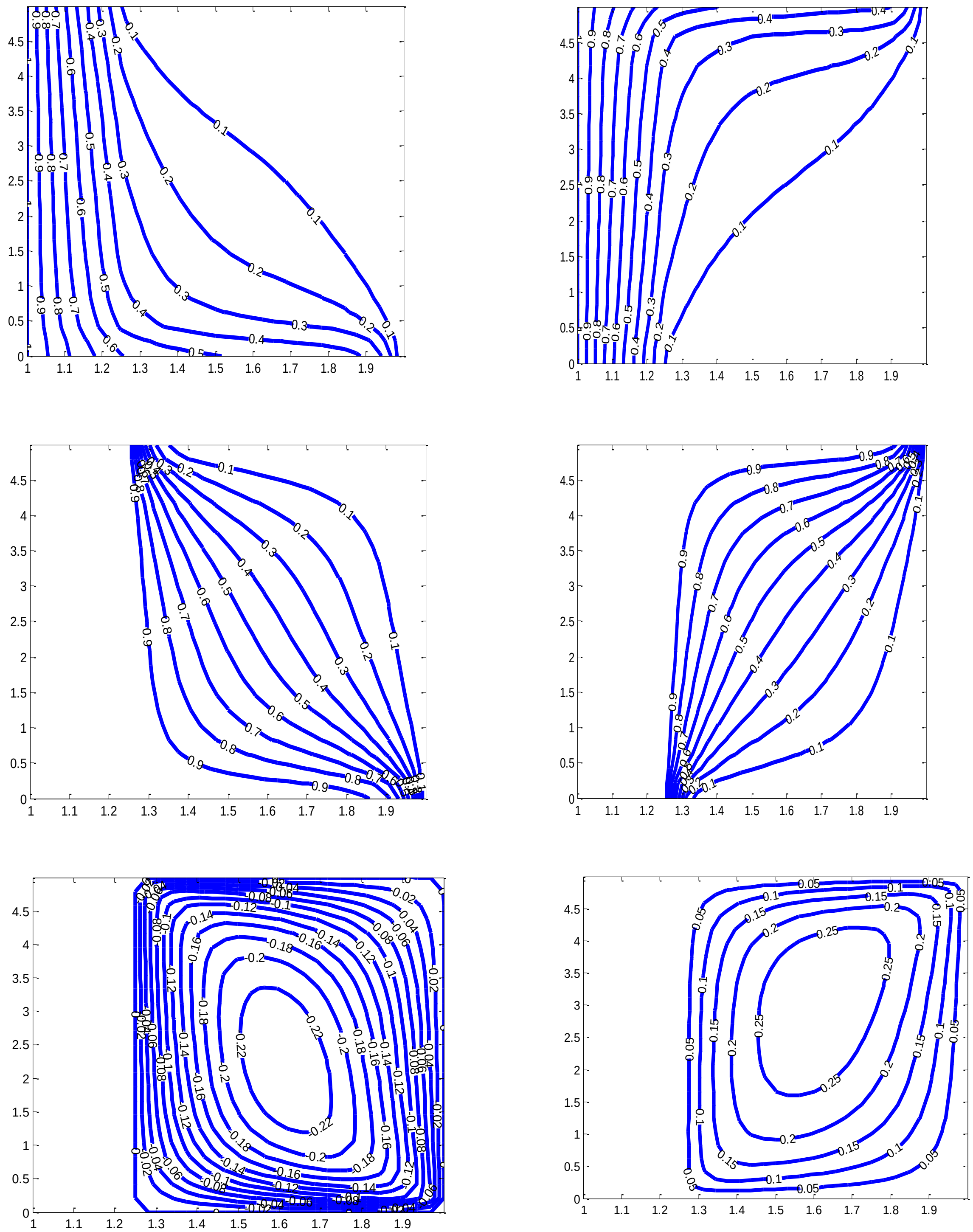

Figure 4.6.7: a) Isotherms b) Isoconcentration c) streamlines for $N=2,-2$, *for* $Ar=5$ $Rr=1$ $D=25$, $R_d=0$ $Le=1$

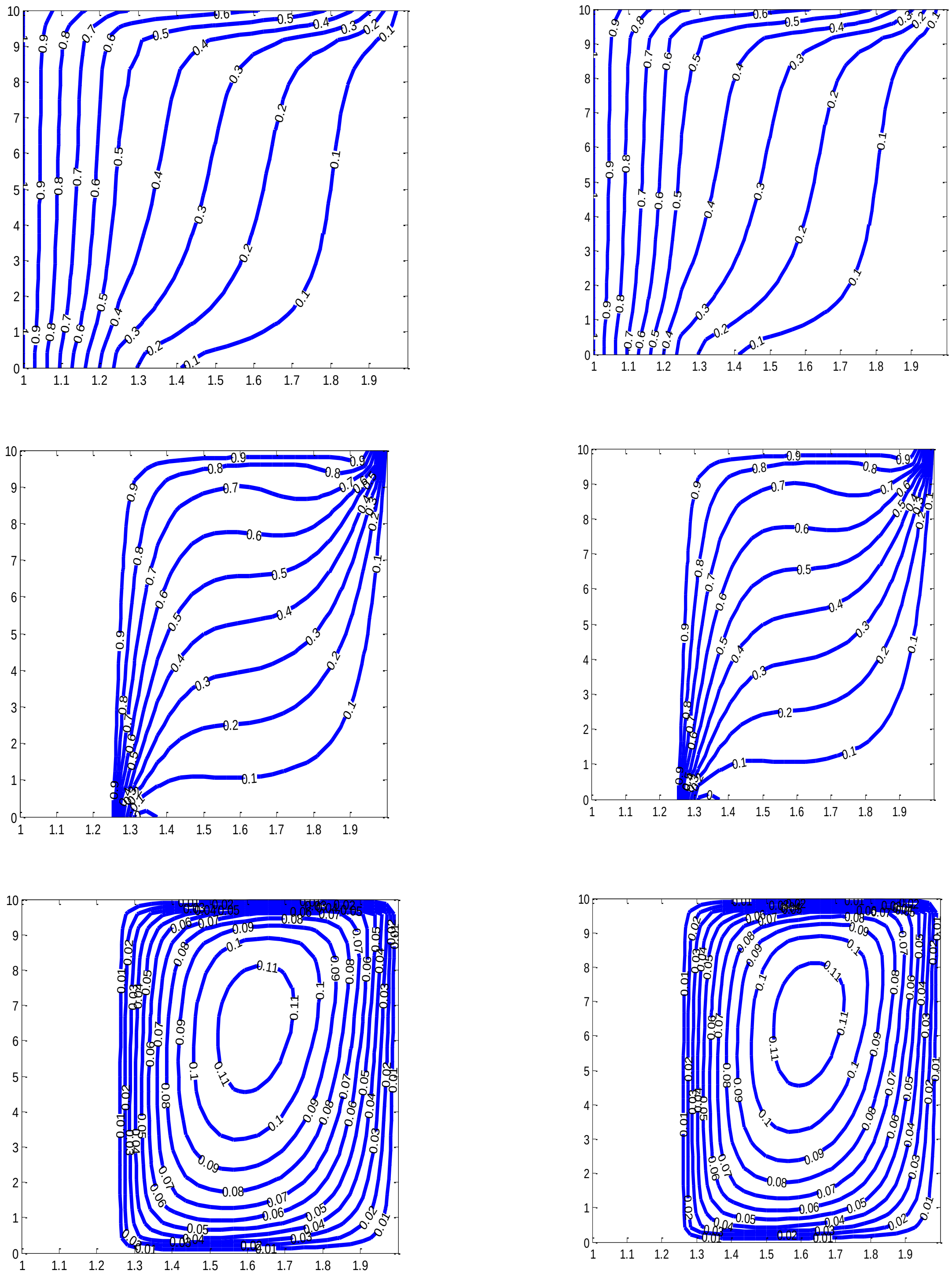

Figure 4.6.8: a) Isotherms b) Isoconcentration c) Streamlines for $Le=1\&10$, for $Ar=10$ $Rr=1$ $D=25$, $R_d=0$ $K=0.5$

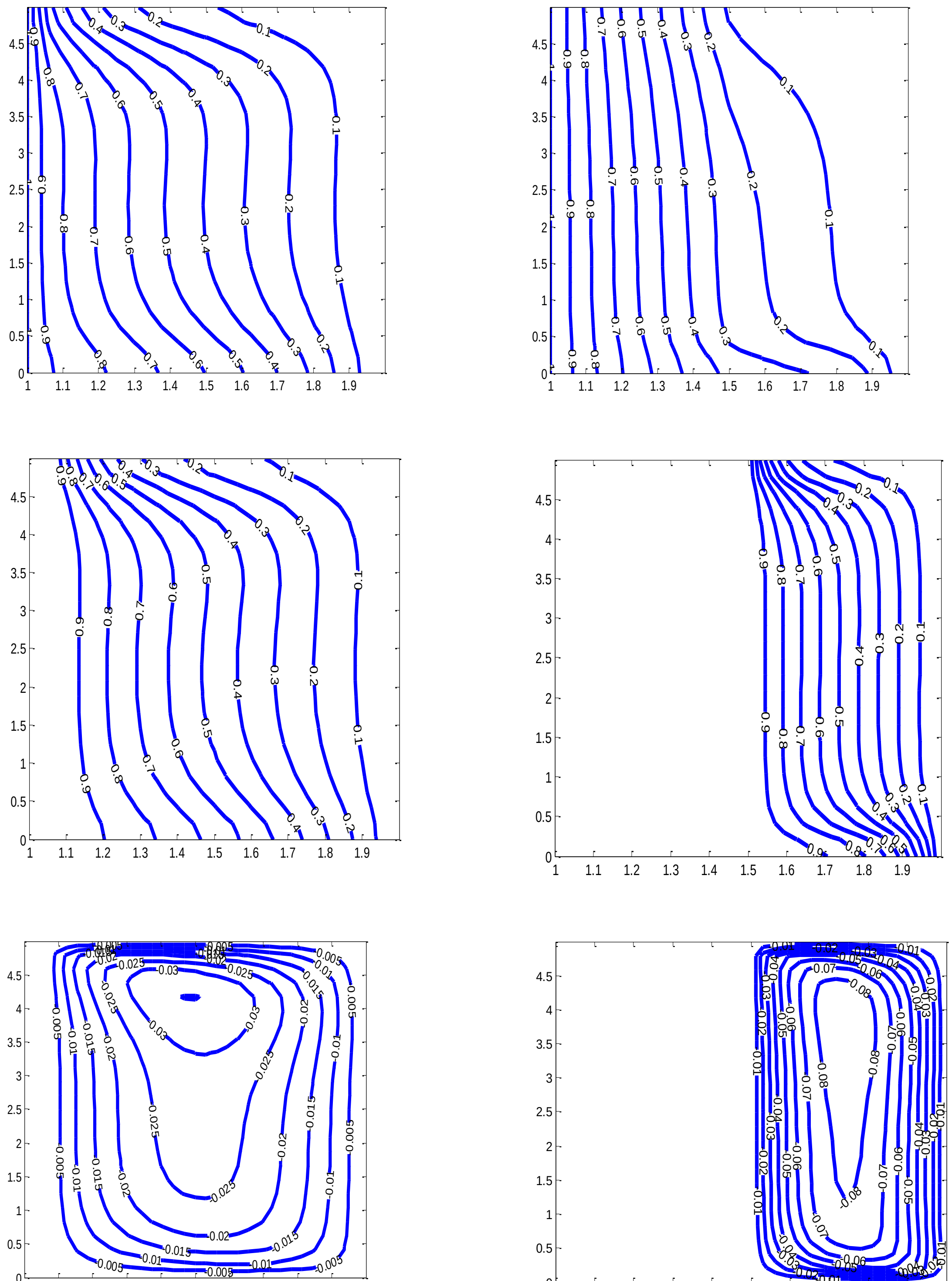

Figure 4.6.9: a) Isotherms b) Isoconcentration c) Streamlines for $D=6.25\&50$, *for* $Ar=5$ $Rr=1$, $Le=1$ $R_d=0$

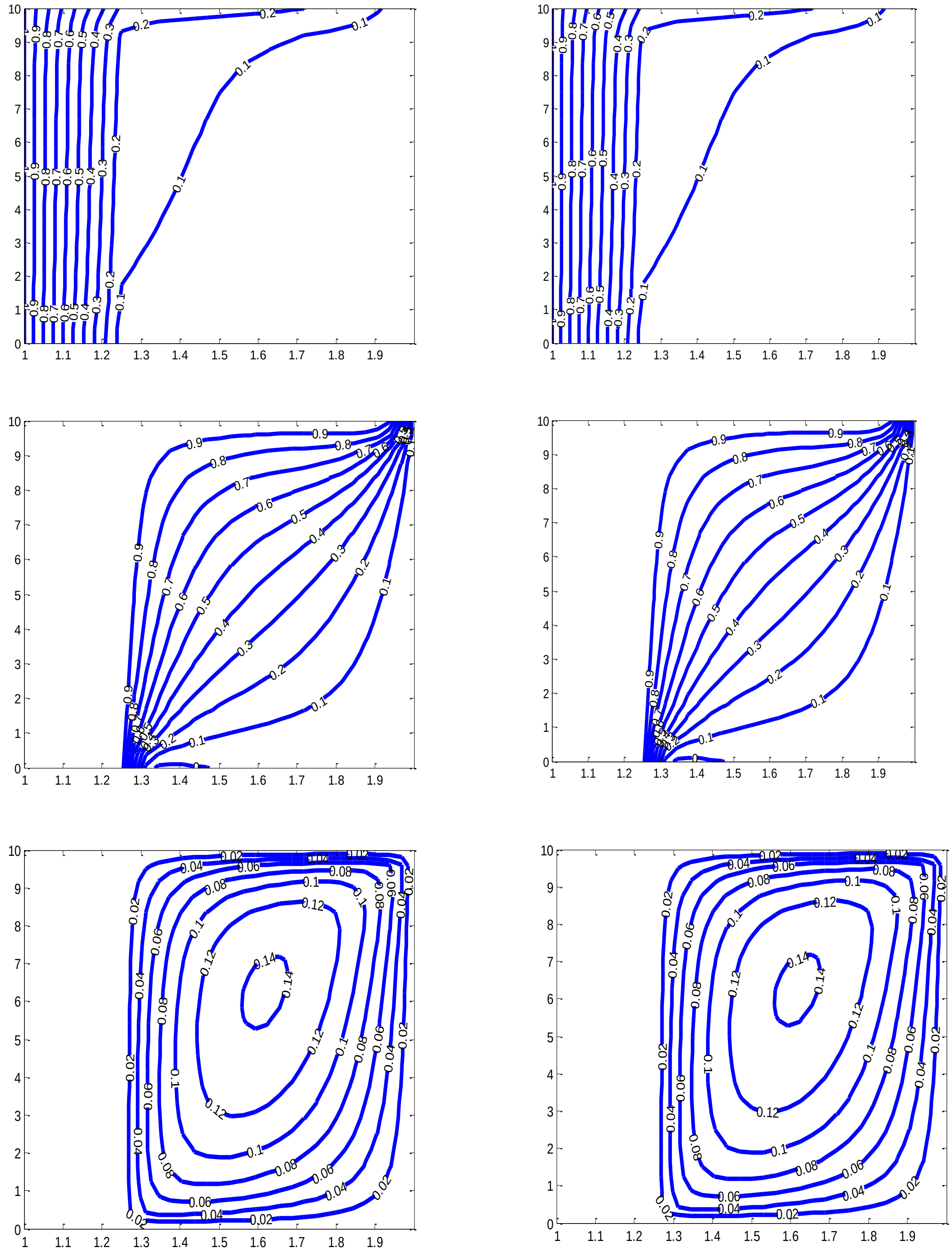

Figure 4.6.10 :a)Isotherms b)Isoconcentration c)Streamlines for *Kr=0.1&10*, *for Ar=10 Rr=1,Le=5,D=25,*R_d*=0,Ra=100 N=-1*

4.6.2b Heat and Mass Transfer in terms of Nusselt and Sherwood Number

The heat and mass transfer in the porous medium is represented in terms of Nusselt and Sherwood numbers respectively. Figure 4.6.11 shows the Nusselt number variation with respect to solid wall thickness. This figure corresponds to $Le = 5, Ra = 50, Rr = 1$. It is found that the heat transfer rate increases with increase in the thermal conductivity ratio between the solid wall and porous medium. This could be related to increased solid-porous interface temperature due to increase in *Kr* which in turn sets high temperature gradient thus increasing the Nusselt number. It is observed that the Nusselt number deceases with increase in the solid wall thickness. The increased solid wall reduces the temperature gradient at the interface leading to reduction in the Nusselt number. It is observed that at low conductivity ratio, the Nusselt number decreases with increase in the solid wall thickness, however at high conductivity ratio, Nusselt number increases with increase in the thickness of the wall. The Nusselt number is high for assisting flow as compared to that of opposing flow. As expected, the heat transfer is high for *Ar = 5* as compared to that of *Ar =10*. The effect of aspect ratio is negligible when conductivity ratio is low. It is further seen that the Nusselt number decreased due to increase in the Lewis number. The influence of solid wall thickness, thermal conductivity ratio along with Lewis number is depicted in Figure 4.6.12 which corresponds to $N = 5, Ra = 50, Rr = 1$. It is seen that the increase in Lewis number reduces the heat transfer rate for all values of *Kr*. It is found that the effect of buoyancy ratio, Lewis number, thermal conductivity ratio and the aspect ratio diminishes as the solid wall thickness increases. This could be related to the fact that the increase in solid wall thickness reduces the temperature at the solid porous interface at which the effect of above mentioned parameters is minimal.

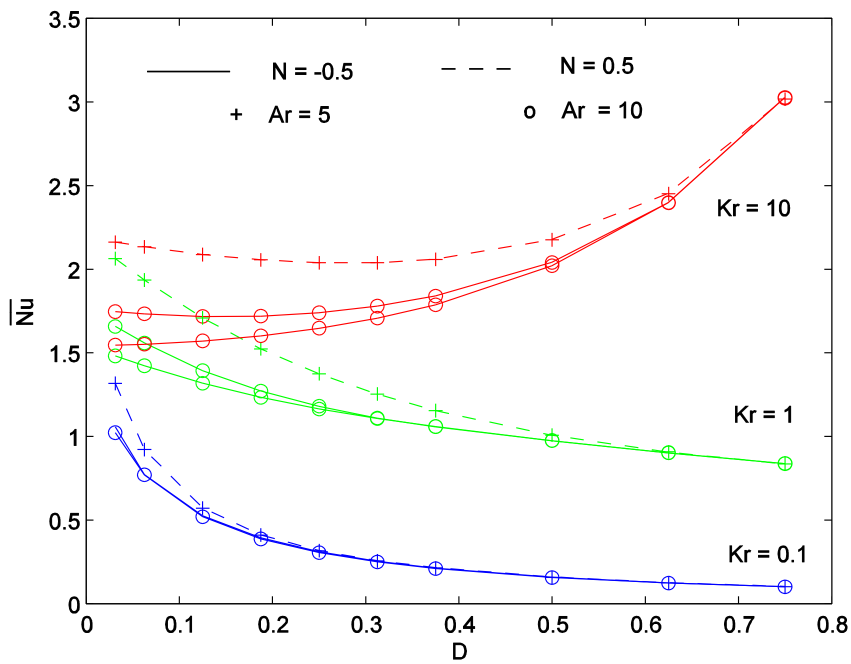

Figure 4.6.11: Nusselt number variation with respect to *D* and *N*

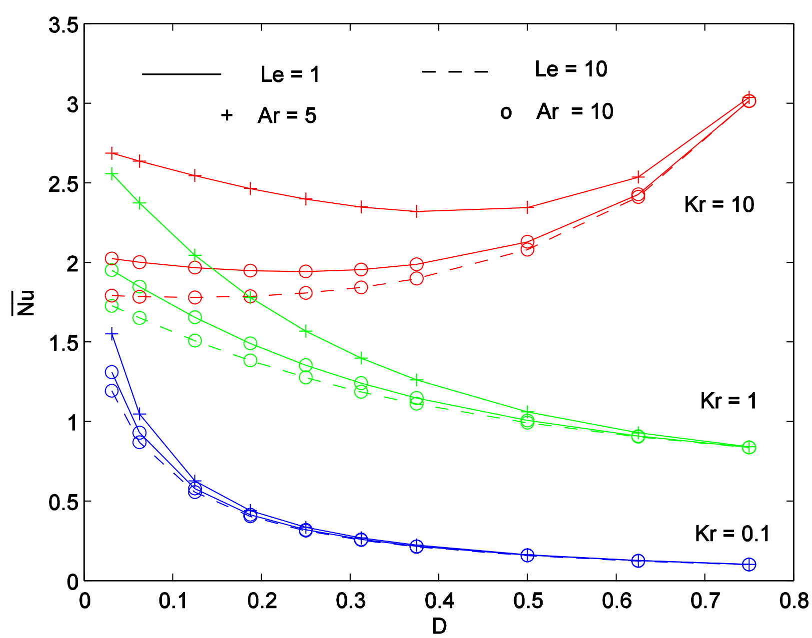

Figure 4.6.12: Nusselt number variation with respect to *D* and *Le*

The mass transfer from the hot surface to the porous medium is represented in terms of Sherwood number. Figure 4.6.13 illustrates the effect of solid wall thickness on the mass transfer for $Le = 5, Ra = 50, Rr = 1$. It is found that the average Sherwood number initially decreases with increase in solid wall thickness until certain thickness and then increases with further increase in D. This trend is seen for higher values of Lewis number. However for *Le=1*, the Sherwood number increases with increase in solid wall thickness for all values of aspect ratio, buoyancy ratio, thermal conductivity ratio etc. as indicated in Figure 4.6.14 which belongs to $N = 1, Ra = 50, Rr = 1$ For a given value of solid wall thickness, the effect of *Kr* is higher at higher Lewis number.

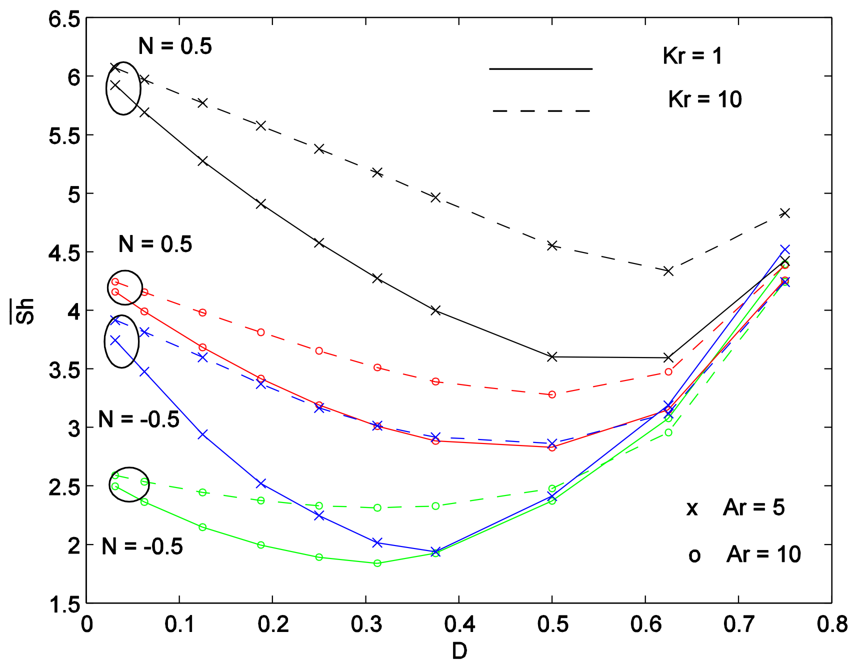

Figure 4.6.13: Effect of *D* and *N* on Sherwood number

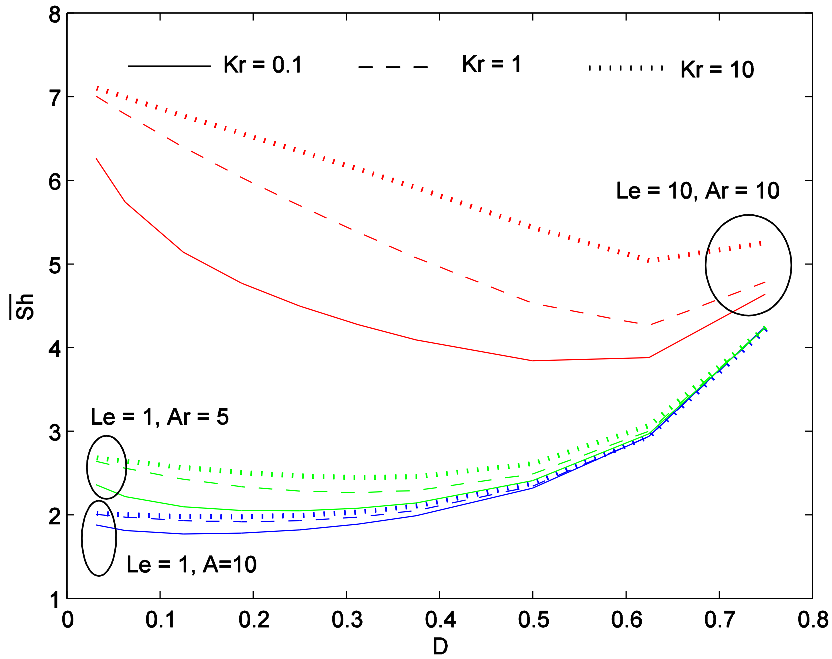

Figure 4.6.14: Effect of *D* and *Le* on Sherwood number

4.6.3 Validation of the Results

The present research work has been validated to the previously published research work by eminent researchers and it is found to be in good agreement with those results. Figure 4.6.15 and Table 4.6.1 shows the comparison and validation of the present results with the published data.

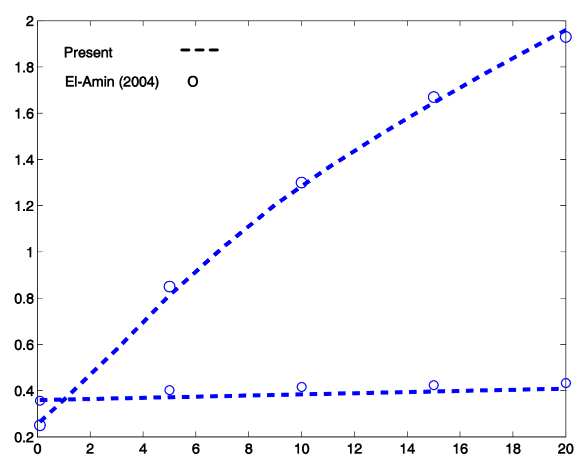

Figure 4.6.15: Comparison of results with previously published work

Table 4.6.1: Comparison of results for different aspect ratio at $Ra = 100, Rr = 1, D = 0$

N	Le	$Nu_z / Ra_z^{1/2}$			$Sh_z / Ra_z^{1/2}$		
		(Yih, 1999)	(Nakayama and Hossain, 1995)	Present	(Yih, 1999)	(Nakayama and Hossain, 1995)	Present
0	1	0.4437	0.444	0.4325	0.4437	0.444	0.4325
0	2	-	0.444	0.4325	-	0.693	0.6912
0	4	-	0.444	0.4325	-	1.053	1.1093
0	6	-	0.444	0.4325	-	1.332	1.4075
0	8	-	0.444	0.4325	-	1.568	1.6357
0	10	0.4437	0.444	0.4325	1.6803	1.776	1.8268
0	100	0.4437	0.444	0.4325	5.5445	6.061	6.3780
1	1	0.6276	0.628	0.6551	0.6276	0.628	0.6551
1	2	-	0.593	0.6307	-	0.937	1.0420
1	4	-	0.559	0.5944	-	1.383	1.5808
1	6	-	0.541	0.5687	-	1.728	1.9535
1	8	-	0.529	0.5496	-	2.019	2.2471
1	10	0.5214	0.521	0.5347	2.2020	2.276	2.4967
1	100	0.4700	0.470	0.4386	7.1389	7.539	7.7022

4.7 The study of the effect of length and location of heater in a porous annulus; a thermal non equilibrium approach

4.7.1 Introduction

The present problem focuses to study the heat transfer in a vertical annular cylinder subjected to discrete heating. The geometry and the corresponding boundary conditions are shown in Figure 4.7.1 along with its description in chapter 3 section 3.6

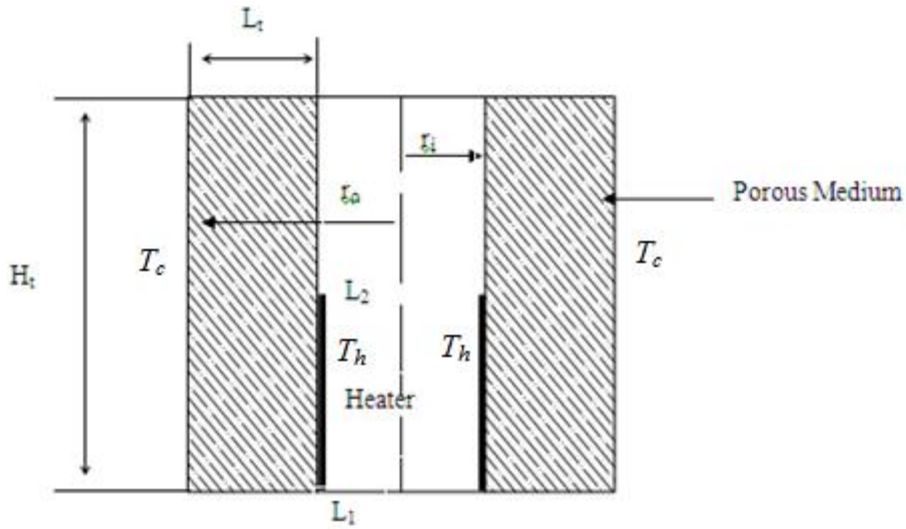

Figure 4.7.1: Schematic of discrete heating in an annular porous cylinder

4.7.2 Analysis

Figure.4.7.2 shows the streamlines and the isothermal lines for fluid and solid when heater is placed at the bottom section of the inner radius. The bottom of the heater always coincides with $\overline{z} = 0$ for three lengths i.e. *HL*= 20%, 35% and 50% indicating that the heater length varies from bottom to upward direction in all the three cases. The streamline and isothermal figures for Case I, corresponds to constant values of$Ra = 100, Rd = 1, A_r = 2, R_r = 1\ H = 15, and\ \ K = 1$. It is seen that the fluid movement is restricted to only a small section at the lower part of the annulus for *HL*=20%. However the circulation region has occupied considerable part of the porous medium when heater length is increased to 35% and beyond. It is also seen that the fluid cell moves towards the central part of the annulus when heater length is increased. The increased heater length leads to higher amount of thermal energy penetration inside the depth of the porous medium along the radial direction in solid as well as fluid phase. It is seen that the increased heater length has higher effect on fluid than the solid phase which is reflected by greater area of porous medium being occupied by higher temperature fluid isotherms as compared to that of solid isotherms. This can be attributed to the fact that the main energy transport mode in solid is by conduction whereas convective current plays vital role in energy transfer in fluid phase.

Figure 4.7.3 shows the effect of heater placement at the center of the inner radius. In this case the center of the heater always coincided with $\bar{z} = A_r$. Careful observation of Figure 4.7.3 reveals that the isothermal lines of solid phase move towards the hot wall indicating that the heat transfer rate increases with the heater length. It is also observed that the isothermal lines (solid phase) in lower part of heater for *HL* =35%, are nearer to hot surface than the upper portion of the heater which reflects that the local Nusselt number increases along the length of the heater. However, Figures 4.7.3a and 4.7.3c indicate that the local Nusselt number does not vary much along the heater length. The fluid isotherms reveals that the local Nusselt number for fluid increase along the heater length for HL=20% and 50%. The fluid is seen to move in an oval shaped cell from lower right to upper left portion of annulus for *HL*=20% but changes the direction towards lover left to upper right portion of annulus when heater length is increased to 50% .

Figure 4.7.4 depicts the streamlines and isothermal lines when heater is placed at the top section of the annulus. The top of the heater always coincides with $\bar{z} = A_r$ for all three heater lengths. It is seen that the fluid moves in two separate regions of the annulus when heater length is 20% of annuls height. The fluid cell moves from lower part to occupy the whole annulus as the length of the heater increases. The fluid movement changes the shape from being circular at *HL*=20% to oval shape at *HL*=50%

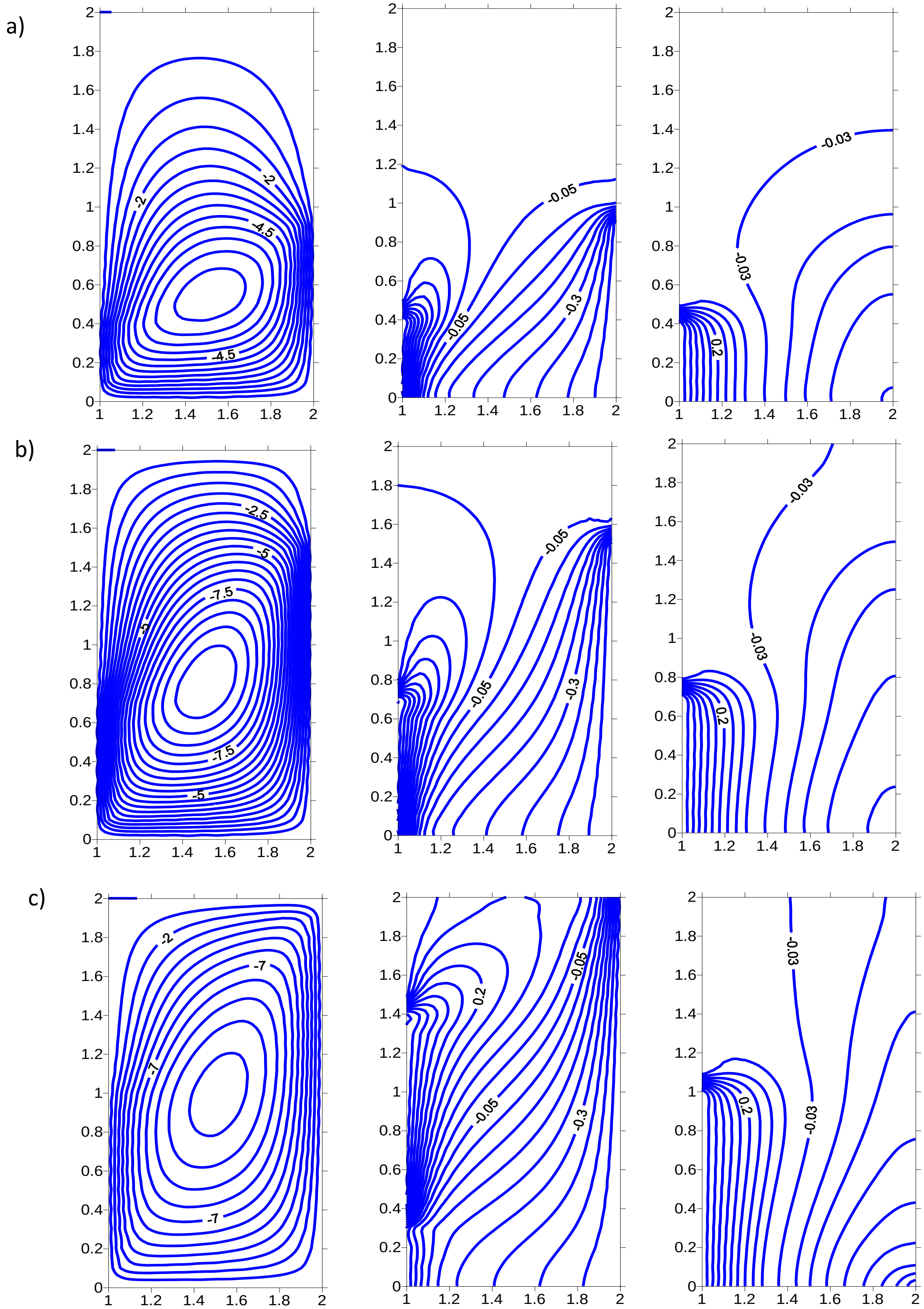

Figure 4.7.2: Streamlines (left) Isotherms for fluid (center) and solid (right) for heart placed at bottom section of the inner radius a) *HL*=20% b) *HL*=35% c) *HL*=50%

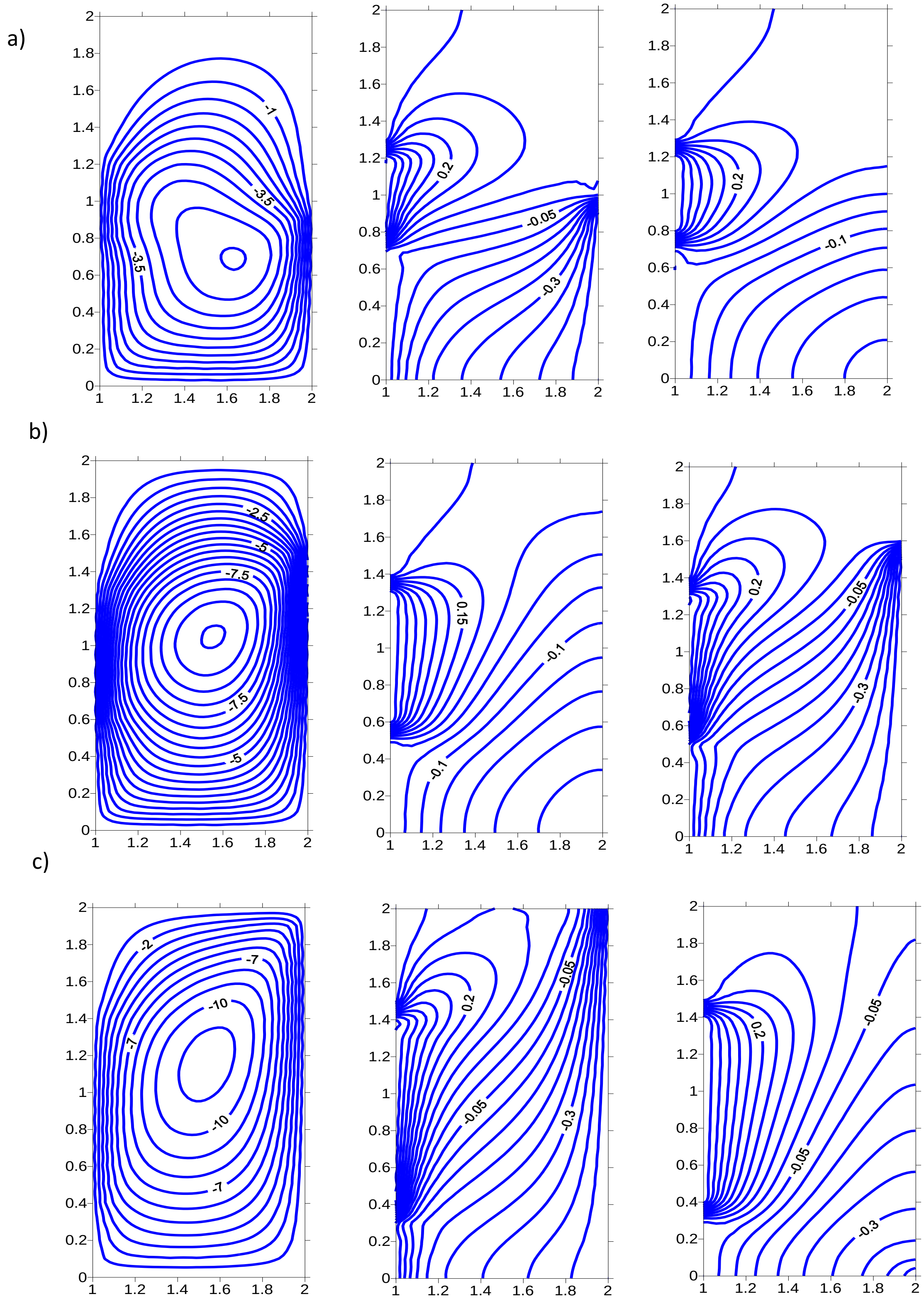

Figure 4.7.3: Streamlines (left) Isotherms for fluid (center) and solid (right) for heater placed at mid-section of the inner radius a) *HL*=20% b) *HL*=35% c) *HL*=50%

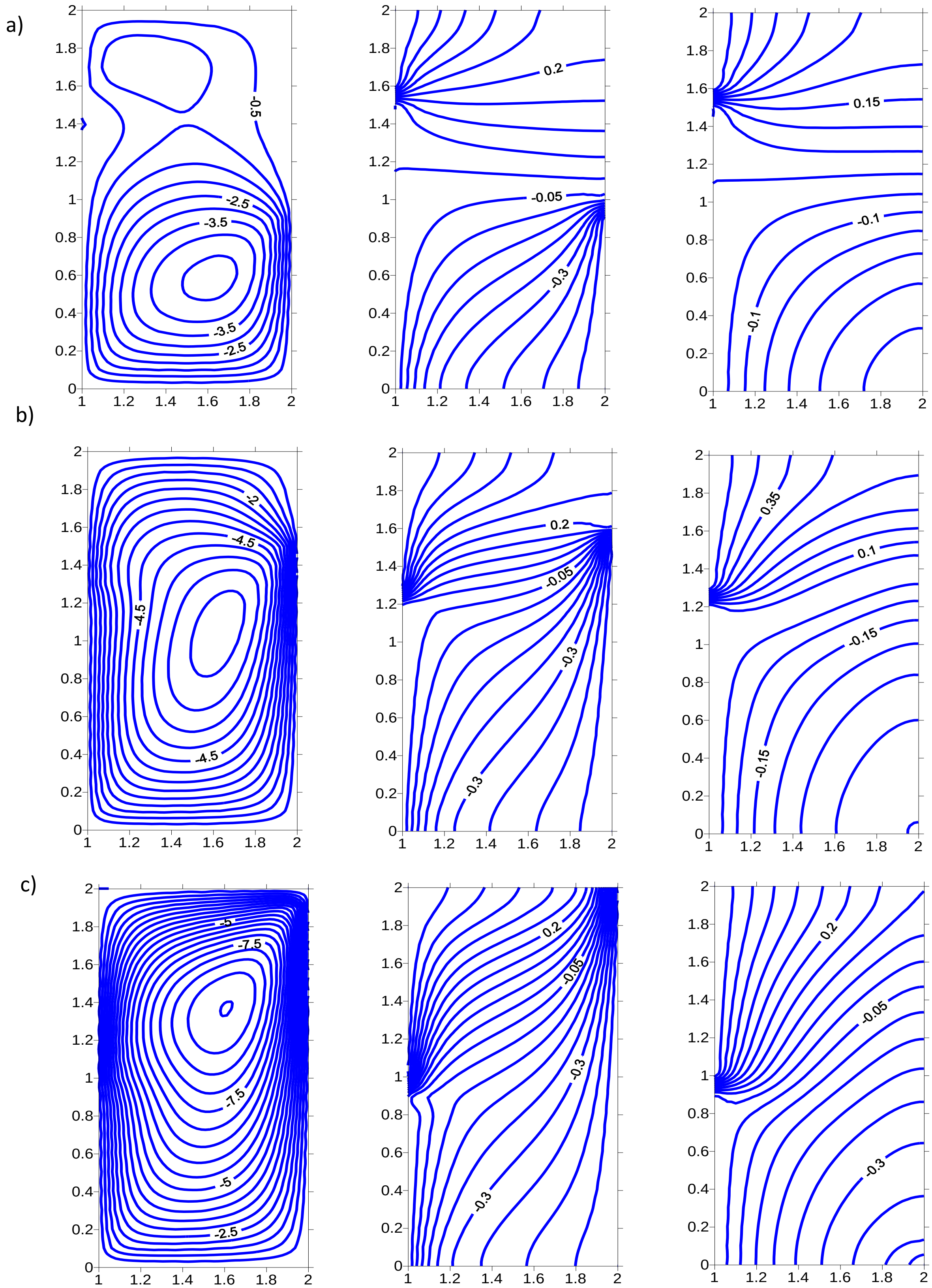

Figure 4.7.4: Streamlines (left) Isotherms for fluid (center) and solid (right) for heater placed at top section of the inner radius a) *HL*=20% b) *HL*=35% c) *HL*=50%

Figure 4.7.5 shows the average Nusselt number variation with respect to the interphase heat transfer coefficient when the heater is placed at the bottom section of the cavity. It may be noted that the heater length is varied in 3 steps i.e. 20%, 35% and 50% of the total height of the cylinder. Figure.4.7.5 corresponds to the constant values of the parameters$= 100, Rd = 1, A_r = 2, R_r = 1 \; and \; Kr = 10$. It is obvious from figure 4.5.5 that the average Nusselt number for fluid ($\bar{N}u_f$), solid ($\bar{N}u_s$) and total Nusselt number ($\bar{N}u_t$) increases with increase in the heater length. It is also evident that average Nusselt number for solid phase is influenced considerably because of change in H. It is evident from figure. 4.5.5 that the heat transfer rate in solid phase initially decreases with increase in interphase heat transfer coefficient until $H \leq 0.6$ and thereafter starts increasing with increase in$H$.

Figure 4.7.6 shows the average Nusselt number variation with respect to the conductivity ratio for heater placed at the central section of annulus. The other parameters relevant to figure 4.5.6 are $Ra = 100, Rd = 1, A_r = 2, R_r = 1 and \; H = 15$. It is clear that the average Nusselt number decreases initially with increase in Kr and then starts increasing at higher values of *Kr* for all the three lengths of heater being investigated. It is also evident that the effect of *Kr* is greater if the heater is of shorter length.

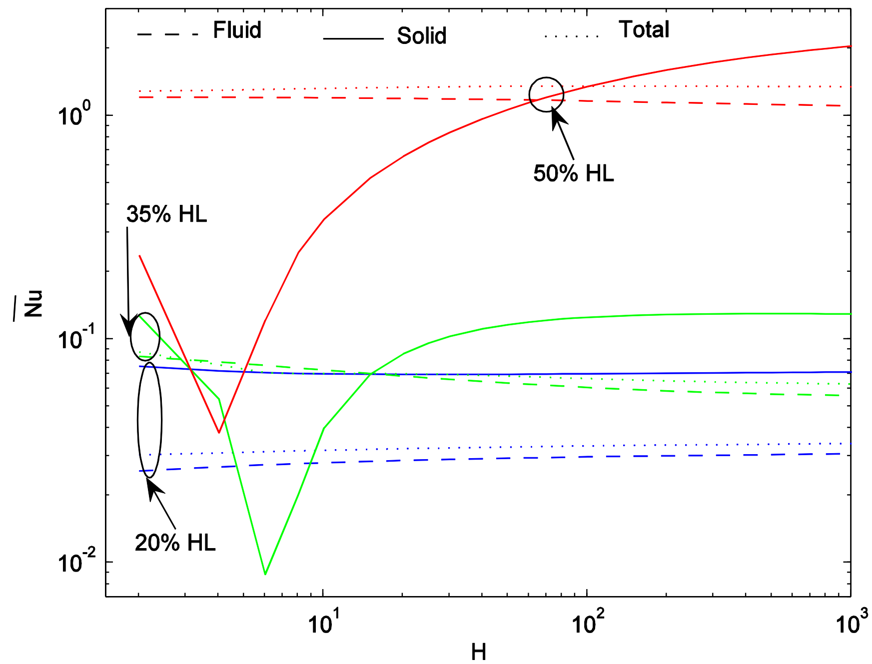

Figure 4.7.5: Average Nusselt number variation with H and different heater length at bottom section of the annulus

Figure 4.7.7 depicts the heat transfer behaviour inside the porous annulus when subjected to varying interphase heat transfer coefficient and also the heater length placed at the mid of the cylinder. It be noted that the mid of the heater coincides with center of the inner surface of annulus in all three cases of heater length i.e. 20%, 35% and 50%. The figure is obtained by taking the values of parameters such as. $Ra = 100, Rd = 1, A_r = 2, R_r = 1 and\ Kr = 10$. As seen from Figure 4.7.7, it is clear that the $\bar{N}u_s$ increases continuously with increase in interphase heat transfer coefficient. It is interesting to note that the average Nusselt number for 20% of heater length is greater than that of 35% and 50% heater length. Thus it is advisable to use shorter heater length if the objective is to have higher heat transfer rate when heater is placed at the center of the annulus.

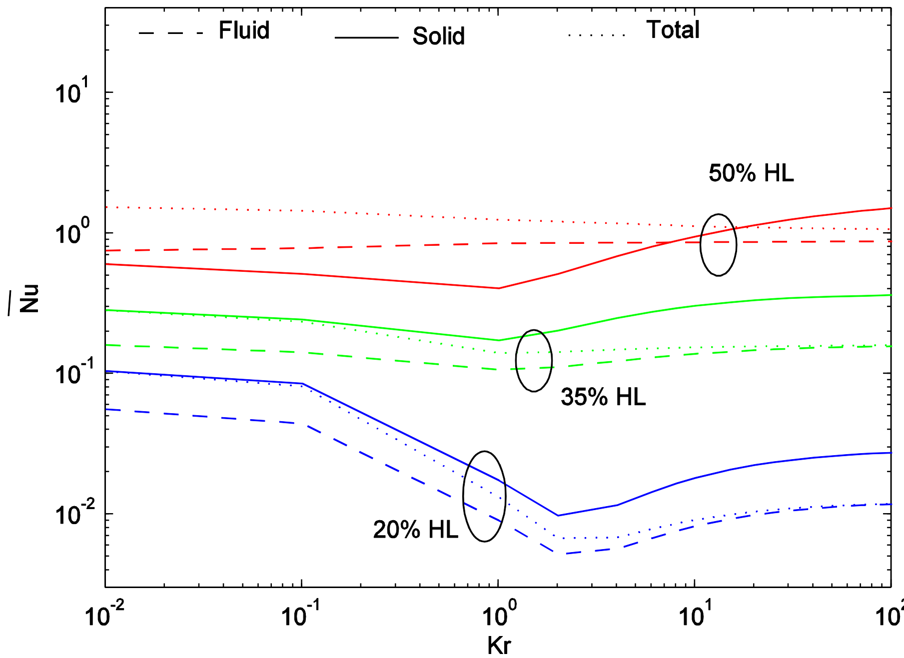

Figure.4.7.6: Average Nusselt number variation with *Kr* and different heater length at Bottom section of the annulus

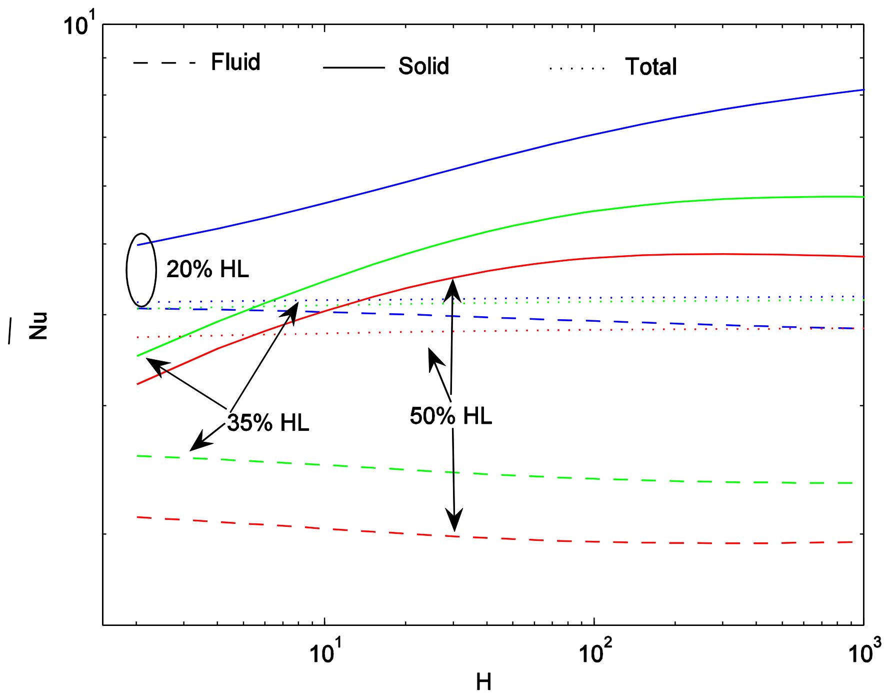

Figure 4.7.7: Average Nusselt number variation with *H* and different heater length at mid-section of annulus

Figure 4.7.8 shows the average Nusselt number variation with respect to H for heater placed at top section of inner radius with $Ra = 50, Rd = 1, A_r = 2, R_r = 1 and\ K = 100$. The fluid Nusselt number remains constant with H as in other cases. The influence of H is higher for the case when HL=50% compared to lower heater lengths.

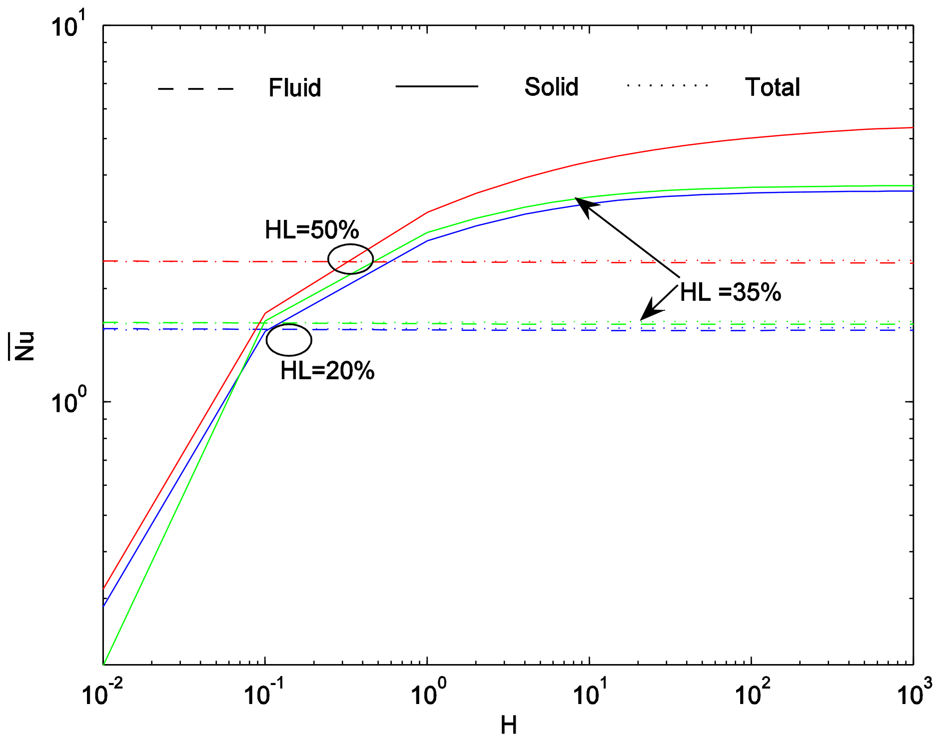

Figure 4.7.8: Average Nusselt number variation with H and different heater length at top section of annulus

Case II

Figure 4.7.9 shows the streamlines and isothermal lines for the boundary conditions corresponding of Case II, when heater is placed at the mid of the annulus**.** The other parameters corresponding to Figure 4.7.9 are set as $Ra = 100, Rd = 1, A_r = 2, R_r 1\ \ and\ H = 15, Kr = 1$. It obvious from figure 4.7.9, that there are two distinct flow regimes due to discrete heating at the inner radius. The smaller flow regime is mostly concentrated near the top inner radius of the annulus. The main flow regime is located in the area covering almost 2/3rd of the annulus and further increases in size with increase in the heater length. This in turn pushes the smaller flow regime to top left corner of the annulus. There is a prominent mismatch between the isotherms of fluid and solid phase showing existence of strong thermal non-equilibrium among solid and fluid phases of porous medium. The effect of increased heater length is to push the low temperature lines of fluid phase towards the outer radius thus increasing the thermal energy content of the fluid phase. It can be seen that there is a marked difference in fluid flow pattern when the heat is supplied to only solid phase at the hot wall as compared to Case I (Figure 4.7.3) where heat is supplied to both solid and fluid phases. The flow pattern is comparatively weaker in Case II. The isotherms of fluid and solid in Figure 4.7.9 indicates the stronger thermal non-equilibrium in case II as compared to case I (Figure. 4.7.3)

Figure 4.7.10 shows the streamlines and isothermal lines when same length of heater (*HL*=50%) is placed at the bottom, mid and top section of the annulus. It is seen that the flow regime is strongest among three positions when heater is placed at the bottom of the annulus followed by mid and then top section of annulus.

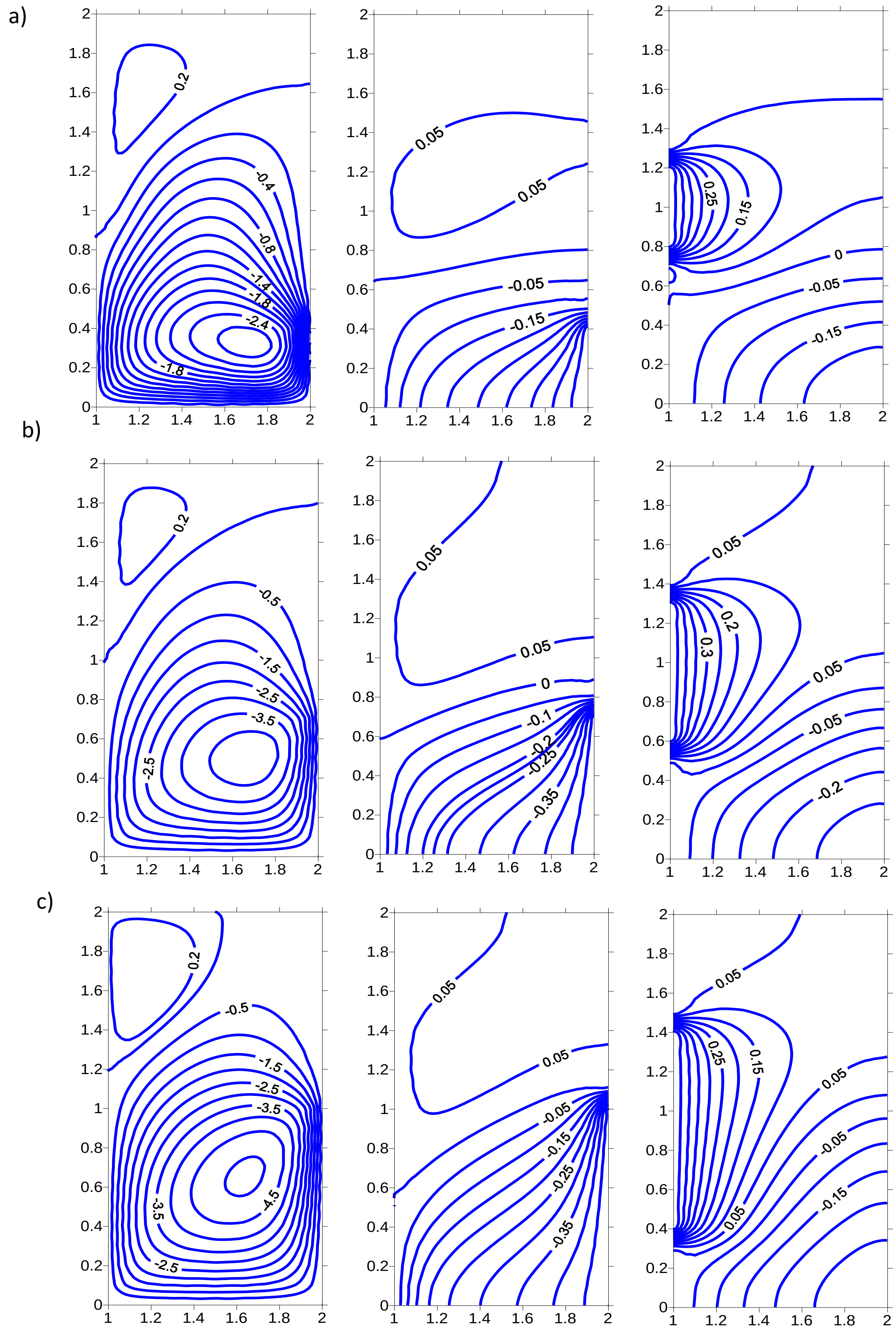

Figure 4.7.9: Streamlines (left) and isothermal lines for fluid (center) and solid (right) when heater is placed at the center of annulus a) *HL*=20% b) *HL*=35% c) *HL*=50%

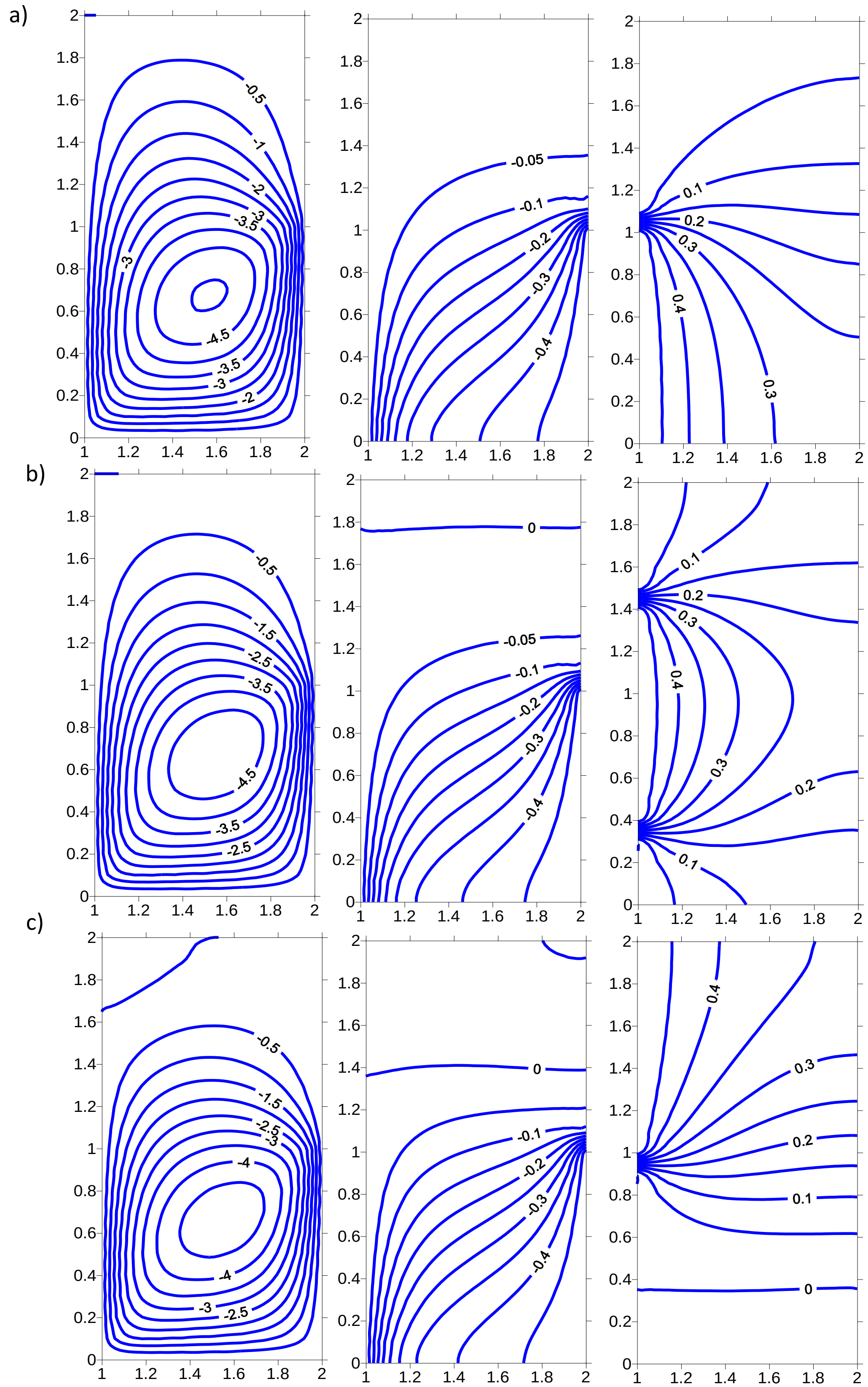

Figure 4.7.10: Streamlines (left) and isothermal lines for fluid (center) and solid when (right) *HL*=50% and heater is placed at a) Bottom b) Mid c) Top, section of annulus

Figure 4.7.11 shows the heat transfer behaviour for the porous medium corresponding to boundary conditions of Case II. The figure corresponds to the situation when heater is placed at the bottom section of the annulus. It may be noted that the Nusselt number variation with respect to H for case II is obtained with the parameters $Ra = 100, Rd = 1, A_r = 2, R_r = 1 and\ Kr = 15$. It is observed that the solid phase heat transfer is higher when the length of the heater is more. The $\bar{N}u_s$ initially decreases for $H \leq 0.1$ and thereafter starts increasing to achieve constant value for heater length of 20% and 35 %. However, the $\overline{Nu}_S$ keep increasing with respect to increase in H for HL=50%. Figure 4.7.12 indicates the variation of Nusselt number with respect to Kr for various heater lengths. It may be noted that the Nusselt number variation with respect to Kr of case II is obtained with the parameter $Ra = 100, Rd = 1, A_r = 2, R_r = 1 and\ H = 15$. It is observed that the heat transfer attains minimum value approximately at $Kr = 1$

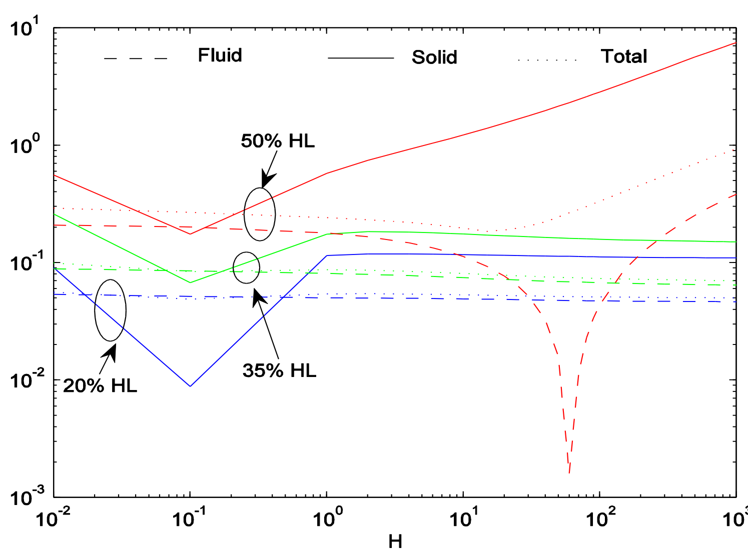

Figure 4.7.11: Average Nusselt number variation with H and different heater length at bottom section of annulus

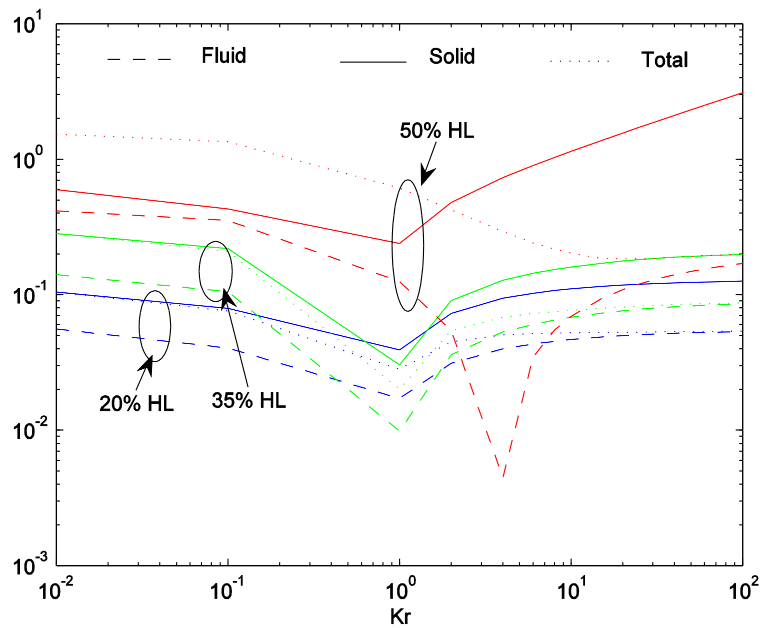

Figure 4.7.12: Average Nusselt number variation with *Kr* and different heater length at bottom of annulus

Figure 4.7.13 shows the Nusselt number variation when the heater is placed at the central section of the inner radius of annulus. The heat transfer in solid phase is not much affected by the length of the heater when it is placed at the center of the annulus. This shows that the local Nusselt number almost remains constant throughout the heater length when placed at the center of the annulus. The fluid Nusselt number initially decreases and then starts increasing with increase in *H*. Figure 4.7.14 depicts the Nusselt number variation with respect to *Kr*. It is interesting to note that the heat transfer rate in solid phase is higher when the heater length is shorter for smaller values of conductivity ratio but the effect of heater length vanishes as the value of *Kr* increases. Contrary to the previous case, the fluid Nusselt number shows noticeable influence of heater length with higher values of *Kr*.

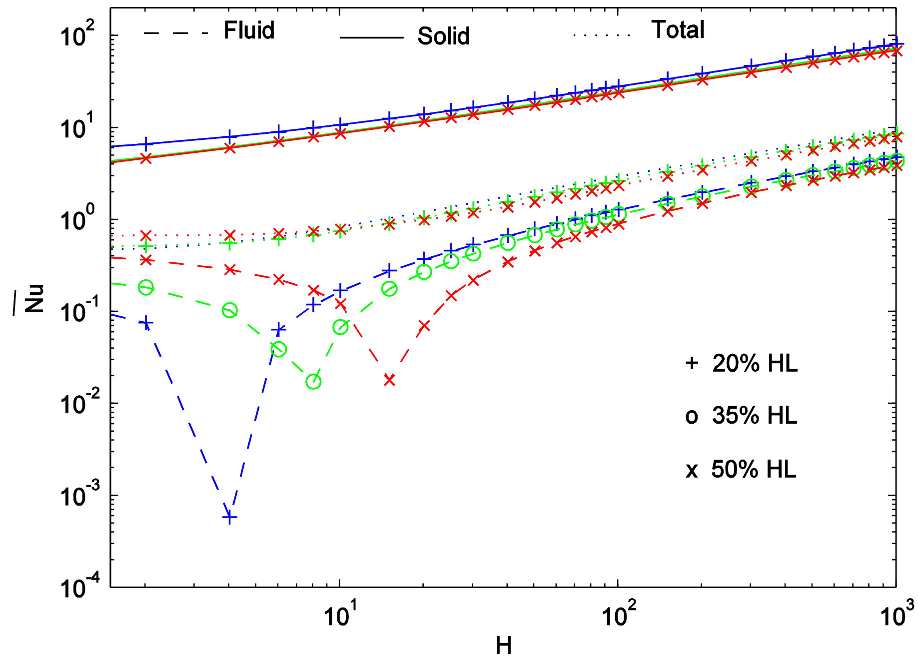

Figure 4.7.13: Average Nusselt number variation with *H* and different heater length at mid-section of the annulus

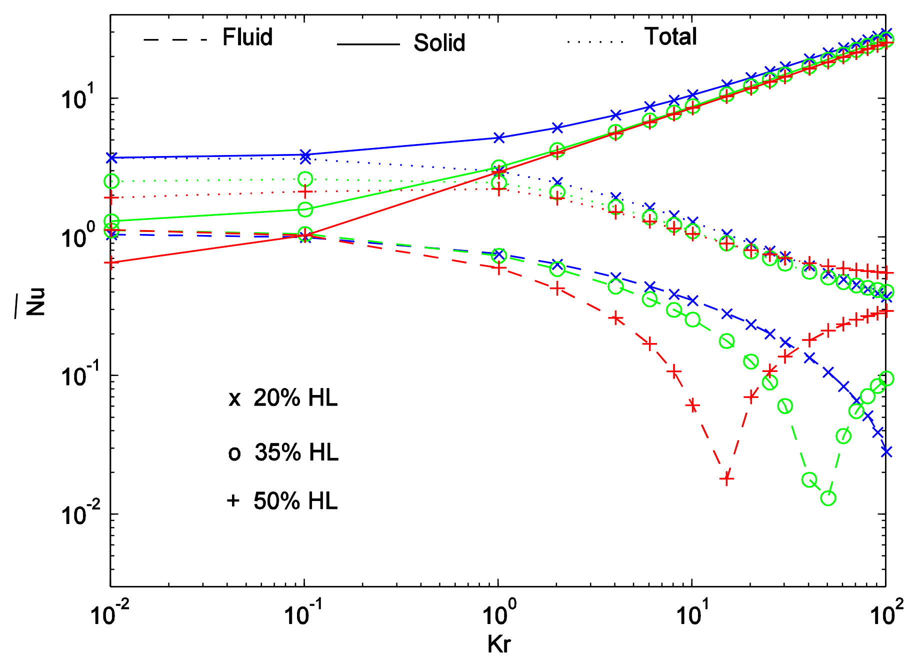

Figure 4.7.14: Average Nusselt number variation with *Kr* and different heater length at mid-section of the annulus

It may be noted that the top of the heater always coincides $\bar{z} = A_r$ for all three lengths with the i.e. 20%, 35% and 50% of heater length.

It is observed that the heat transfer rate is not affected much when heater length is varied from 20% to 35 %, however further increase in heater length enhances heat transfer rate considerably in solid phase of porous medium.

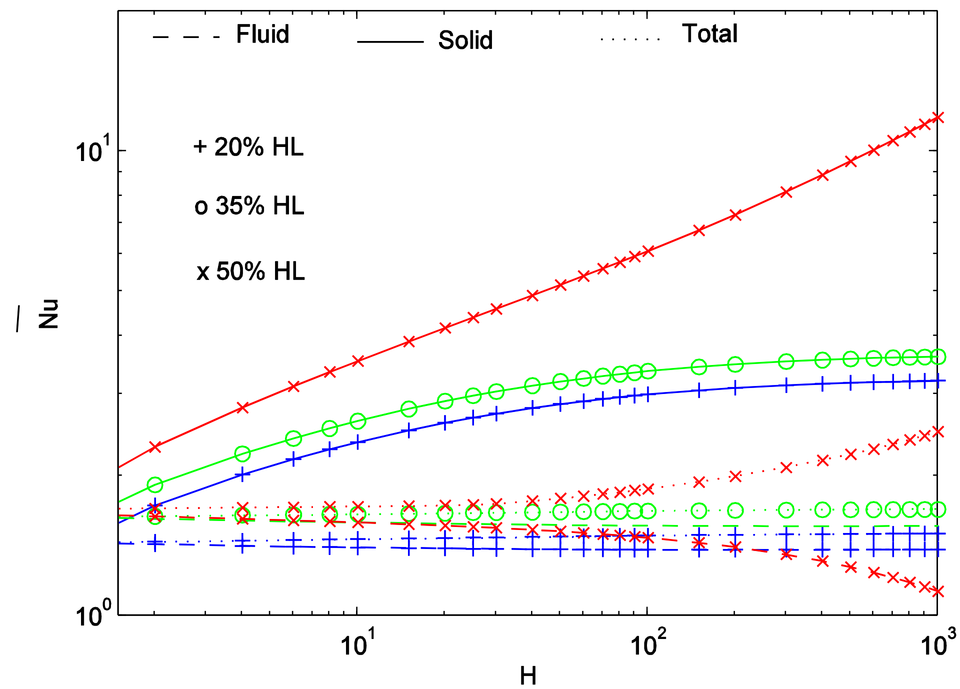

Figure 4.7.15: Average Nusselt number variation with *H* and different heater length at top section of annulus

4.8 Mixed convection analysis in a vertical cylinder with discrete heating

4.8.1 Introduction

The following section describes the heat transfer characteristics of mixed convection in a porous medium for aiding and opposing flow. The aiding and opposed flow is dictated by the direction of applied velocity. It may be noted that the aiding flow refers to a condition when the applied velocity and the buoyancy force act in the same direction assisting each other. However, the buoyancy force and applied velocity act in the opposite direction for the case of opposed flow. The annulus is subjected to discrete heating of 20%, 35% and 50% at bottom, mid and top sections of the annulus. One such case of 20% heating at bottom section for aiding and opposing flow is depicted in Figure 4.8.1 and its mathematical formulation is given in chapter 3, section 3.7.

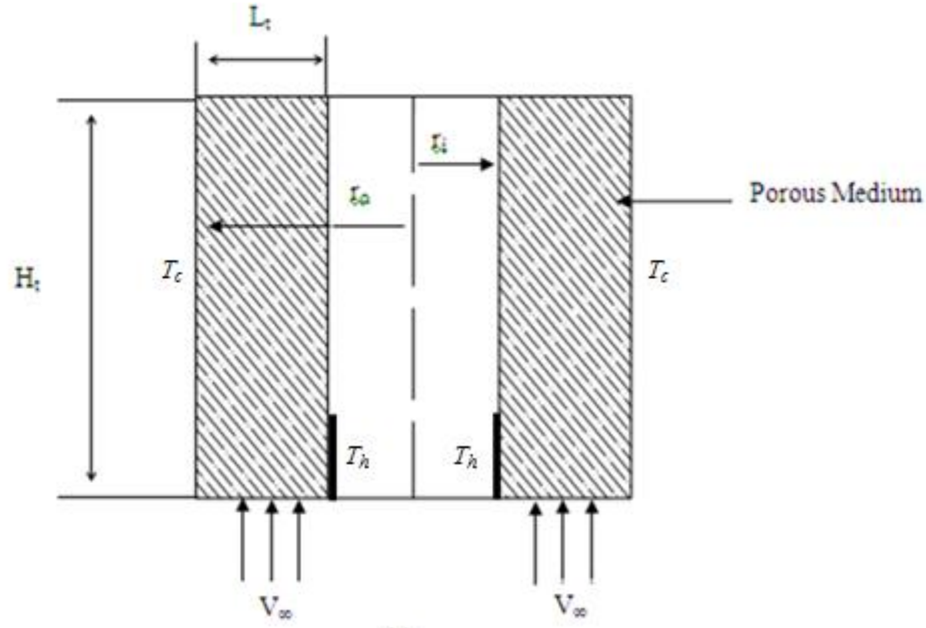

(a)

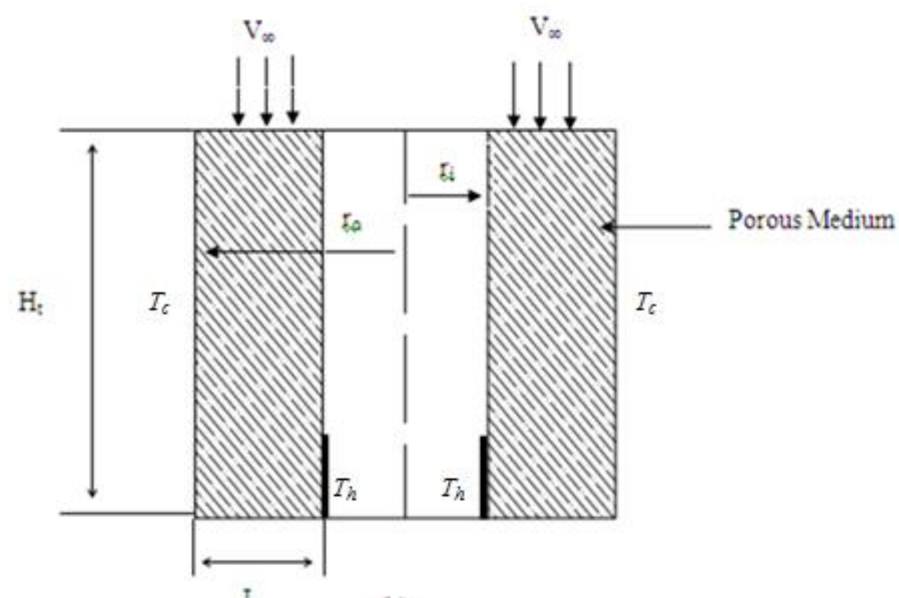

(b)

Figure 4.8.1: Schematic of mixed convection in porous annulus a) aiding flow b) opposing flow

4.8.2 Aiding flow analysis

4.8.2 Aiding flow analysis

Figure 4.8.1 shows the average Nusselt number variations with respect to the thermal conductivity ratio between solid matrix and fluid phase of porous medium when 20% of the length of annulus is heated isothermally to temperature T_h and the rest of the height is adiabatic. It may be noted that the heater length is varied in 3 steps i.e. 20%, 35% and 50% of the height of the annular cylinder. When the bottom portion is heated then the lower edge of the heater always coincides with the lower edge of annulus in all three cases of 20%, 35% and 50% heating. Figure 4.8.1 is obtained by setting $Ra = 25, H = 1, A_r = 2, R_r = 1, R_d = 1.$ It is observed that the Nusselt number of the solid phase is higher than the Nusselt number of the fluid phase for Peclet number 0.1, 0.5 and 2. As expected, the Nusselt number increases with the conductivity ratio. For lower conductivity ratios, the heat transfer rate is better when the Peclet number is higher whereas this trend reverses when thermal conductivity ratio increases. The difference between the solid phase and fluid phase Nusselt number increases with decrease in the Peclet number.

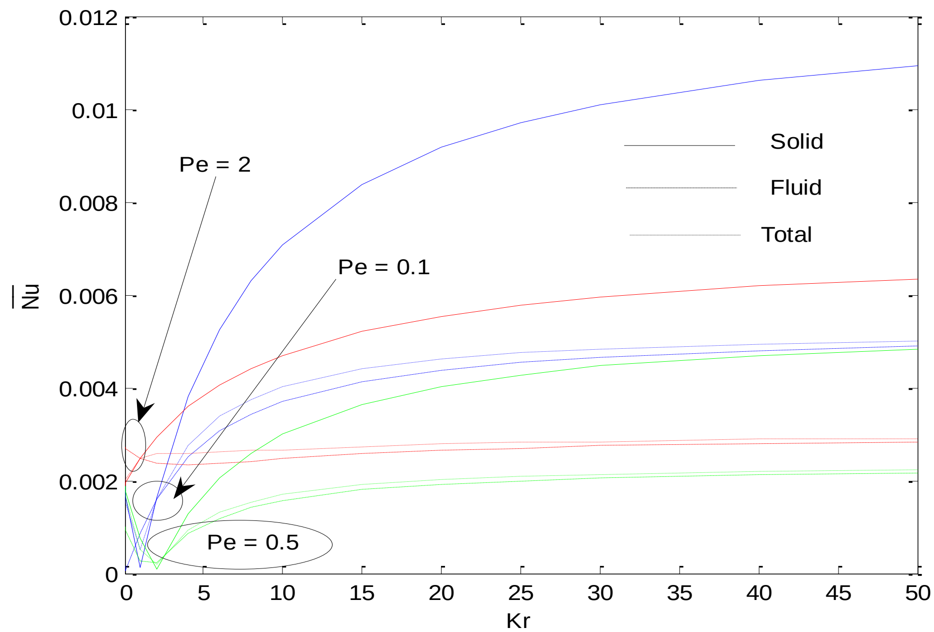

Figure 4.8.2: Variation of average Nusselt number with the respect to conductivity ratio for the 20% heater at the bottom section of the annulus

Figure 4.8.2 shows the average Nusselt number variation when the heater length is 35% of the total height of the annulus, keeping all other parameters similar to that of 20% heater length. It is interesting to note that the Nusselt number of fluid, solid phase as well as the total Nusselt number decreases initially with respect to the thermal conductivity ratio and then further increases in conductivity ratio leading to enhancement of heat transfer due to an increase in the Nusselt number. The initial decrease of Nusselt number with respect to *Kr* is particularly true when the Peclet number is low but this effect diminishes with an increase in the Peclet number as illustrated by lines corresponding to *Pe = 2* in Figure 4.8.2

Figure 4.8.3 shows the average Nusselt number with respect to conductivity ratio and Peclet number for heater length of 50% of cylinder height with all other parameters kept same as that of the previous case. It is noted that the heat transfer rate increases with increase in the length of the heated section of the annulus as illustrated by comparison of

Figures 4.8.1-34.8. This can be explained as the greater length of the heater provides extra heat to be conducted into the medium which in turn increases the fluid activity, increasing the buoyant force of fluid. It can be seen that the maximum Nusselt number reached is 0.52 for 50% heater length as compared to 0.25 and 0.0028 for 35% and 20% *HL* when *Kr* approximates zero. This illustrates that the heat transfer rate increases with heater length. It is seen that the solid Nusselt number increases predominantly with the conductivity ratio but fluid Nusselt number remains almost constant with respect to *Kr*. It is further observed that the total Nusselt number decreases until a point with respect to *Kr* and then the decrease in Nu is negligible. This illustrates that the temperature gradient at close vicinity of the heated section is higher for the solid phase which allows more heat to be transferred between the wall and the solid matrix of the porous medium.

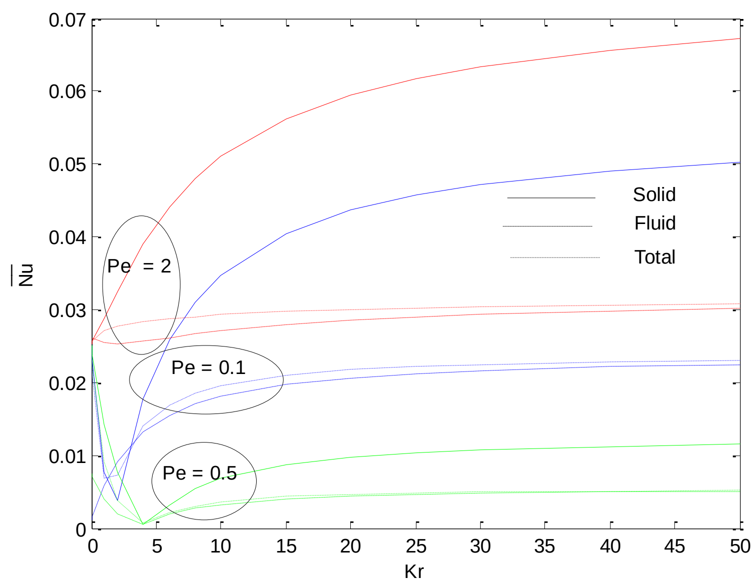

Figure 4.8.3: Variation of average Nusselt number with the respect to conductivity ratio for the 35% heater at the bottom section of the annulus

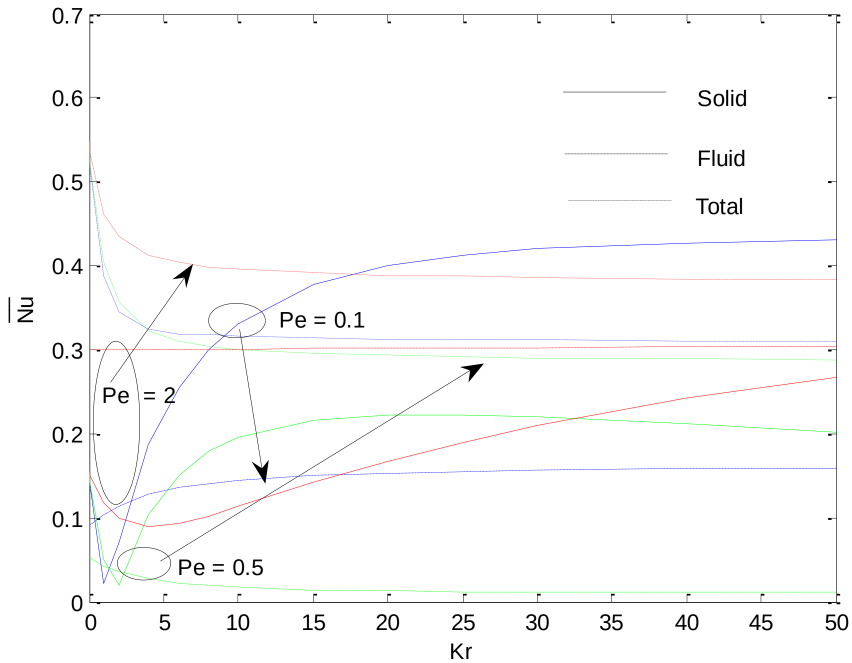

Figure 4.8.4: Variation of average Nusselt number with the respect to conductivity ratio for the 50% heater at the bottom section of the annulus

Figures 4.8.4, 4.8.5 and 4.8.6 show the heat transfer behaviour when the heater is placed at the center of the hot surface for 20%, 35% and 50% *HL* respectively. All other parameters are kept constant as in the previous case except the location and length of the heater. It is observed that the trend of the Nusselt number variation is considerably different from when the heater is placed at the bottom section of the annulus. In the current case, the Nusselt number of the solid phase increases continuously whereas variation of the fluid Nusselt number is minimal although it increases with respect to the concavity ratio *Kr*. For a given value of *Kr*, the solid Nusselt number decreases with increase in the Peclet number. At very large values of *Kr*, the fluid and the total Nusselt numbers are almost equal. The increase in the length of the heater to 35% and 50% (Figures 4.8.5 and 4.8.6) leads to increase in total Nusselt number initially and then decreases marginally contrast to the case of 20% *HL* (Figure 4.8.4)

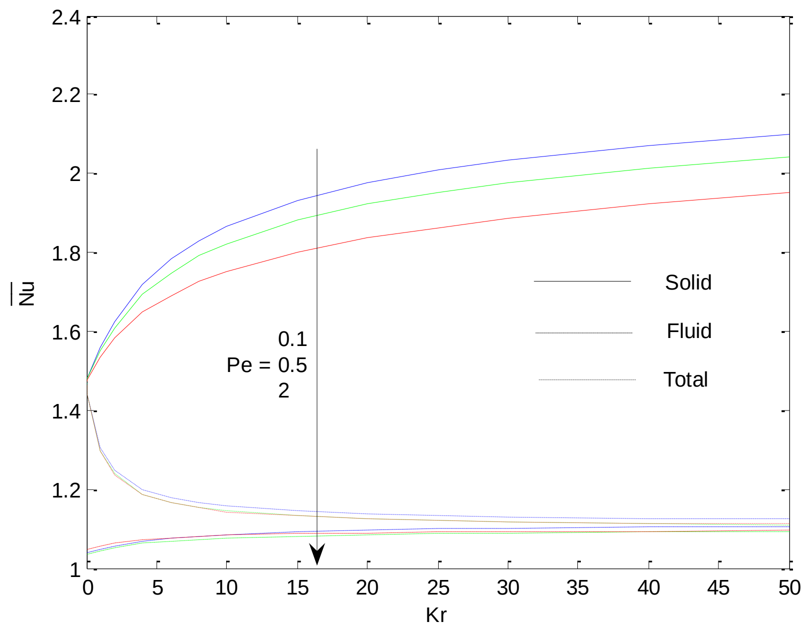

Figure 4.8.5: Variation of average Nusselt number with the respect to conductivity ratio for the 20% heater at the mid-section of the annulus

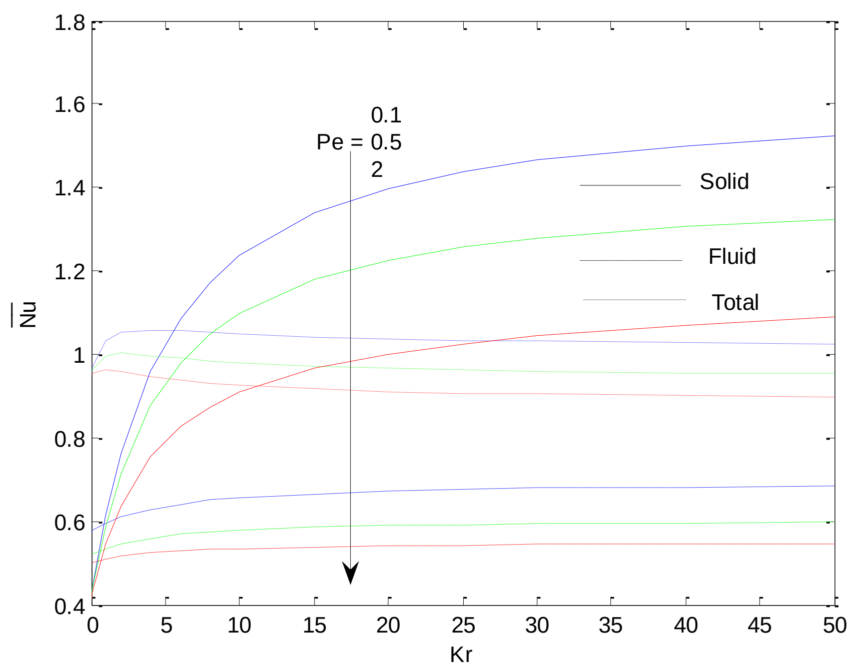

Figure 4.8.6: Variation of average Nusselt number with respect to conductivity ratio for the 35% heater at the mid-section of the annulus

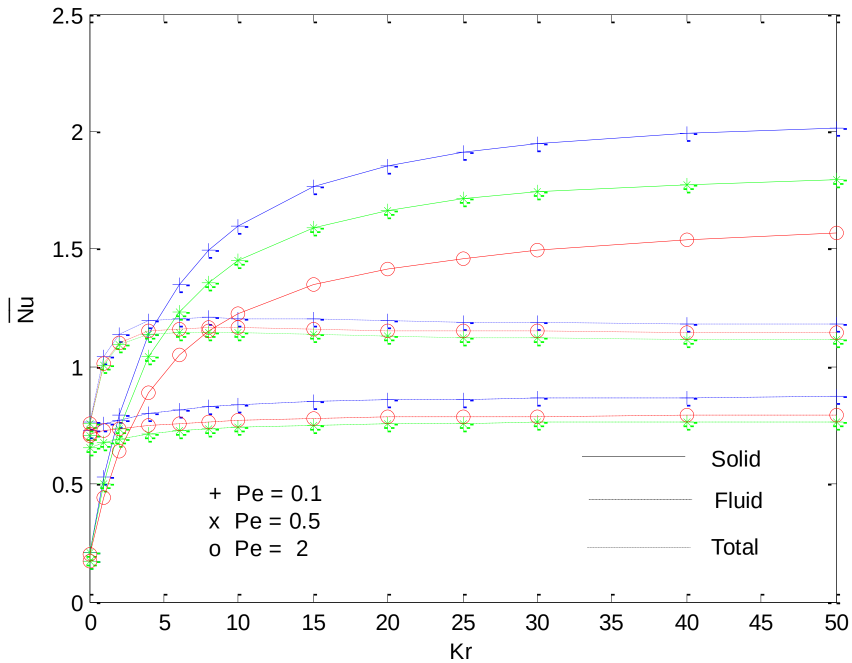

Figure 4.8.7: Variation of average Nusselt number with the respect to conductivity ratio for the 50% heater at the mid-section of the annulus

Figure 4.8.7-4.8.9 illustrates the effect of heater length when it is placed at the top of a hot surface of an annulus. The top edge of the heater always conjoins with the edge of the inner radius for all three cases of 20%, 355 and 50% *HL*. All other parameters are kept constant as in previous cases. It is found that the Nusselt number for fluid, solid and total Nusselt number increases with increase in the conductivity ratio *Kr*. However, this increase in heat transfer tends to cease at higher values of *Kr*. It is found that the fluid and total Nusselt numbers are almost equal to each other. It is seen that the Nusselt number increases with an increment in the Peclet number. The low value of the Peclet number indicates that the flow is buoyancy-driven with minimal applied external velocity. For the case of the heater placed at the top section of the hot surface (Figure 4.8.7-4.8.9), the heat transfer is dominated by an increase in the applied velocity while it is dominated by a buoyancy force for the heater placed at the bottom and middle of the hot surface (Figures 4.8.1-4.8.6)

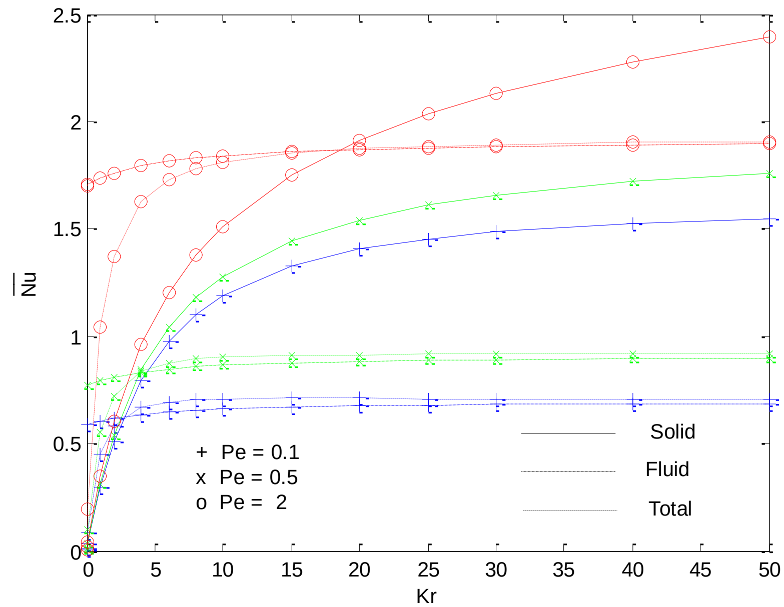

Figure 4.8.8: Variation of average Nusselt number with respect to conductivity ratio for the 20% heater at the top section of the annulus

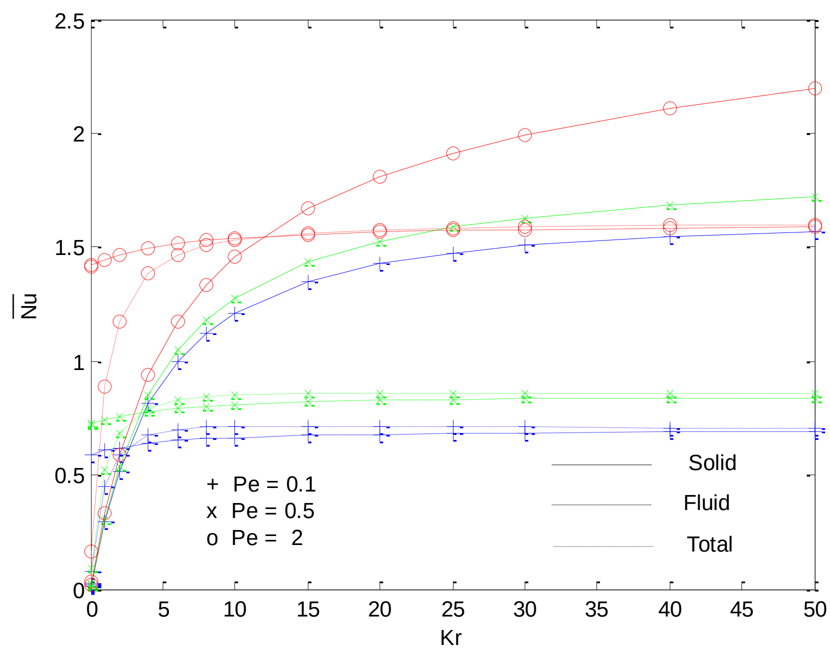

Figure 4.8.9: Variation of average Nusselt number with respect to conductivity ratio for the 35% heater at the top section of the annulus

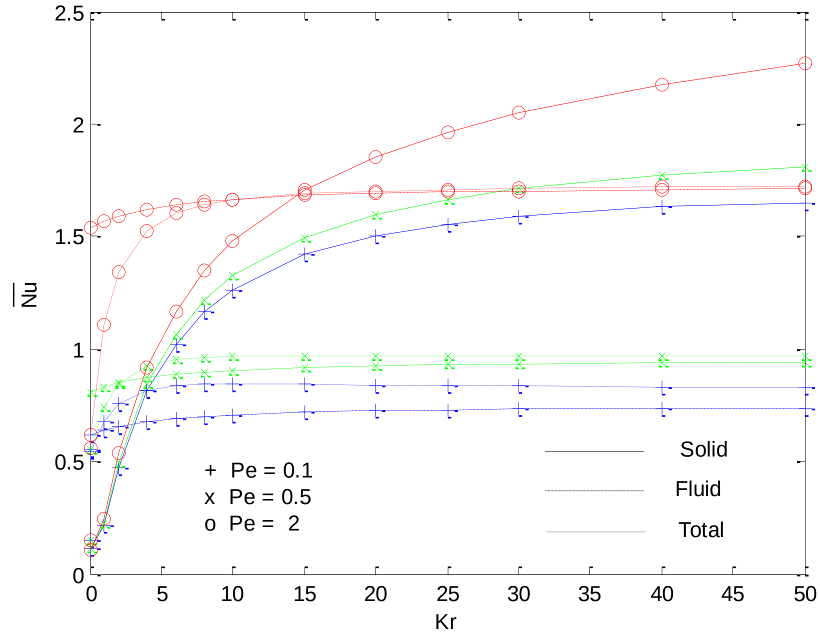

Figure 4.8.10: Variation of average Nusselt number with respect to conductivity ratio for the 50% heater at the top section of the annulus

Figure 4.8.19-4.8.21 illustrates the heat transfer behaviour of the heater being placed at the top section of the annulus. It is found that in general the heat transfer rate of the heater at the top section of the annulus is less than that of the heater placed at the middle section (Figures 4.8.16-4.8.18). The pattern of heat transfer of the heater at the bottom and top sections is similar but with some variation from that of the middle section. In all the cases it was found that the effect of the Peclet number is prominent on the solid phase Nusselt number as compared to the fluid phase and total Nusselt number.

Figures 4.8.10-4.8.12 show the isothermal lines of the fluid and solid phases along with the streamlines for various values of Peclet number for the case of 50% heating at bottom, middle and top of the annulus respectively. These Figures are obtained at$Ra = 25$, $Kr = 50,\ H = 1,\ A_r = 2,\ R_r = 1, R_d = 1$. It can be seen that the isotherms of the fluid tend to move towards the hot surface when the Peclet number is changed from 0.1 to 2 thus indicating that there is higher thermal gradient due to increased Peclet number that in turn leads to improved heat transfer rate. It is further observed that the isotherms of the solid phase are almost vertical near the hot surface which shows that the local heat transfer rate along the hot surface does not vary much for the solid phase. However the local heat transfer rate of the fluid phase is higher at the lower section of the heater causing ~~making~~ the heat transfer rate to vary along the length of the heater. The fluid appears to flow in two distinct patterns with an obvious oval circulation in the majority of the annulus and a small movement of incomplete circulation near the bottom section. For the case of the heater being placed at the middle section as shown in Figure 4.8.11, the fluid heat transfer rate is higher at the lower part of the heater compared to the upper section for the fluid phase. For the solid phase, the heat transfer rate improves at the lower section of the heater due to an increase in the Peclet number but that of the upper section of the heater decreases in the larger proportion rendering the overall effect to be less heat transfer when the Peclet number is increased to 2. The fluid circulation is moved to the center of the annulus when the heater is placed at the middle of the hot surface. The isothermal lines get divided into two distinct sections when the heater is placed at the top of the hot section as shown in Figure 4.8.12. The upper section of the annulus is occupied by high temperature lines and lower section is occupied by low temperature lines. The fluid moves in a twisted oval shape cell indicating that there is weak fluid circulation near the bottom unheated section of the annulus.

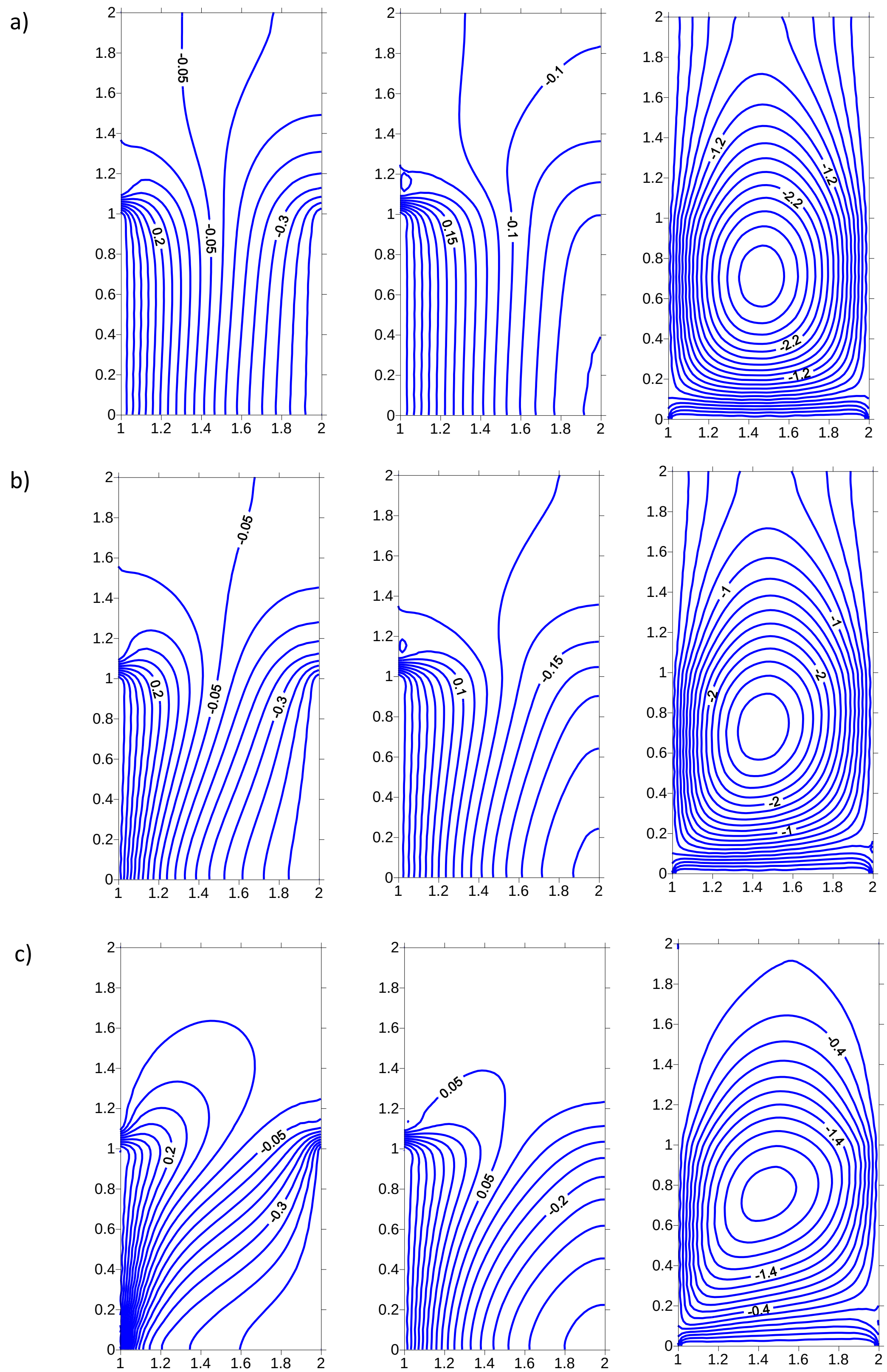

Figure 4.8.11: Isotherms of fluid (left), solid (center) and Streamlines (right) for bottom-section heating a) Pe = 0.1, b) Pe = 0.5 c) Pe = 2

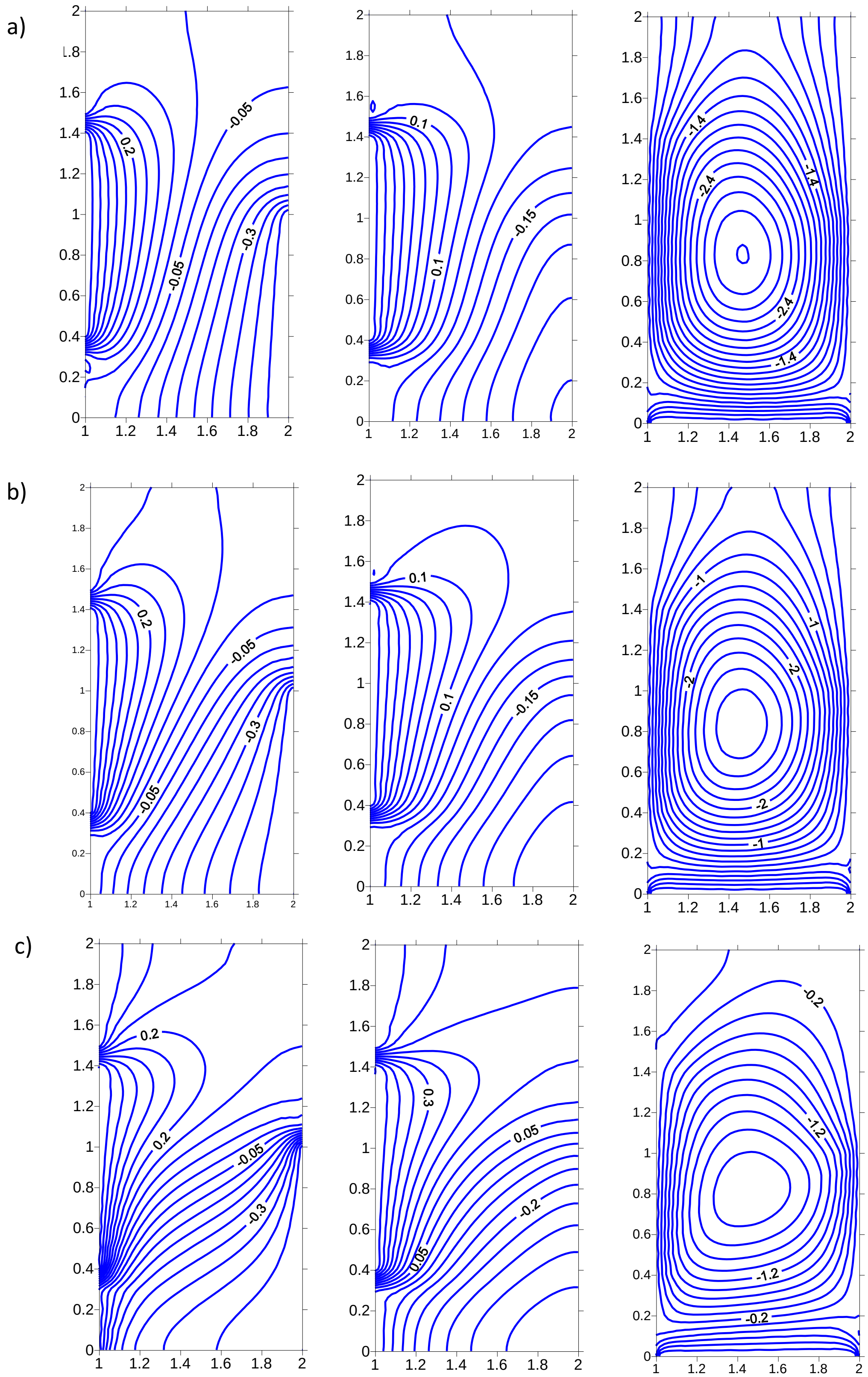

Figure 4.8.12: Isotherms of fluid (left), solid (center) and streamlines (right) for mid-section heating a) Pe = 0.1, b) Pe = 0.5 c) Pe = 20.5 c) Pe = 2

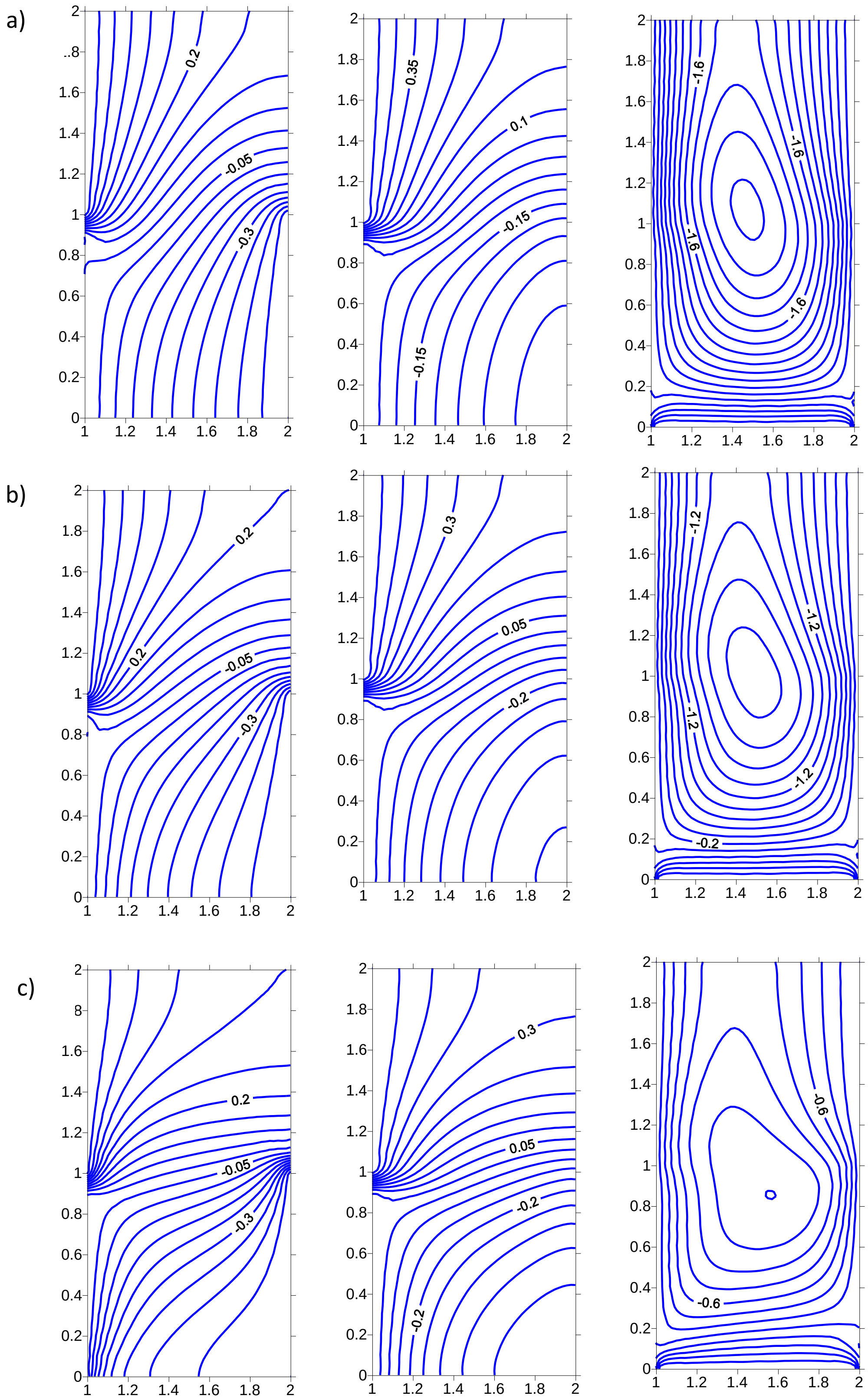

Figure 4.8.13: Isotherms of fluid (left), solid (center) and streamlines (right) for top-section heating a) Pe = 0.1, b) Pe = 0.5 c) Pe = 20.5 c) Pe = 2

4.8.3 Opposing flow analysis

Figure 4.8.13 shows the Nusselt number behaviour of opposing flow with respect to conductivity ratio *Kr*, and Peclet number *Pe* for the case of bottom heating with 20% HL. As expected, the heat transfer rate increases with the conductivity ratio *Kr*. The Nusselt number for $Pe = 0.1$ and 0.5 decreases initially with increase in *Kr* while that of $Pe = 2$ increases continuously with respect to increase in *Kr*. It is seen that the Nusselt number for $Pe = 0.1$ is higher than that of $Pe = 0.5$ and highest Nusselt number is found to be the case when $Pe = 2$ for fluid, solid and total Nusselt number. This shows that the Nusselt number initially decreased with increasing Peclet number and then increased with further increase in *Pe*. The fluid and total Nusselt number are almost equal. The increase in the heater length leads to a sharp decrease in the Nusselt number for Pe=0.1 and 0.5 as illustrated in Figures 4.8.14 and 14.8.5. The increase in heater length changes the pattern of fluid and solid phases and total Nusselt number. The increase in heater length causes the ~~leads~~ total Nusselt number to have a prominent value in comparison to that of the fluid and solid phases Nusselt number (Figure 4.8.15). The overall heat transfer rate increases with the heater length as illustrated by Figures 4.8.13-4.8.15.

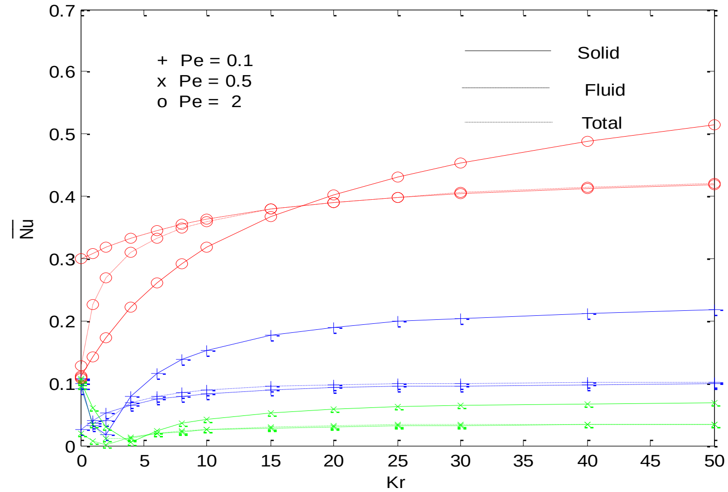

Figure 4.8.14: Variation of average Nusselt number with respect to conductivity ratio for the 20% heater at the bottom section of the annulus

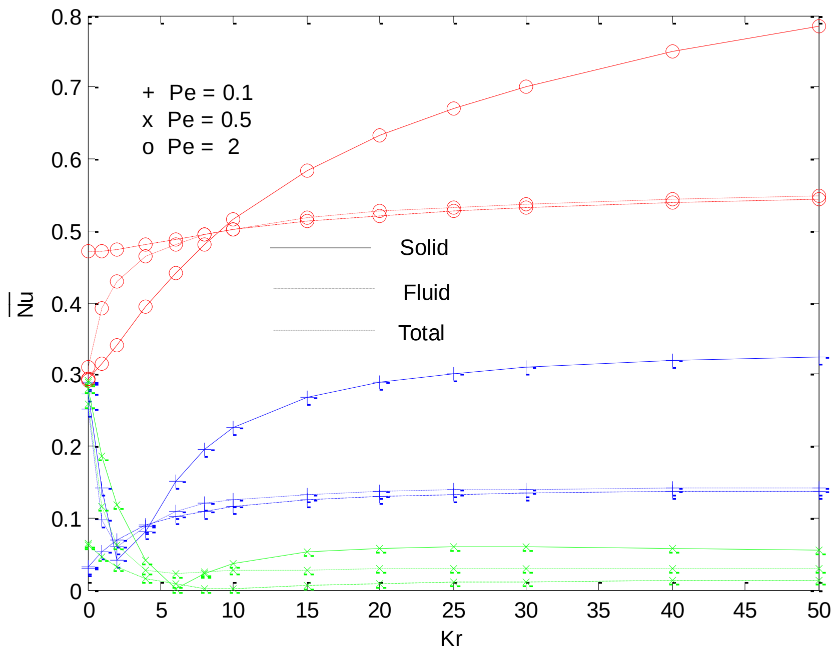

Figure 4.8.15: Variation of average Nusselt number with respect to conductivity ratio for the 35% heater at the bottom section of the annulus

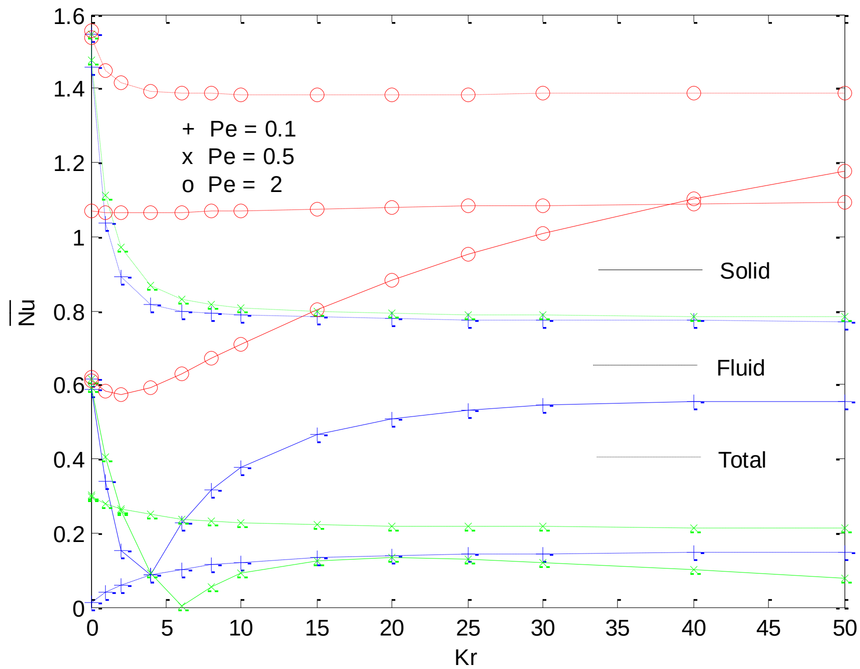

Figure 4.8.16: Variation of average Nusselt number with respect to conductivity ratio for the 50% heater at the bottom section of the annulus

Figures 4.8.16-4.8.18 demonstrates the effect of heater length for opposing flow along the middle portion of the annulus with all other parameters being held constant as in previous cases. It is observed that the Nusselt number for the heater being placed at the upper portion of annulus is higher than the case when the heater is placed at the bottom section of the annulus. For this case, the Nusselt number of the fluid and solid phases decreases with increase in the Peclet number as opposed to the case when the heater is placed at bottom section.

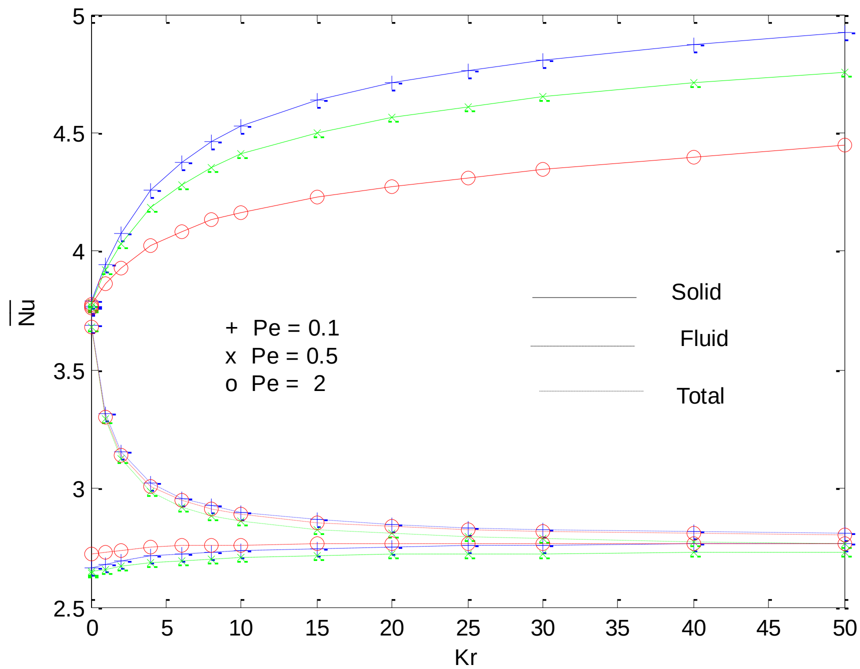

Figure 4.8.17: Variation of average Nusselt number with respect to conductivity ratio for the 20% heater at the mid-section of the annulus

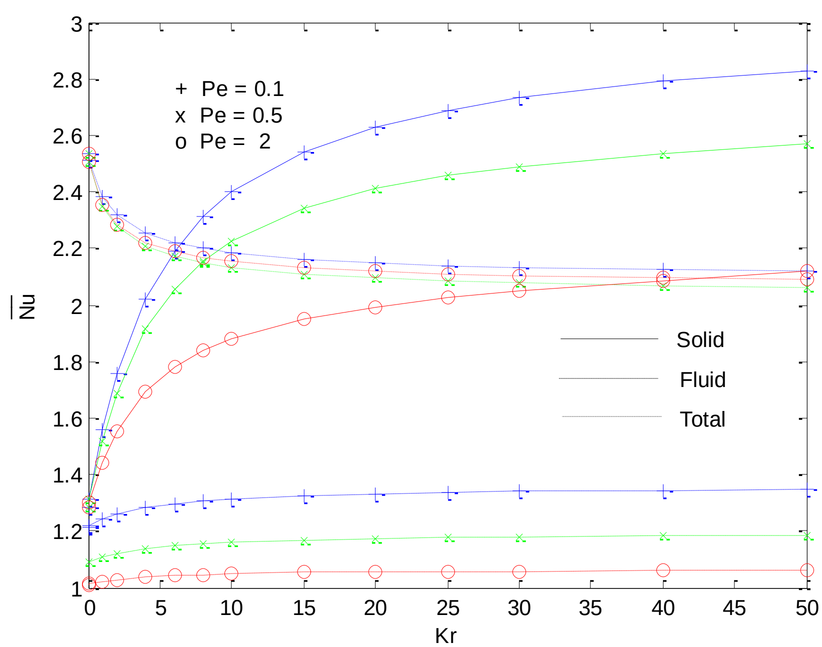

Figure 4.8.18: Variation of average Nusselt number with respect to conductivity ratio for the 35% heater at the mid-section of the annulus

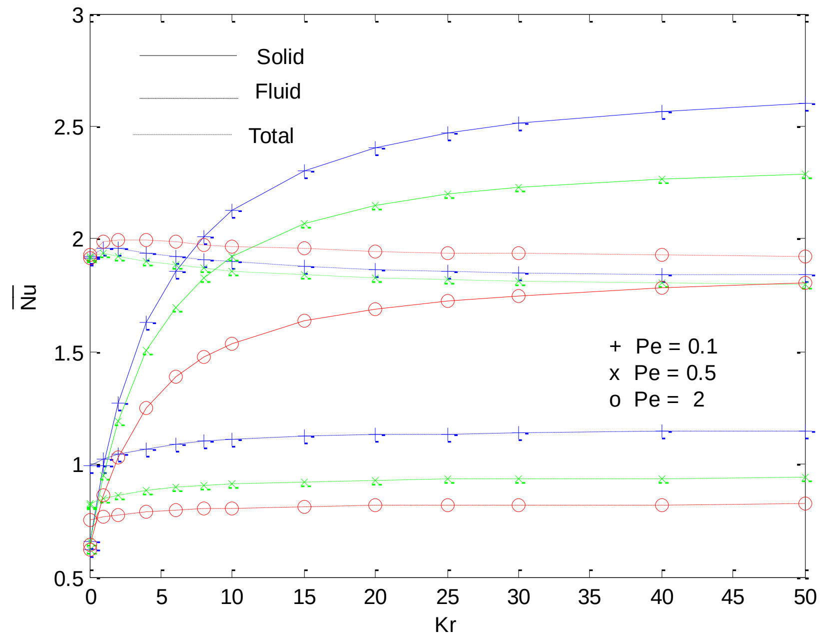

Figure 4.8.19: Variation of average Nusselt number with respect to conductivity ratio for the 50% heater at the mid-section of the annulus

Figures 4.8.19- 4.8.21 illustrate the heat transfer behaviour corresponding to the heater is placed at the top section of the annulus. It is found that in general, the heat transfer rate from the heater at the top section of the annulus is less than that when the heater is placed at middle section (Figures 4.8.16-4.8.18). The pattern of heat transfer from the heater at the bottom and top sections varies slightly from, the heater placed at the middle section. In all the cases, it is found that the effect of the Peclet number is prominent at the solid phase Nusselt number compared to fluid phase and total Nusselt number.

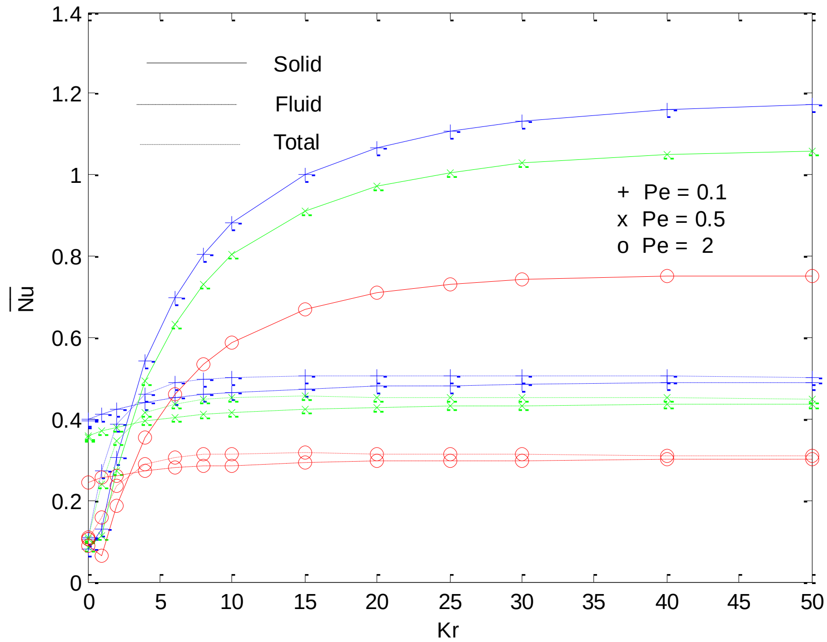

Figure 4.8.20: Variation of average Nusselt number with respect to conductivity ratio for the 20% heater at the top section of the annulus

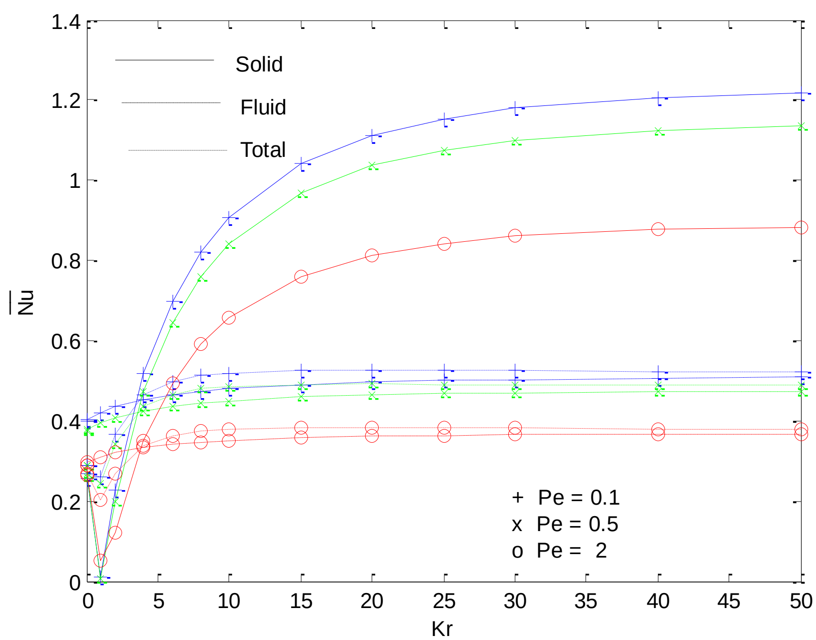

Figure 4.8.21: Variation of average Nusselt number with respect to conductivity ratio for the 35% heater at the top section of the annulus

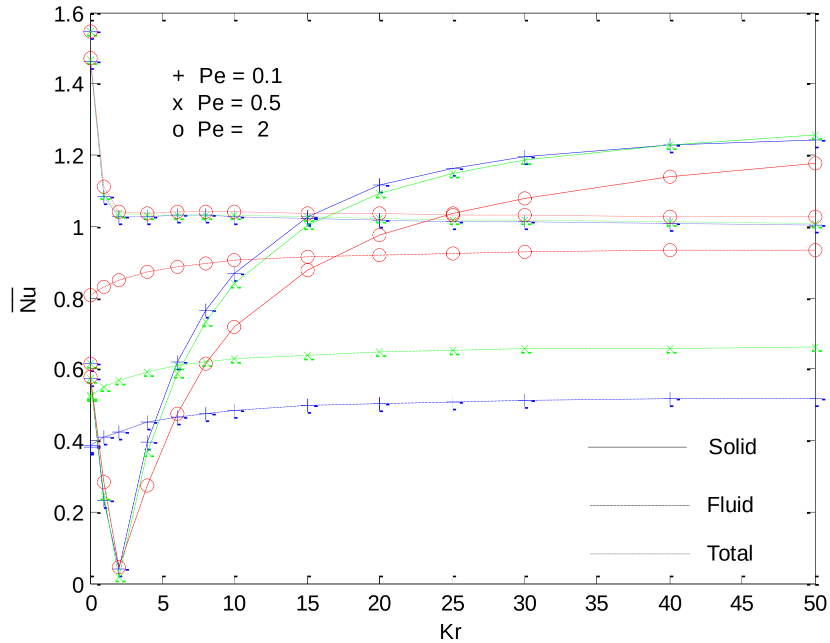

Figure 4.8.22: Variation of average Nusselt number with the respect to conductivity ratio for the 50% heater at the top section of the annulus

Figures 4.8.23-4.8.25 illustrate the temperature distribution and fluid flow activity in terms of isothermal lines and streamlines respectively for the case of opposing flow at $Ra = 25,\ Kr = 50,\ H = 1,\ A_r = 2,\ R_r = 1, R_d = 1$ when 50% of the annulus is heated at the bottom, middle and top sections of the annulus respectively. For the case of bottom section heating (Figure 4.8.23), it is found that the fluid does not complete the circulation but flows in a semi-circle culminating at the base of the annulus. However, the placement of the heater at the middle section brings in a smoother flow of fluid with few complete circulation cells at the centre of the annulus. The fluid movement of opposing flow is found to be more ovoid compared to the circular shape of aiding flow (Figures 4.8.10-4.8.12). It is obvious by comparing the Figures 4.8.10-4.8.12 and Figures 4.8.22-4.8.24 that the applied velocity in a downward direction in case of the opposing flow does not allow the thermal energy to reach from hot to cold surface. Instead, it reduces the energy before it can reach the cold surface as illustrated by the two distinct patterns of isothermal lines and the streamlines.

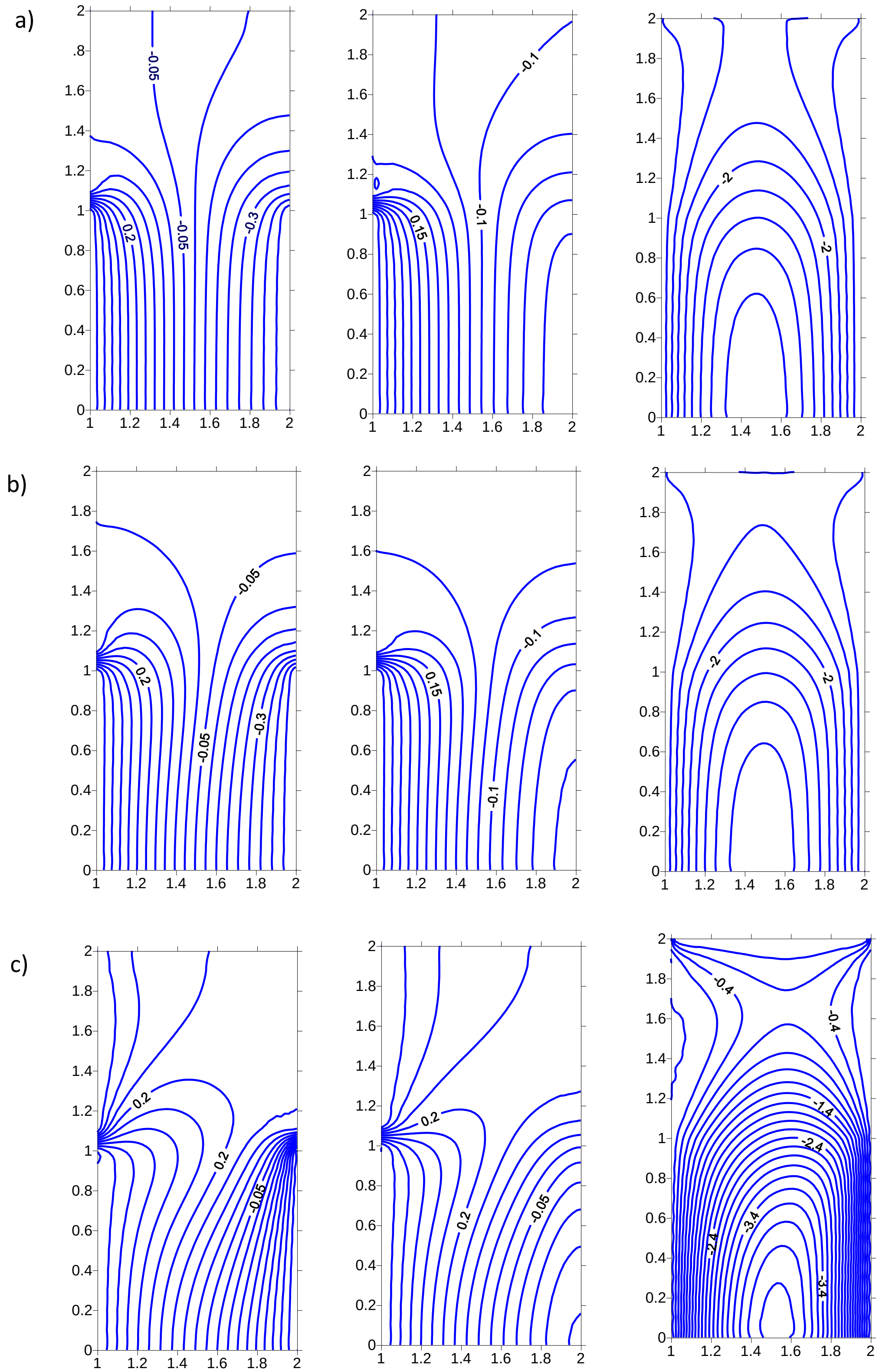

Figure 4.8.23: Isotherms of fluid (left), solid (center) and streamlines (right) for bottom section heating a*) Pe = 0.1, b) Pe = 0.5 c) Pe = 20.5 c) Pe = 2*

a)

b)

c)

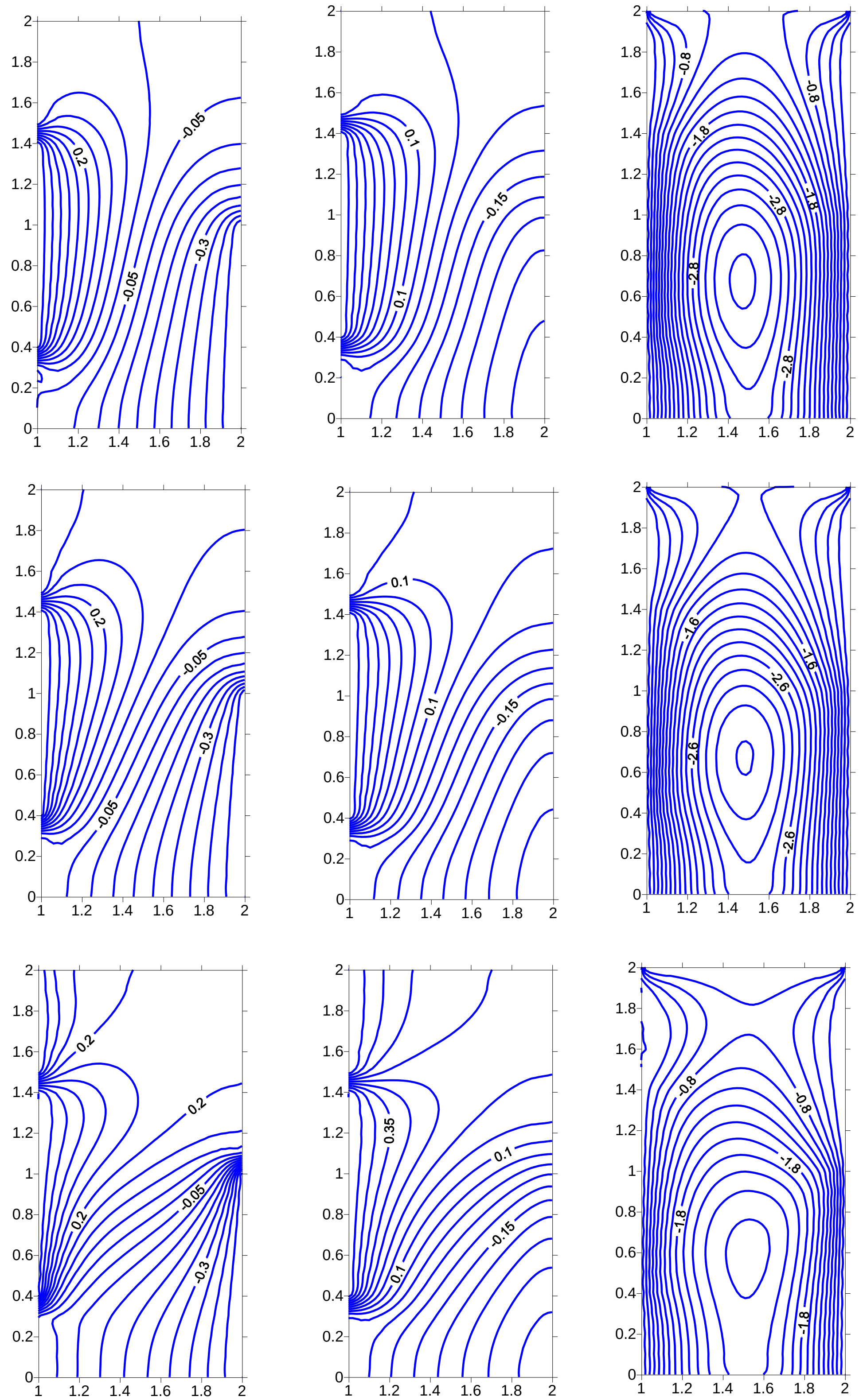

Figure 4.8.24: Isotherms of fluid (left), solid (center) and streamlines (right) for middle section heating a) *Pe = 0.1, b) Pe = 0.5 c) Pe = 20.5 c) Pe = 2*

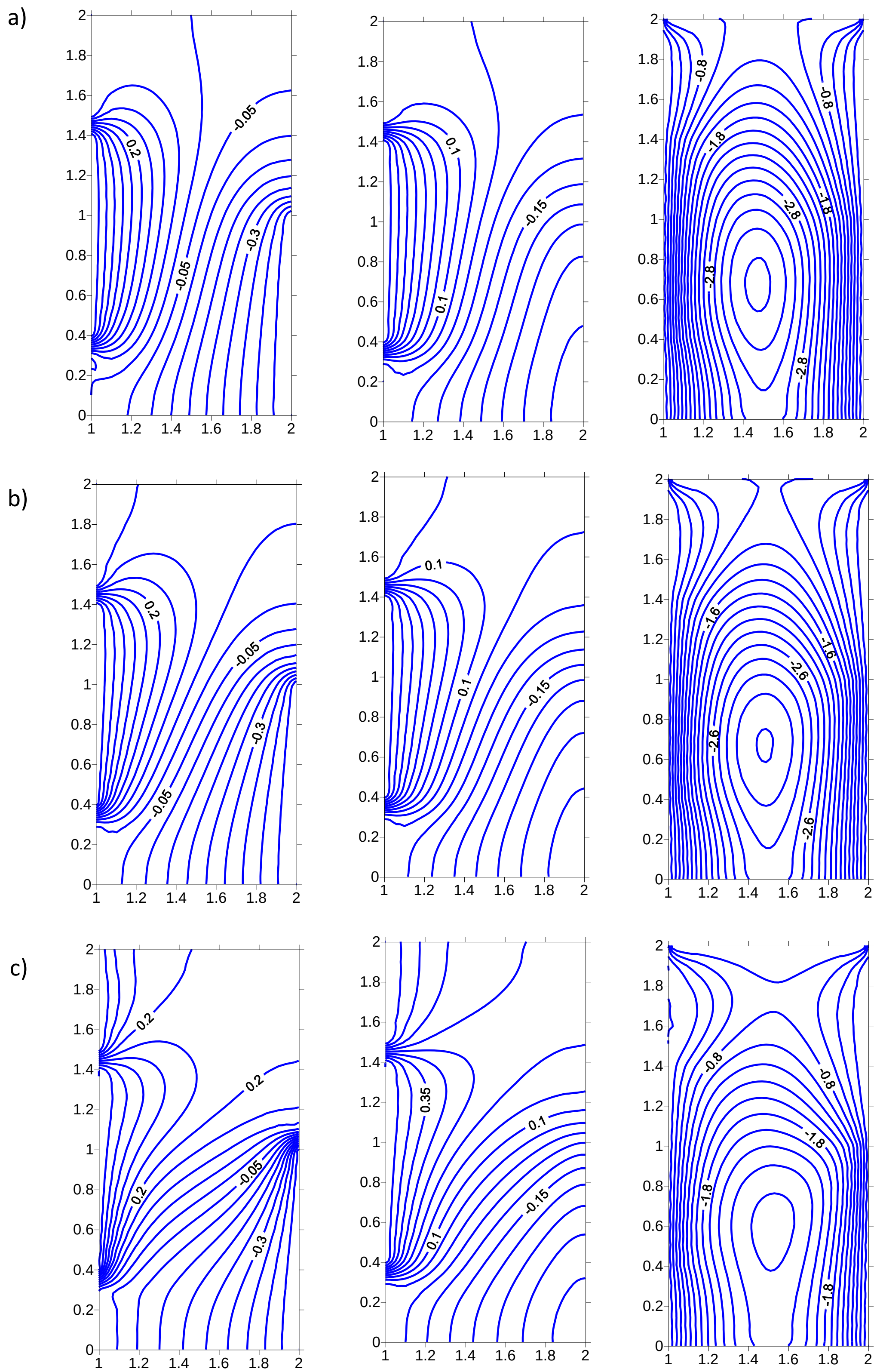

Figure 4.8.25: Isotherms of fluid (left), solid (center) and streamlines (right) for top section heating a) *Pe = 0.1, b) Pe = 0.5 c) Pe = 20.5 c) Pe* = 2